UNIVERSIDADE FEDERAL FLUMINENSE

Rafael Heitor Correia de Melo

Using Fractal Characteristics such as Fractal Dimension, Lacunarity and Succolarity to Characterize Texture Patterns on Images

NITERÓI

2007

UNIVERSIDADE FEDERAL FLUMINENSE

Rafael Heitor Correia de Melo

Using Fractal Characteristics such as Fractal Dimension, Lacunarity and Succolarity to Characterize Texture Patterns on Images

A Dissertation submitted to the Post-Graduate program in Computing of Universidade Federal Fluminense in partial fulfillment of the requirements for the degree of Master in Computing. Area: Computação Visual e Interfaces (Visual Computing and Interfaces).

Supervisor: Aura Conci

NITERÓI

2007

Ficha Catalográfica elaborada pela Biblioteca da Escola de Engenharia e Instituto de Computação da UFF

M528 Melo,Rafael Heitor Correia de.
Using Fractal Characteristics such as Fractal Dimension,Lacunarity and Succolarity to Characterize Texture Patterns on Images / Rafael Heitor Correia de Melo. – Niterói, RJ : [s.n.], 2007.
97 f.

Orientador: Aura Conci
Dissertação (Mestrado em Computação) - Universidade Federal Fluminense, 2007.

1. Processamento de imagem-Técnica digital.. 2. Dimensão Fractal. 3.Textura de imagens-análise.4.Fractais. 5.Imagem 3D. I. Título.

CDD 006.42

Using Fractal Characteristics such as Fractal Dimension, Lacunarity and Succolarity to Characterize Texture Patterns on Images

Rafael Heitor Correia de Melo

A Dissertation submitted to the Post-Graduate program in Computing of Universidade Federal Fluminense in partial fulfillment of the requirements for the degree of Master in Computing. Area: Visual Computing and Interfaces.

Approved by Dissertation Examining Committee:

Profª. Aura Conci – IC/UFF (Supervisor)

Prof. Anselmo Antunes Montenegro – IC/UFF

Prof. Estevam Barbosa de Las Casas - UFMG

Niterói, August 24th, 2007.

To God;

To all my family and friends;

Acknowledgements

I would like to thank all my family, specially my parents, Julio and Dayse, for the education that made possible for me to reach this point in my life, and for the understanding of the stress on the work hours.

Another person who helped me very much on the period I was writing this dissertation was Evelyn Vieira. I have to thank her for the incentive she gave me to hold on.

I also have to specially thank my supervisor, Professor Aura Conci, who trusted me and my potential, for the teachings, for the way that she treats her students, as equals, always with patience, availability and recognition.

A special thank to all my friends of work on ADDLabs, specially Paula Yamada, Robson Vinicio, Fernando Pinto, Giovanni Arbasi, Professor Inhaúma Ferraz and Professor Ana Cristina, that, through all these years, contributed to my professional growth, as well as on my personal growth.

Talking about friends, I could never forget to thank two of my best friends, Marcio Nunes and Rodrigo Prado, that on many times, even without knowing, turned bad moments into good moments during this work.

The support of the Computer Institute of UFF and all of its staff is acknowledged, a special thank to Maria, that helped me on many things, many times.

Thank you all.

Resumo

A geometria fractal possui três medidas para caracterizar texturas: Dimensão Fractal (FD), Lacunaridade e Sucolaridade. A Dimensão Fractal é a mais conhecida e estudada. É também a que possui mais metodologias para o cálculo por imagens. Pode ser calculada para imagens em preto e branco bem como para imagens de satélite com várias bandas. A FD pode ser avaliada por diversos métodos, desde o simples método do "Box-Dimension" a mais complexa dimensão de Hausdorff. O mesmo não acontece com as duas outras medidas. Embora cada vez mais trabalhos tenham explorado as características da Lacunaridade, a Sucolaridade, até então não tem sido calculada.

Este trabalho apresenta um método para calcular a Sucolaridade. Demonstra a sua usabilidade em imagens reais, bem como as semelhanças e diferenças de cada medida fractal. A proposta de cálculo para esta medida se baseia no método "Box Counting" com adaptações para que este atenda as noções da Sucolaridade. O passo a passo de um exemplo simples explica a forma de cálculo proposta para imagens binárias e para objetos 3D. Além disso, este trabalho apresenta uma abordagem para o cálculo da Lacunaridade de objetos 3D. Esta proposta inclui uma forma de calcular também a Lacunaridade de imagens em tons de cinza de duas formas distintas.

O principal objetivo deste trabalho é mostrar que a Sucolaridade pode ser usada como uma nova característica em processos de reconhecimento de padrões, especialmente na identificação de texturas naturais. Além disso, esta medida, combinada com a Dimensão Fractal e a Lacunaridade, é muito útil para identificar diferentes tipos de texturas em imagens.

Palavras chaves: Sucolaridade, Dimensão Fractal, Lacunaridade 3D, medidas fractais, análise binária, imagens preto e brancas.

Abstract

Three aspects of texture are considered by the fractal geometry: Fractal Dimension (FD), Lacunarity and Succolarity. Fractal Dimension has been well studied; a great number of approaches have been presented to extract it from images. It can be computed from black-white to multi-band image. There are many approaches also, from the simple Box-Dimension to the most complex Hausdorff Dimension. The same does not happen with the other two measures. Although Lacunarity has been more and more used in works exploring its characteristics, Succolarity, until now, has not been computed.

This work presents a method to compute Succolarity, as well as a demonstration of its applicability, differences and similarities of each fractal measure. The proposed method for this computation is based on the Box Counting approach adapted to the notions of Succolarity. A simple example is shown step by step to easily explain how to compute the Succolarity for binary images and for 3D objects. Moreover, this work presents a procedure to calculate the Lacunarity of 3D objects. This proposal is organized in a way that it could be used to evaluate also the Lacunarity of grey-scale images in two different manners.

The main goal of the work is to show that the Succolarity can be used as a new feature in the pattern recognition process, especially for identification of natural textures. The combination of this measure with fractal dimension and Lacunarity is useful to identity different types of texture on images.

Key words: Succolarity, Fractal Dimension, 3D Lacunarity, fractal measures, binary image analysis, black & white images.

List of Figures

List of Tables

Contents

1 INTRODUCTION

Although the denomination *Computer Graphics* is dated from 1959, the use of computer graphics is directly connected to the MIT development (on 1950) of the first computer with graphic resources which enables the visualization of numeric data. This made possible the construction of the computer system SAGE, on 1955. This system converts information captured from the radar to images with the possibility of points under suspicion being pointed by the user through an optic pen.

Despite being considered a novel area, the evolution on this field was enormous, as it can be easily seen by comparing old and new films. Tron, shown in Figure 1.1 (a) and (b) (LISBERGER, 1982), was one of the first films (from a major studio) that used computer effects extensively. The Polar Express (ZEMECKIS, 2004), figure 1.2 (a) and (b), presents real 3D character movements.

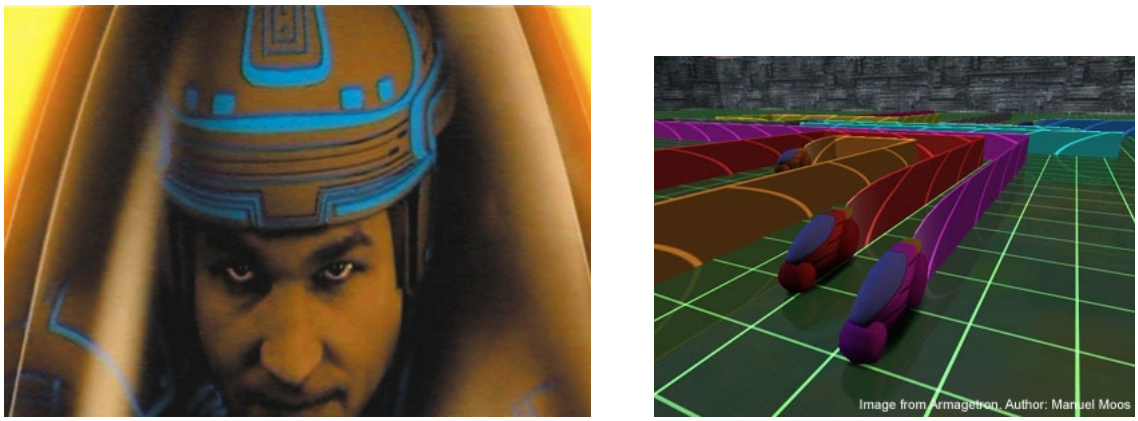

(a) (b)

Figure 1.1. Two images of the film Tron: (a) Using a real image and computer effects; (b) A scene 100% generated by computer.

The first film, Tron, illustrates some basic computer graphic techniques (figure 1.1). In "The Polar Express" (figure 1.2), the actors made all the scenes in front of an empty screen, sensors of movement captured details of their motion. The data of these sensors were transmitted to computers and served as mold for the creation of the characters of the film. And because of these sensors, the characters created do not need to have the same body of the actor that play the role. This permitted Tom Hanks to play 5 roles on this film, one of them as a kid. These two examples of movies show how fast is the evolution of the techniques of computer graphics.

(a) (b)

Figure 1.2. Images of two of the five personages interpreted by Tom Hanks on the film Polar Express: (a) The conductor; (b) The kid.

The ability to represent nature on computers attracts the attention of all the scientific community. The fractals are the best examples on how to produce images with a high degree of realism. This statement could be seen on a simple example of a fractal landscape generated by computer using FLG, a fractal landscape generator program (BROWN, 2005) in figure 1.3. These computer generated images are useful to show the incredible complexity of images generated with great simplicity through fractal equations.

Figure 1.3. Fractal landscape to simulate the Arizona desert (BROWN, 2005).

Computer graphics could be classified in three main areas of interest: image synthesis, image processing and image analysis. The image synthesis regards the synthetic creation of images; creating images by the computer is very useful to simulate a great number of phenomena. Image processing is used to enhance the characteristic of images and sometimes enables the visualization, perception of particularities that cannot be seen

on the image before the processing. The image analysis involves feature extraction from the image that is useful on the process of pattern recognition.

1.1 MOTIVATION

Nowadays computer graphics can be found on many important areas like movies (special effects), medicine (exams, diagnostics and treatments), engineering (solid/fluid mechanics and simulation), meteorology (weather prevision), public security (training and recognition), industry (quality control and product development), entertainment (games and cartoons) and others (AZEVEDO and CONCI, 2003).

This dissertation is concerned with image processing and analysis. Image synthesis was used too, on the generation of synthetic images to validate some ideas presented here. The work presented here continues with the fractal line of research that produced several papers since 1995, beginning with CONCI&CAMPOS, 1995 through 2006, with MELO et al, 2006, MELO et al, 2006a, NUNES&CONCI, 2006-2007 and MELO& CONCI, 2007.

A great number of applications treat the identification of characteristics using fractal dimension: BATTY and LONGLEY, 1994; BLOCK et al., 1990; BARROS FILHO and SOBREIRA, 2005 and MELO and CONCI, 2007, some use Lacunarity to this end, like FERNANDES and CONCI, 2004a; BARROS FILHO and SOBREIRA, 2005a and MELO et al, 2006. Nevertheless up to now, none has used Succolarity to characterize patterns through images. With the definition of Succolarity and its computational method here presented we intend to start a discussion on why not use this fractal characteristic to image processing. This work also shows that Succolarity presents good results on images that have flow characteristics.

1.2 GOALS

An important point of this work is to demonstrate to the readers the positive aspects of the Succolarity and to show that, despite the simplicity of the method proposed here, it attends to the notions of Succolarity (MANDELBROT, 1977) and preserves similar characteristics with the fractal measures already known.

The computation of the Succolarity is organized to be a direct and simple natural evolution of the other fractal measures already known, like the box counting method (BLOCK et al., 1990) for Fractal Dimension estimation (that is the easiest way to calculate

it) and the gliding box method (ALLAIN and CLOITRE, 1991) to Lacunarity evaluation (that is an effective method to calculate its value).

All fractal indices that are considered in this work could be used on pattern recognition processes, but it is not the idea of this dissertation to define a complete application to this purpose. Neural networks, nearest neighbor or any kind of decision method are out of the scope of this work. So, as seen in figure 1.4, which demonstrates a general pattern recognition model through images, one can notice that this work has some pre-processing methods, but the main idea of this dissertation stands for the feature extraction step of this model.

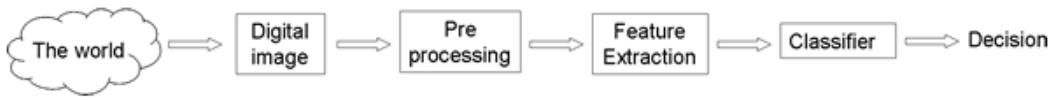

Figure 1.4. General pattern recognition model by images.

Finally, the main achievement of this work is that it could be used as a starting point to researchers and applications in this area. Moreover, new approaches could be proposed for this evaluation as well as this work could also be continued and improved in many ways.

1.3 CONTRIBUTIONS

One of the contributions is to present a text that explains the theory of fractal measures in an easy and understandable way. It explains the fractal measures of Fractal Dimension and Lacunarity, with the already known methods that calculate them, respectively, box counting and gliding box, through simple examples. The other fractal measure, Succolarity, is shown also, through simple examples, but now presenting a completely novel formal definition, as well as a totally new method. The only definition for this measure that has been known is a descriptive one presented by Mandelbrot. Here, a formal definition and an original method are both proposed. The method is based on the box counting approach but with adaptations to attend the notions of Succolarity. This text could then be a basic tutorial for people who would like to initiate their studies in this area.

Moreover, the implemented techniques that could be seen as contributions are: the box counting method (to calculate the fractal dimension of binary images), the gliding box

method (to calculate the Lacunarity of binary images), a new approach to calculate the Lacunarity of 3D objects, two approaches for gray-scale images (based on the 3D method defined) and the completely new methods to calculate the binary Succolarity and the sucolarity of the 3D objects. All these techniques were developed on C++ with paradigms of object orientation. The development was done using CxImage (PIZZOLATO, 2003), an open source library for image processing and visualization.

1.4 WORK ORGANIZATION

This dissertation is organized as follows. The second chapter presents an introduction to the fractal geometry and describes the concepts of Fractal Dimension, Lacunarity (with a definition of computation for 3D objects, applied also to gray-scale images in two different approaches; it also explains two other approaches already made for gray-scale images) and Succolarity. The calculations of these measures are illustrated through their evaluation on synthetic images. With these examples, the characteristics of the methods to computed Fractal Dimension and Lacunarity are explored. On chapter three, the proposed methods to calculate the Succolarity for images and 3D objects or images are presented. Simple examples are used to easily explain the idea of the presented approaches. Chapter four explains the advantages of using more than one fractal measure on a pattern recognition process. On chapter five, the preparation of the images before submitting it to the three methods described in this work is considered. Then, all the methods described are demonstrated through their results on real images. Comparisons with other methods are made to validate and demonstrate their advantages or disadvantages. The results obtained show the usability of the method and the possibility of combinations of all these results on pattern recognition processes. Finally, chapter six presents the conclusions of this work and proposes future extensions that could be studied on the same subject.

2 FRACTAL GEOMETRY AND MEASURES

Geometry is the mathematical language to describe, relate and manipulate shapes. Fractals are recent issues with respect to its uses on science; this potential was recognized only on the last thirty years.

The Euclidean forms have only one or a few characteristics (side, radius, etc) that could be reduced or could change in scale and proportion. Fractal forms do not present characteristic parameters; they are independent of scale and are always self-similar. The Euclidian geometry shows a concise and adequate description to man made objects but this description is not appropriate for natural shapes like the fractal geometry.

Euclidean forms have simple geometric formulas. Fractal forms are results of recursive algorithms and their construction and representation need computers. An example of fractal form is the von Koch Curve (KOCH, 1904). On figure 2.1 this fractal is represented to show the above commented differences.

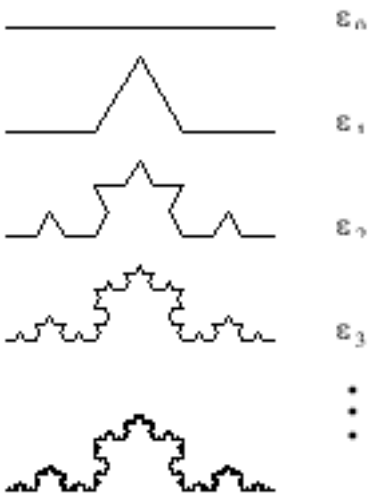

Figure 2.1. Construction of the von Koch Curve.

To build the triadic von Koch Curve we have to execute the following steps:

1 - Start with a line segment of length r;

2 - Divide this line in 3 parts of the same size (each piece of length d is scaled from the original line by d=1/3×r);

3 - Remove the central piece and add two other pieces (the other two sides of an equilateral triangle) of the same size of the one that have been removed;

4 - Repeat the process over and over.

At each new stage, the corresponding drawing will be added by a piece that will be 1/3 of the previous and we will have 4 of these new pieces. So, its length at each new step will increase 4/3 in relation with the previous step.

This construction rule identifies the figure, not its formula as is common on the case of Euclidean forms. This curve has the same shape independence of the scale of observation (self-similarity). Any little detail, when magnified or "zoomed in", can be seen a copy of itself. At each new stage, the length of the curve will grow 4/3 with relation to the previous length. On the limit, this process yields the von Koch Curve, which will have an infinite length on a finite area of the plane without any intersection. Although its construction is simple, there is no equation to determine all its points.

The occurrence of self-similarity on nature is easily found as illustrated in figure 2.2.

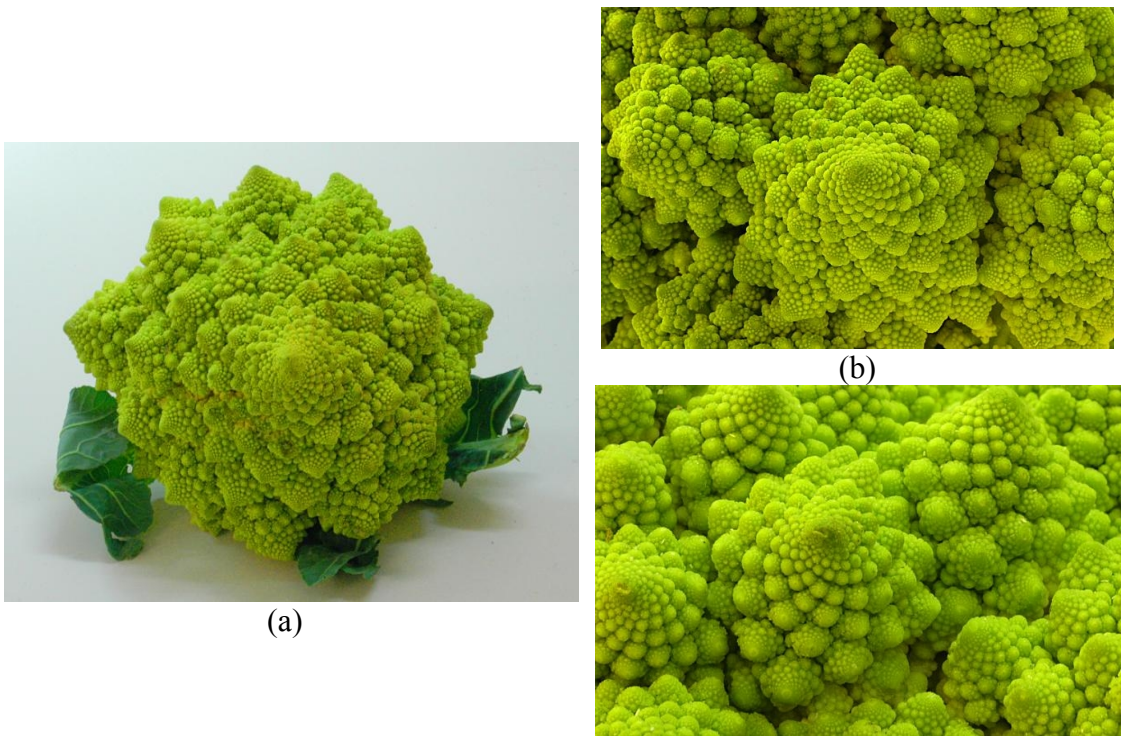

(a) (b) (c)

Figure 2.2. Example of a Romanesco broccoli (WALKER, 2007): a) The whole; b) first zoom; c) a deeper zoom.

The word “Self-similarity” needs no explanation, and at this point it is only an example of a natural structure with that property: a broccoli (figure 2.2). There are many others in nature. The broccoli contains branches or parts, which, when removed and compared with the whole, are very much the same, only smaller. These parts again can be decomposed into smaller parts, which again look very similar to the whole as well as to the first generation branches. After a certain number of stages, the structures became too small for a further dissection. In a mathematical idealization, the self-similarity property of a fractal may be continued through infinitely stages. This leads to new concepts such as Fractal Dimension which are also useful for natural structures that do not have exactly ‘infinite condition’.

2.1 FRACTAL DIMENSION

There are many definitions of Fractal Dimension and, in this section we will see some of them, including: the similarity dimension (D_S) (MANDELBROT, 1977); the Hausdorff dimension (D_H) (GRASSBERGER, 1981 and FALCONER, 1990); the box counting dimension (D_B) (BLOCK et al., 1990); the information dimension (D_I) (FALCONER, 1990; ADDISON, 1997 and WEISSTEIN, 2006); the correlation dimension (D_C) (ADDISON, 1997 and WEISSTEIN, 2006); the pointwise dimension (D_P) (ADDISON, 1997); and the averaged pointwise dimension (D_A) (ADDISON, 1997).

2.1.1 SIMILARITY DIMENSION

One of the most intuitive notions of dimension is associated with scale and self-similarity. A 1D object (of dimension 1), a line for example, if divided in N parts, each part will be equal to the previous one scaled by the factor $d = 1/N$, and $N \times d^1$ will reconstruct the object.

A 2D object (of dimension 2), a square, for example, could be divided in N equal parts, each will be equal to the previous one scaled by $d=\sqrt{1/N}= (1/N)^{0.5}$ and $N \times \delta^2$ reconstructs the object.

A example in 3D, a cube for example, could be divided in N equal parts, each will be equal to the previous one scaled by $d=\sqrt[3]{1/N}= (1/N)^{1/3}$ and $N \times d^3$ reconstructs the object.

The powers of d in each case are the dimensions D of the objects. On fractals, D is fractional. This definition of dimension, denoted by D_S, that is D with the subscript 'S' , is named similarity dimension.

Figure 2.3. Example of line divided in 64 parts. If N=64 → d=1/64 and $N \times d^1$=1.

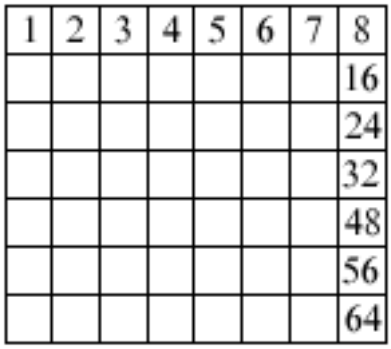

Figure 2.4. Example of square divided in 64 parts. If N=64 → d=1/√64=1/8 and $N \times d^2$=1.

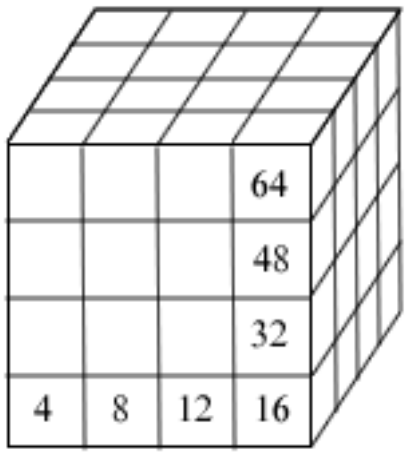

Figure 2.5. Example of cube divided in 64 parts. If N=64 →d=1/$\sqrt[3]{64}$=1/4 and $N \times d^3$=1.

So, the dimension D_S should be (FALCONER, 1990 and WEISSTEIN, 2006):

$$N \times (d)^{D_S} = 1 \qquad (2.1)$$

$$N = \frac{1}{d^{D_S}} = \left(\frac{1}{d}\right)^{D_S} \Rightarrow \log N = D_S \times \log\left(\frac{1}{d}\right) \quad (2.2)$$

$$D_s = \frac{\log N}{\log(1/d)} \quad (2.3)$$

where, N is the number of parts to reconstruct the original figure, and d is the ratio between consecutive steps.

For the von Koch curve (figure 2.1), the original figure is scaled by d=1/3 and 4 parts reconstruct the figure, so N=4, then:

$$D_s = \frac{\log N}{\log 1/\delta} = \frac{\log 4}{\log 3} \cong 1{,}26$$

The same equation 2.3 can be used to calculate the dimension of all fractals that we know the rules of construction and are composed with parts of same proportion. Let's see another example, now on 2D: Sierpinski Carpet (MANDELBROT, 1977) which construction scheme is represented in figure 2.6.

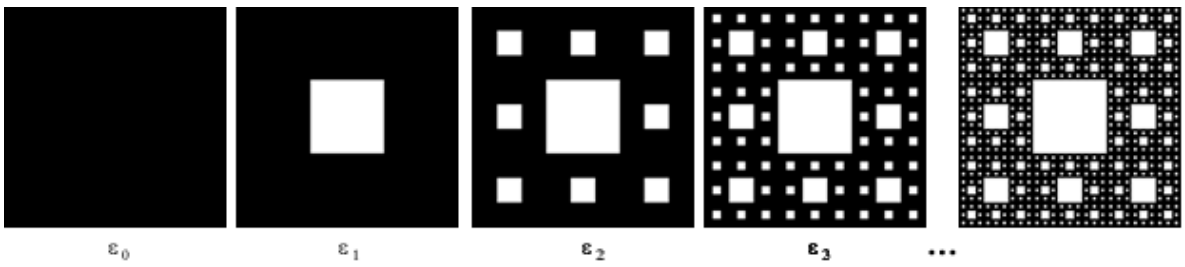

Figure 2.6. Construction of the Sierpinski Carpet. Start with a square and at each stage divide each remaining square into nine equal squares and cut out the middle one.

To divide the square in nine equal squares we use a scale factor of d=1/3. The number of pieces to reconstruct is eight (because we cut out only the middle one), so N=8. Then, the similarity dimension (D_S) of the Sierpinski Carpet (figure 2.6) is:

$$D_s = \frac{\log 8}{\log 3} \cong 1{,}89$$

A fractal dimension for a 3D figure, like a cube, can also be computed using this formula as we see on the next example for the fractal Menger's Sponge (MANDELBROT, 1977), also knew as Sierpinski Sponge, which construction is represented in figure 2.7.

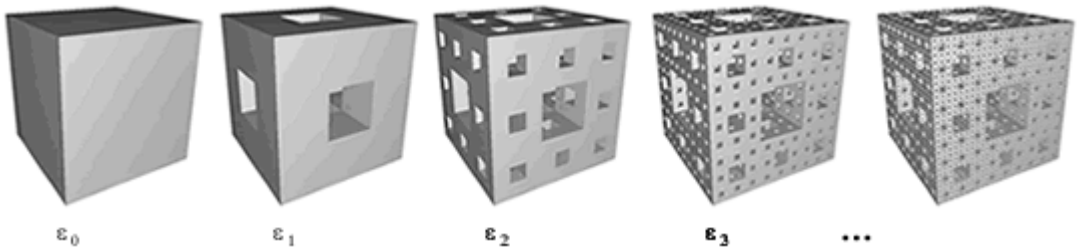

Figure 2.7. Construction of the Menger's sponge. Start with a cube and at each stage divide each remaining cube into twenty seven equal cubes and cut out the central one and all the other six that share faces with it.

This example presents an idea similar to the Sierpisnki Carpet dividing the cubes with a scale factor of d=1/3. But now, the number of pieces to reconstruct is twenty (because we cut out seven pieces: the middle one and other six), so N=20. Then, the dimension of the Menger's Sponge (figure 2.7) is:

$$D_s = \frac{\log 20}{\log 3} \cong 2{,}73$$

Although this way to measure the Fractal Dimension (FD) is extremely simple, it only could be applied when we know the rules of construction of the object (as observed earlier) and all parts have the same relations. This occurs only on the so called determinist fractals, like those showed until now. When more complex objects are under consideration as natural elements like: clouds, trees, neurons, dusts, tissues, wave frequency, color radiation, surfaces of the sea, etc; then we have lots of other ways to measure the fractal dimension experimentally as we will see next.

The FD quantifies the density of fractals or any images on its metric space. The fractal dimensions are then an objective way to compare one fractal (or figure) to another.

The relation:

$$D_s = \frac{\log N}{\log(1/d)}$$

leads to several important methods of estimating the fractal dimension D for a given set S as we present in figure 2.8.

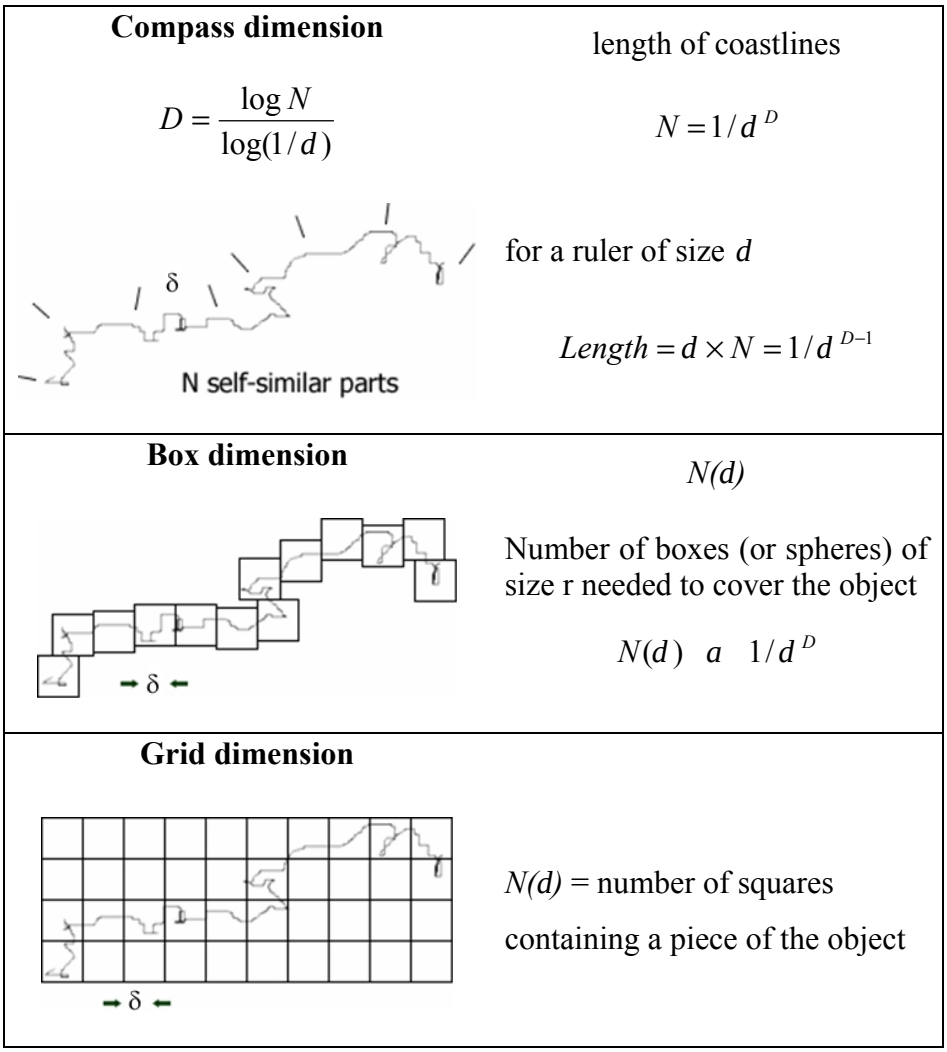

Figure 2.8. Basic techniques for estimating fractal dimension from experimental images (BARNSLEY et al., 1988).

2.1.2 HAUSDORFF DIMENSION

The Hausdorff dimension, D_H, (also called Hausdorff-Besicovitch dimension) is the oldest dimension, among the variety of fractal dimensions in use. It presents the advantage of being defined for any set. It is also mathematically convenient, as it is based on measures, which are relatively easy to manipulate. On the other hand, a problem with this dimension is how to calculate it by computational methods, which is hard in many cases. However, the comprehension of this dimension is essential to understand the mathematics of fractals.

Let U be any non-empty subset of a n-dimensional Euclidean space, $\hat{A}^n$. The diameter of U is defined as $|U|=sup\{|x-y|: x, y \hat{I} U\}$, i.e. the greatest distance between any pair of points in U. Suppose that F is a subset of $\Re^n$ and s is a non-negative number. If $\{U_i\}$

is a countable (or finite) collection of sets of diameter at most d that covers a set F, i.e. $F \subset \bigcup_{i=1}^{\infty} U_i$ with $0 < |U_i| \le d$ for each i, we say that $\{U_i\}$ is a d-cover of F.

For any $d>0$ we define:

$$H_d^s(F) = \inf\left\{\sum_{i=1}^{\infty} |U_i|^s : \{U_i\} \ \ is \ \ a \ \ d-\text{cover} \ \ of \ \ F\right\} \qquad (2.4)$$

Thus, we look at all covers of F by sets of diameter at most d and seek to minimize the sum of the s^{th} powers of the diameters (figure 2.9). As d decreases, the class of permissible covers of F in (2.4) is reduced. Therefore, the infimum $H_d^s(F)$ increases, and so approaches a limit as $d \to 0$. We write

$$H^s(F) = \lim_{d \to 0} H_d^s(F) \qquad (2.5)$$

This limit exists for any subset F of $\hat{A}^n$, though the limiting value can be (and usually is) 0 or ∞. We call $H^s(F)$ the s-dimensional Hausdorff measure of F.

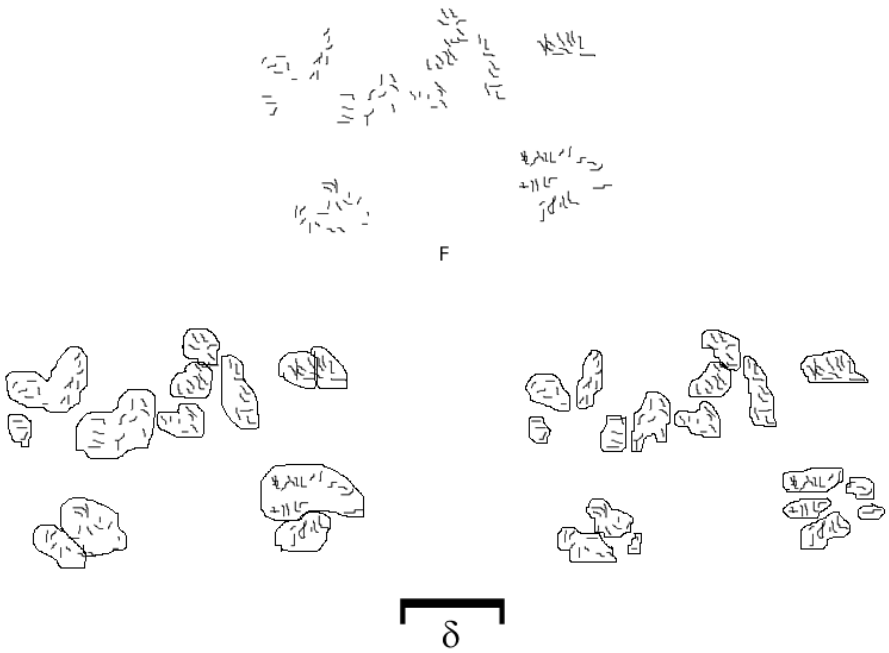

Figure 2.9. A set F and two possible d-covers for F. The infimum of $\sum|U_i|^s$ over all such d-covers $\{U_i\}$ gives $H_d^s(F)$

On the equation 2.4 it is clear that for any given set F and d<1, $H_d^s(F)$ non-increasing with s, so by 2.5 $H^s(F)$ is also non-increasing. In fact, if t>s and $\{U_i\}$ is a d-cover of F we have:

$$\sum_i |U_i|^t = \sum_i |U_i|^{t-s} |U_i|^s \le d^{t-s} \sum_i |U_i|^s \qquad (2.6)$$

So taking the infima, $H_d^t(F) \le d^{t-s} H_d^s(F)$. Letting $d \to 0$ we see that if $H^s(F) < \infty$ then $H^t(F) = 0$ for t>s. A graph of $H^s(F)$ jumps from ∞ to 0 on a value s. The critical value (that is the value of the jump) is called the Hausdorff dimension of F ($D_H(F)$).

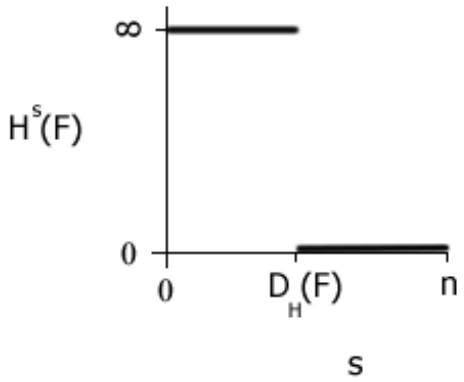

Figure 2.10. Graph of $H^s(F)$ against s for a set F. The Hausdorff dimension is the value of s at which the jump from ∞ to 0 occurs.

Formally (FALCONER, 1990, WEISSTEIN, 2006):

$$D_H(F) = \inf\{s : H^s(F) = 0\} = \sup\{s : H^s(F) = \infty\} \qquad (2.7)$$

so that

$$H^s(F) = \begin{cases} \infty & if \quad s < D_H(F) \\ 0 & if \quad s > D_H(F) \end{cases} \qquad (2.8)$$

If $s = D_H(F)$, the $H^s(F)$ may be zero or infinite, or it presents any finite value that satisfies:

$$0 < H^s(F) < \infty$$

To show how to calculate the D_H of a set, let U denote the Menger's sponge (figure 2.7). This set is constructed from a cube by a sequence of repeatedly removing its middle third volume and other 6. Taking the obvious covering of U by $(20)^n$ cubes of side $(1/3)^n$ we get $H_d^s(U) \leq (20/3^s)^n$ for the *infimum* in equation (2.4). As $n \to \infty$ so $d \to 0$ giving $H^s(U) = lim_{n \to ¥}(20/3^s)^n$ so the D_H of U is $s = ln\ 20 / ln\ 3 = 2.73$. We get an estimate of $H^s(U)$ by presenting an approximation of this set to the DBC-Differential-Box Counting (SARKAR and CHAUDHURI, 1994) or to the MDBC-Modified Differential-Box Counting (CONCI and PROENÇA, 1998). We consider an approximation of Menger's sponge with 729x729 pixels and 729 total gray levels (that is a box with 729x729x729 space-intensity cells). Then DBC or MDBC algorithms present the results in table 2.1. Where N_r is the union of non-overlapping blanked (surface and thickness) boxes that intersect the set U on resolution r. Both algorithms consider $N_r = å\ n_r(i,j)$, where $n_r(i,j) = u_r - b_r + 1$; u_r and b_r are related with (blanket idea) the maximum and minimum gray level of the image in the grid (i,j) on box resolution r (figure 2.11) (CONCI and MONTEIRO, 2000).

r	pixels in box	$\|U\|=1/(3^r)^p$	$N_r(U)=20^r$	$N_r(U)\ \|U\|$
1	243x243x243	1/3	20	20/3
2	81x81x81	1/9	400	$(20/3)^2$
3	27x27x27	1/27	8000	$(20/3)^3$
4	9x9x9	1/81	160000	$(20/3)^4$
5	3x3x3	1/243	3200000	$(20/3)^5$

Table 2.1. Fractal dimension approximation of Menger's sponge.

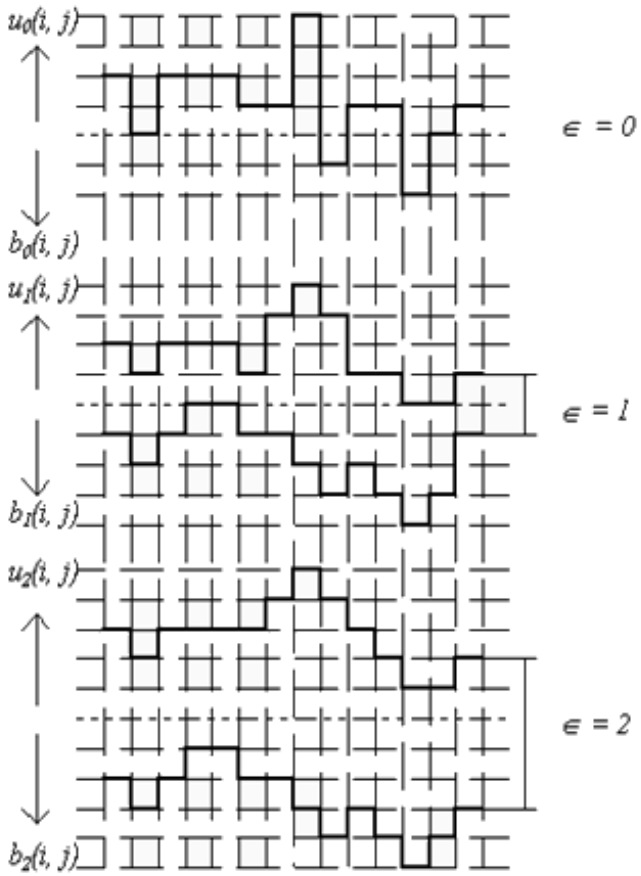

Figure 2.11. The blanket method idea (thickness).

2.1.3 BOX COUNTING DIMENSION

This is the approach used to calculate the fractal dimension that is used on sections 4.2 and 5.2.

To examine an object to compute its box counting dimension we cover the object with elements or 'boxes' of side length d. The number of boxes, N, required to cover the object is related to d through its box counting dimension, D_B. The method for determining D_B is illustrated in the example of figure 2.12, where a straight line (a one-dimensional object) of unit length is covered by cubes (3D objects) of side length d. We require N cubes (volume d^3) to cover the line. If squares of side length d (area d^2) or line segments (length d^1) are used, we would again have required N of them to cover the line. Equally, we could also have used 4D, 5D, or 6D elements to cover the line segment and still required just N of them (FALCONER, 1990). In fact, to cover the unit line segment, we may use any elements with dimension greater than or equal to the dimension of the line

itself, namely one. For simplicity, the line in figure 2.12 is specified as exactly one unit in length. The number of cubes, squares or line segments required to cover this line is then Nd (= 1), hence $N = 1/d^1$.

$$D_B = \lim_{d \to 0} \left[\frac{\log(N)}{\log(1/d)} \right] \qquad (2.9)$$

Note that the exponent of d remains equal to one regardless of the dimension of the probable elements, and it is in fact the box counting dimension, D_B, of the object under investigation. Note also that for the unit (straight) line $D_E = D_B = D_T$ (= 1), hence it is not a real fractal, as the fractal dimension, here given by D_B, does not exceed the topological dimension, D_T. D_E is the Euclidean dimension (MANDELBROT, 1977).

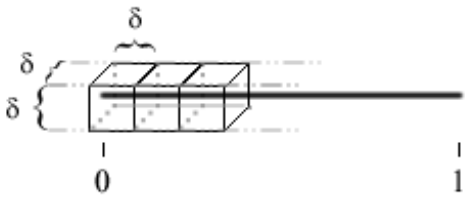

Figure 2.12. Considering a unit line (1D) using boxes/cubes (3D). Number of cubes required to cover the line: *N=1/d*.

As an experimental example of measuring the box counting dimension, consider the set F in figure 2.13. To measure it, we put this set onto a regular mesh with grid size d, and simply count the number of grid boxes which contain some of the set. This gives a number, say $N(d)$, because as we could see by the two examples, this value depends of d. Then we progressively change δ to smaller sizes and count the corresponding $N(d)$. Next we plot the measurements in a graph *log(N(d)) by log(1/d)*. We then fit a straight line to the plotted points of the graph and measure its slope D_B. This number is the box counting dimension. All of this process is illustrated in figure 2.13 where we use two measurements to find a slope, which is approximately D_B=1,25.

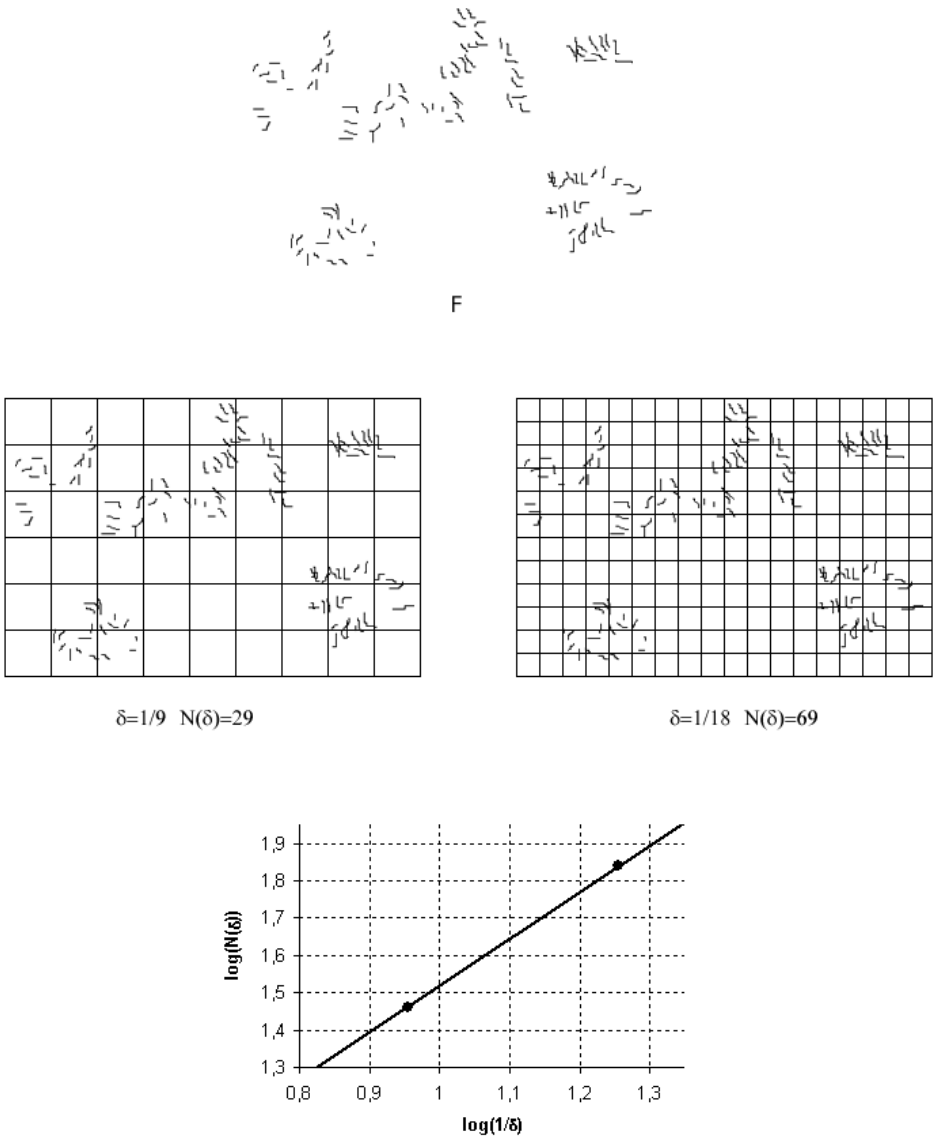

Figure 2.13. The set F is box-counted using two grids. The slope of the line is log(69/29)/log2≈1,25 (FALCONER, 1990).

It is easy to note that in the plane a box counting dimension (D_B) will never exceed 2. The self similarity dimension (D_S), however, can easily exceed 2 for a curve in the plane. For that, we only have to construct an example where the scale of the original figure (d) is equal to 1/2 and the number of parts to reconstruct is equal to $N(d)>4$. Then:

$$D_s = \frac{\log \mathrm{N}(d)}{\log(1/d)} > 2$$

This is because a curve generated with this rules of construction will have overlapping parts, which, by principle, are counted only once in the box counting method (which happens due to the impossibility of representation of this concept on images

because parts that match over other, on the same pixel, are counted only once), but with corresponding multiplicities in the computation of the self similarity dimension. An example of self similarity dimension in a plane with *N(d)*=5 and *d*=1/2 will result

$$D_s = \frac{\log(5)}{\log(2)} \approx 2{,}32$$

An example of a fractal with similarity dimension exceeding 2 is in figure 2.14, where we starts with a line; divide using $d = 4$ as factor; an use *N(d)*=18 to reconstruct the step; the process is repeated over and over for all remaining lines. The similarity dimension of this example is:

$$D_s = \frac{\log(18)}{\log(4)} \approx 2{,}08$$

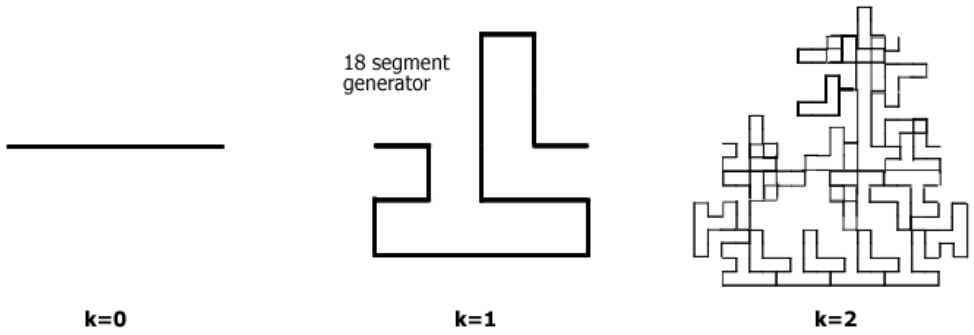

Figure 2.14. Three first steps of generation of a fractal in a plane with similarity dimension greater than two.

The box counting dimension is the most used one in all sciences. The reason for its dominance lies in the easy and automatic computability by machine. It is straightforward to count boxes and to maintain statistics allowing dimension calculation. The program can be carried out for shapes with and without self similarity. Moreover, the objects may be embedded in higher dimension spaces. For example, when considering objects in common three-dimensional space, the boxes are not flat but real three dimensional boxes with height, width and depth. But the concept also applies to fractals such as the Cantor set (figure 2.15) which is a subset of the unit interval, in which case the boxes are small intervals.

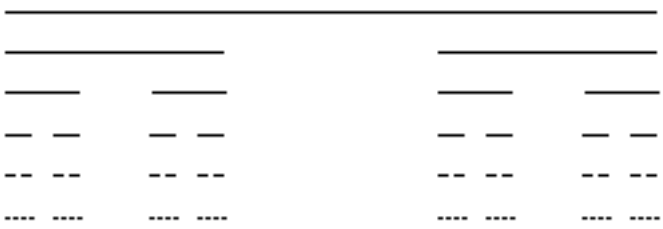

Figure 2.15. Cantor Set or Cantor Dust starts with a line segment of unit length. Recursively remove the middle thirds of the segments at each step.

2.1.4 INFORMATION DIMENSION

Another way to estimate the dimension is called the information dimension (D_I). The idea is similar to the box counting dimension. The set is also covered with cubes of side length d. But this measure takes into account how much of the set is contained within each cube instead of simply counting the cubes (FALCONER, 1990; ADDISON, 1997 and WEISSTEIN, 2006).

$$D_I = \lim_{d \to 0} \left[\frac{I(d)}{\log(1/d)} \right] \qquad (2.10)$$

Where $I(d)$ is given by Shannon's entropy formula:

$$I(d) = -\sum_{i=1}^{N} P_i \log(P_i) \qquad (2.11)$$

where P_i is the probability of part of the set occurring within the i^{th} cube of side length d. For a special case of a set with an even distribution of points, an identical probability, $P_i=1/N$, is associated with every box. Hence, $I(d)=\log(N)$, and the equation 2.10 reduces to the box counting dimension equation (2.9). Thus, D_B simply counts all cubes containing parts of the set, while D_I measure how much of the set is within each cube.

2.1.5 CORRELATION DIMENSION

An alternative to estimate the dimension that requires less computation time is the correlation dimension (D_C). To define D_C is necessary that we first define the correlation sum C_r, as follows (ADDISON, 1997 and WEISSTEIN, 2006):

$$C_r = \frac{1}{N(N-1)} \sum_{i=1}^{N} \sum_{j=1; j \neq i}^{N} q\left(r - \left|X_i - X_j\right|\right) \qquad (2.12)$$

where q is the Heaviside function, r is the radius of an n-dimensional sphere centered on each sampled point on the trajectory of the set, X_i, $i=1,2,3,...,N$. X_i denotes the multidimensional vector that is the i^{th} phase space coordinate of the set, i.e. for a set in 3D phase space with coordinates x, y and z, $X_i=(x_i,y_i,z_i)$. The Heaviside function counts the number of points of the set within the sphere centered on one point (that is not counted).

For a system of n first-order ordinary differential equations, the 2 n-dimensional space consisting of the possible values of ($x_1, \dot{x}_1, x_2, \dot{x}_2, ..., x_n, \dot{x}_n$) is known as its phase space (WEISSTEIN, 2006).

The Heaviside function is equal to the unity if the value inside the brackets is positive and zero if the value is negative. X_i are the points on the reference trajectory and X_j are other points on the attractor in the vicinity of X_i. $|X_i - X_j|$ is the separation distance between the two points. $q\left(r - \left|X_i - X_j\right|\right)$ return a value of unity if the distance between the two points is less than the sphere radius; otherwise a zero value is returned.

"An attractor is a set of states (points in the phase space), invariant under the dynamics, towards which neighboring states in a given basin of attraction asymptotically approach in the course of dynamic evolution. An attractor is defined as the smallest unit which cannot be itself decomposed into two or more attractors with distinct basins of attraction.

Basin of Attraction is the set of points in the space of system variables such that initial conditions chosen in this set dynamically evolve to a particular attractor" (WEISSTEIN, 2006).

The calculation of the correlation sum of equation (2.12) involves following the reference trajectory, stopping at each discrete point on this trajectory and counting the number of other set points within a sphere of radius r. The cumulative sum of all the counted points is then divided by $N(N-1)$ to give the correlation sum, C_r. The maximum value of C_r is unity.

The correlation sum scales with the sphere radius according to a power law of the form:

$$C_r \quad a \quad r^{D_C} \qquad (2.13)$$

where the exponent (D_C) is the correlation dimension. Examining the set in the method described for many different sphere radii, D_C is obtained from the slope of the scaling region of a $log(r)$ x $log(C_r)$ plot as shown in figure 2.16. In general, good estimates of D_C require large number of data points, N; however, the computational time required to calculate C_r increases with N^2.

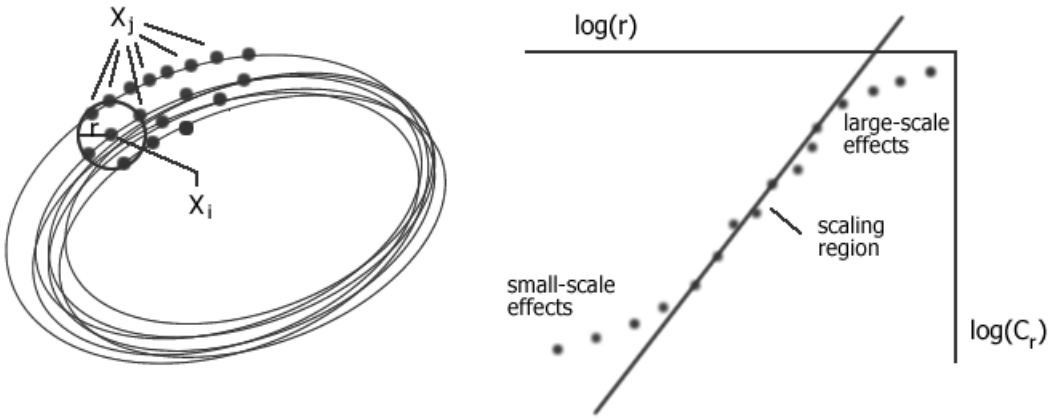

Figure 2.16. Determining the correlation dimension: (a) Probing sphere on the set. (b) The *log(r) x log(C_r)* plot.

The correlation dimension, information dimension and box counting dimension are related. In fact, they are part of a generalized collection of dimensions, known as Renyi dimensions (BADII and POLITI, 1987). It can be shown that D_C forms a lower bound to D_I which in turn forms a lower bound to D_B,

$$D_C \leq D_I \leq D_B \qquad (2.14)$$

In addition, D_C and D_I asymptotically approach the value of D_B as the attracting set becomes more uniformly distributed in phase space. If the points on the attractor are uniformly distributed, then $D_C = D_I = D_B$. In many practical cases D_C gives a very close estimate of D_B.

2.1.6 POINTWISE AND AVERAGED POINTWISE DIMENSION

Another dimension estimator, closely related to the correlation dimension described above, is the pointwise dimension, D_p (ADDISON, 1997). Rather than looking at the scaling properties of the set as a whole, we turn our attention to localized scaling of the set at a specific point on the set, say at point X_i. To do this we count only the number of neighboring points, P_r, contained within the sphere at this location over a range of radii, r, more formally,

$$P_r = \frac{1}{(N-1)} \sum_{j=1; j\neq i}^{N} q\left(r - \left|X_i - X_j\right|\right) \qquad (2.15)$$

P_r has a power law dependence on the radius r, given by

$$P_r \quad a \quad r^{D_p} \qquad (2.16)$$

where the exponent, D_p, is the point wise dimension. D_p may be computed at a specific location (point) on the set from a *log(r) x log(P_r)* curve in a manner analogous to the correlation dimension. The point wise dimension is a localized dimension estimate and in practice may vary over the entire set. To this end, an averaged point wise dimension, D_A (ADDISON, 1997), may be defined as

$$D_A = \frac{1}{N} \sum_{i=1}^{N} D_p \qquad (2.17)$$

Although it has been suggested by some authors that this dimension estimate, D_A, is preferable to D_C as a measure of the average fractal properties of strange attractors, the correlation dimension is more popular due to its computational speed and the wealth of background literature on its use.

2.2 LACUNARITY

When talking about fractals a intuitive definition about Lacunarity is that a fractal is to be called *lacunar* if its gaps tend to be large, in the sense that they include large intervals (discs, or balls) (MANDELBROT, 1977). Lacunarity is a counterpart to the fractal dimension that can improve the texture description of a fractal. It has to do with the size distribution of the holes. Roughly speaking, if a fractal has large gaps or holes, it has high Lacunarity; on the other hand, if a fractal is almost translational invariant, it has low Lacunarity. Different fractals can be constructed that present the same dimension but that look very different because they have different Lacunarity. There are applications of Lacunarity in image processing, ecology, medicine, and other fields (RAUCH, 2007).

A low Lacunarity, generally, indicates homogeneity, while high Lacunarity indicates heterogeneity. The higher the Lacunarity, the bigger will be the variation of pixels distribution in an image. In other words, high Lacunarity means that pixels are grouped in a wide variety of sizes of island, surrounded by a widely variant emptiness, indicating heterogeneity of spatial pattern or texture (BARROS FILHO and SOBREIRA, 2005).

The approach presented on the next section to calculate the local Lacunarity is based on the gliding box algorithm, used to analyze the mass distribution on one-dimensional generalized Cantor sets (ALLAIN and CLOITRE, 1991).

It considers a box of side s, which glides in the object on all possible manners, computing the mass distribution, used for the Lacunarity measure. The notion of location is added to make it possible to distinguish among different parts of the same set. Figure 2.17 shows a fractal used on the tests in this section.

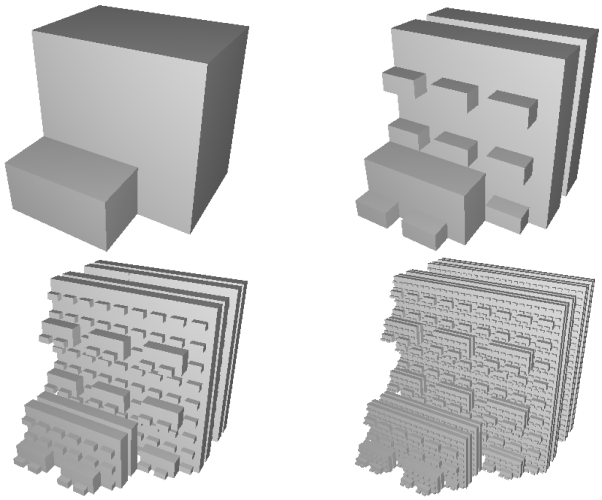

Figure 2.17. Initial steps of the reproduction of a fractal object made as figure 2.7 of 20 parts each one scaled by 1/3, but grouped without gap. In this object the seven eliminated pieces are all on the same face where only two consecutive pieces kept their positions.

The proposition to compute Local Lacunarity (LL) consists in the following steps (MELO et al., 2006):

1 - Objects are first adjusted to a bounding box (BB) (see example in figure 2.18). The size of this box is a function of the object's size: *S*, in a specific resolution.

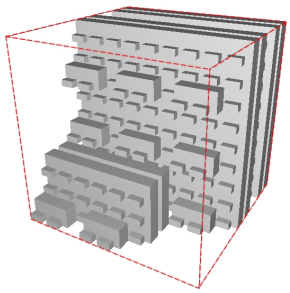

Figure 2.18. In dashed, the example of a bounding box (BB) for the third image in figure 2.17.

2- The gliding box method is used to get the mass probabilities for the BB in all possible combination of parameters: gliding box size, *s*, object resolution, *r*, and size, *S*, thresholds levels, *t*, and position *(i,j)*. Note that the gliding boxes may overlap.

3- The probability obtained as a function of all parameters is used to define the Lacunarity associated with the local parameters of the object or image.

In step 1, if the object is an image, then it is equalized, to compensate for possible differences in acquisition conditions before the beginning of Local Lacunarity (LL) computation. Colour and grey scale information are important aspects on texture (CONCI and CASTRO, 2002) and must be considered if available. Lacunarity can be computed on 2D grey-scaled images by: (1) threshold on a specific level to convert it to binary images or (2) the third coordinate can be used and the images can be seen as collection of voxels. In a specific resolution, each voxel can only be considered as empty or full. It is important to stress that the term "local" for Lacunarity is related to the BB position, *(i,j)*, on the original image and to the BB resolution, *r*, but mainly to the threshold mass or grey value, *t*.

In the step 2, the incremental analysis of each parameter is associated with the gliding box procedure. In this procedure the first voxel of an *s x s x s* voxels gliding box is initially placed on the corner at first voxel of the images. The computation is performed and then the first voxel of the box is positioned at the second voxel of the images and so on until it reaches the last possible position. Name *N* this last possible position. The box of *s x s x s* voxels glides over the entire image, registering each time, the number *I* of non void voxels related to that resolution, and its side, s. As s^3 is the maximum possible number of voxels, for the box side *s*, the sequences of the number of non void voxels, $\{n_i\}$, $i \in \{1,2,....N\}$ can be organized to define the frequency of boxes of size s, with mass *M*: *n(M, s)*. For 3D objects, the total number of boxes of size *s*, *N(s)*, is also a function of the size of the object, *S*, that is:

$$N(s) = (S - s + 1)^3 \qquad (2.18)$$

The frequency distribution of boxes of size s voxels with mass *M*, *n(M, s)*, defines a probability function *Q(M,s)* by dividing it by the total number of boxes:

$$Q(M, s) = \frac{n(M, s)}{N(s)} \qquad (2.19)$$

where Q(M,s) represents the probability that a gliding box (GB), with side s voxels, contains M non void voxels. In other words, it is easy to show that *Q(M, s)* satisfies all the axioms of probability (PAPOULIS, 1965). Local Lacunarity (for box side *s*) is defined as the ratio between the second moment and the first moment squared:

$$\Lambda(s) = \frac{\sum_{i=1}^{N} M^2 Q(M,s)}{\left(\sum_{i=1}^{N} MQ(M,s)\right)^2} \qquad (2.20)$$

When considering all GB positions, (i,j,k), resolution, r, and possible threshold values, t, it is clear that the above expression is not only a function of the box side s, but related to a set of parameters ($L_{i,j,k}(r,t,s)$). Lacunarity is a function of the postion *(i,j,k)* for each GB (Local Lacunarity), the global result is only a function of *(r,t,s)*. Although this method is easily implemented in section 2.2.1, we here consider some manual results in order to promptly interpret some aspects, resulting of this measure, that can be useful in many recognition applications. Highest value for a given image will always be found for a gliding box with size of one voxel, i.e. *s*=1. However, this computation need not be performed since at s=1, *Q(1,1)* represents the occupied ratio and $\Lambda(1)$ is the inverse of this value. This value is: (i) only a function of the percentage of occupied sites; (ii) independent of the overall size of the image; and (iii) not related with details of the distribution. Local Lacunarity then must be computed by equation (2.20) for box side s ranging from 2 to r (or to a representative value).

Differently from objects, 2D grey level images present no gaps, unless some thresholds are performed over these images. Once using digital images it is possible to identify constrains related to the limits of resolution. These limits are related in the lower bound to the pixel or voxel and in the upper bound to the image resolution, r, in 2D or 3D, that is, the number of pixels (r x r) or voxels (r x r x r) it contains. In other words, in the lower bound, Lacunarity reflects the degree of space occupancy similarly to the FD. On the opposite side, the larger possible value is the entire image and Lacunarity is similarly constrained at this limit.

Considering equation (2.20), if the denominator (mean), goes to zero, the Lacunarity, Λ, goes to ∞. If the box size contains the entire image (s = r), then the variance of the masses in the box is zero and $\Lambda(r)=1$. Although, far from the limits that the values (measuring the texture) are realistic, hence, the above discussion of boundary limitation can be useful (e.g. for algorithm verification or as edge representation on graphical visualization of the results). The average mass increases with the box size, then the probability that box masses greatly differ from the average decreases as relative variance decreases.

Two approaches are proposed here to analyze grayscale images through the described 3D method. The first one, named 3D, considers all possible values for the pixels of the image (from 0 to 255) to the k^{th} position of the BB. The second one, named 3D min-max, considers only the existing values of pixels on the image. The second approach is intensity-invariant. This is useful on applications were this property is of interest. A comparison illustrating this property is shown in figures 2.19, 2.20 and 2.21.

(a) (b)

Figure 2.19. Synthetic images to illustrate the intensity-invariant approach, images with two distinct pixels values: (a) backgroung pixels = 1, foregroung square pixels = 192 named (1,192); (b) backgroung pixels = 51, foregroung square pixels = 242 named (51,242).

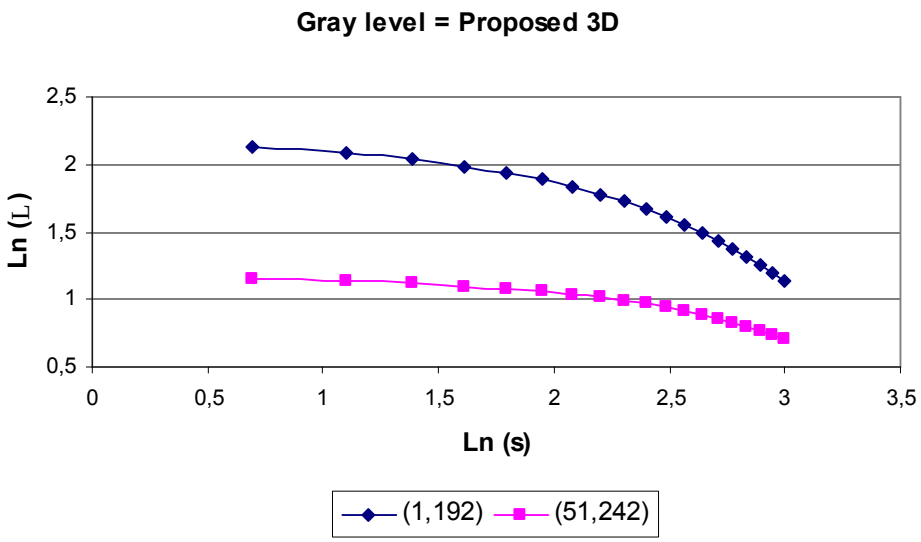

Figure 2.20. Result of the Lacunarity of the proposed method 3D for the input images in figure 2.19.

The only difference on the two images in figure 2.19 is that image on (b) is equal to image on (a) with an increase of 50 on the grey value for all the pixels on the image. After this, we expect to obtain in figure 2.21 the same result for the processing of the two images through the 3D min-max method, which does not happen on the 3D method.

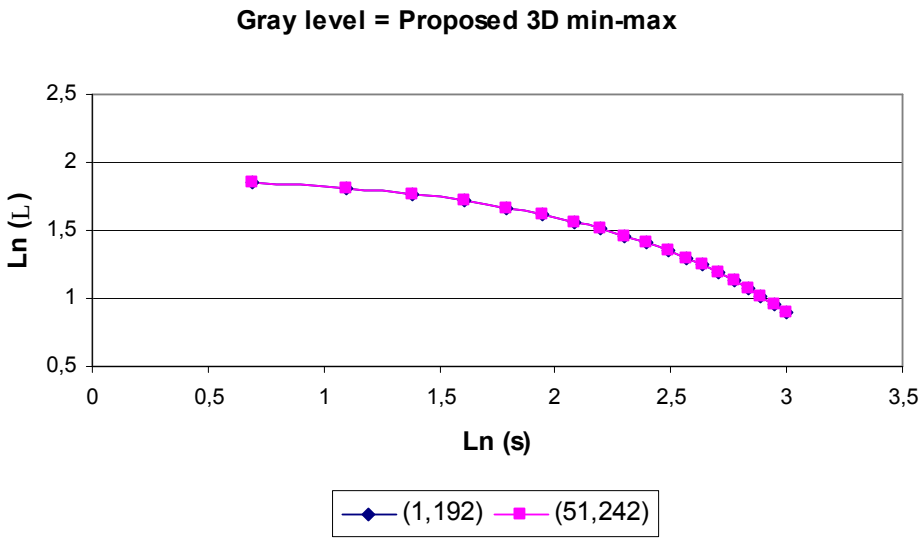

Figure 2.21. Result of the Lacunarity of the proposed method 3D min-max for the input images in figure 2.19.

With the results in figure 2.20 and 2.21, we easily see that, for an application where the changes on illumination are not important or should not be considered (for any reason) is better use the 3D min-max method than the 3D one.

2.2.1 COMPUTING THE MASS DISTRIBUTION (PROPOSED METHOD)

Let us compute the mass distributions for the first object in figure 2.17, suppose it is represented by 3x3x3 boxes. The total number of boxes of size s=2 that can glide inside the object is 8. If the "gliding" process begins from the farthest to the nearest viewer position, the number of occupied voxels n_i is:{8, 8, 6, 5, 8, 8, 4, 4}. Then n(M,s) for s=2 is defined in table 2.2.

From table 2.2 and equation (2.20) we have: $\Lambda(2) \approx 43.625/(6.375)^2 \approx 1.073$. The positional parameters in this computation are not important and the threshold level is obviously at void voxel but the obtained result is related to the used BB resolution of r=3. That is, in fact, $\Lambda(3, 0.5, 2) \approx 1.073$.

Considering the first object in figure 2.7 and supposing that it is represented by 3x3x3 voxels, for s=2, the number of occupied voxels n_i registered for all positions of a gliding box is 4. Then n(M,2)=8 and Q(M,2)=0 for M≠4 and Q(4,2)=1. So we have: $\Lambda(2)$ =1. That is, for the first iteration of this approximation of Sierpinski's Sponge

$\Lambda^1(3,0.5,2)=1$. Other results are $\Lambda^1(81,0.5,2) \approx 1.3449$ and $\Lambda^1(3,0.5,3)=1$ considering both the first iteration on the object construction. For the same object but in another iteration, as the second, third and fourth objects in figure 2.7, we have respectively: $\Lambda^2(81, 0.5, 2) \approx 1.7672$, $\Lambda^3(81, 0.5, 2) \approx 2.1619$ and $\Lambda^4(81, 0.5, 2) \approx 2.1577$.

mass: $_i$	frequency $n(M_i,s)$	Probabiblity $Q(M_i,s)$	$M_iQ(M_i,s)$	$M_i^2Q(M_i,s)$
0	0	0	0	0
1	0	0	0	0
2	0	0	0	0
3	0	0	0	0
4	2	0.25	1	4
5	1	0.125	0.625	3.125
6	1	0.125	0.75	0
7	0	0	0	4.5
8	4	0.5	4	32
Σ	8	1	6.375	43.625

Table 2.2. Lacunarity computation for iteration 1 of figure 2.17 represented with 9 voxels, considering gliding box with s=2.

Then, an additional point is that, for real fractals, as these in figures 2.7 and 2.17, the LL results change with the iteration. For the same object, but in other iteration, as the second, third and fourth object in these figures we have the values that can be seen on the graph in figure 2.20 and 2.21. Note: LL is a function of one more parameter, here represented by the index *I*: $L^I_{i,j}(r,t,s)$.

Figures 2.20 and 2.21 show the results for all possible parameters of the objects in figures 2.7 and 2.17, that is $\Lambda^I(r , 0.5, s)$ for r=9,27,81; s = 2,3,4, ...,80,81 and I=1,2,3. The entire object is considered, so positional parameters (i,j) are irrelevant.

It is interesting to note that all the objects in figures 2.7 and 2.17 will be real fractals only if the generation goes to infinity. As it is impossible for representation of digital objects or images, they are, mathematically, only approximations of real fractal objects. Its constructions are limited by the voxel, limit that is digitally or physically the lower limit of representation.

Figure 2.7 - step 1

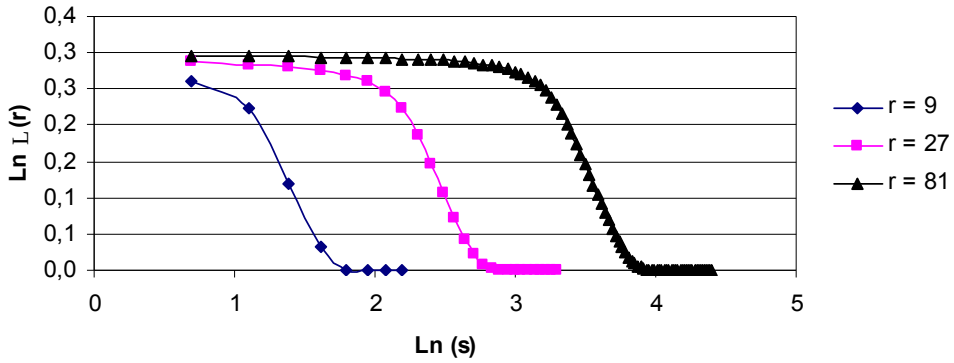

Figure 2.7 - step 2

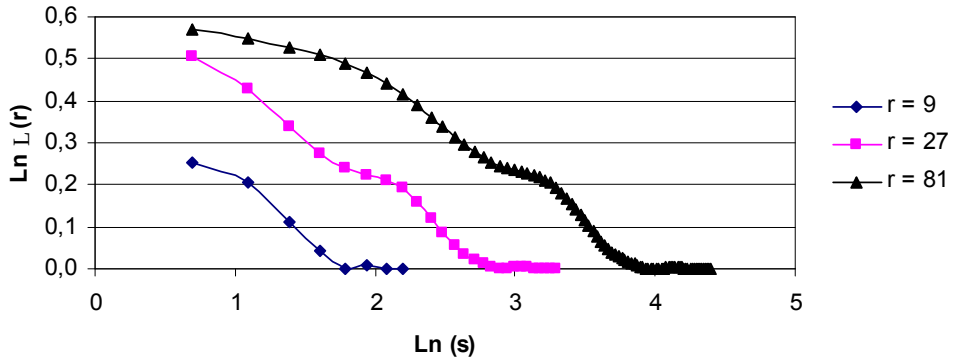

Figure 2.7 - step 3

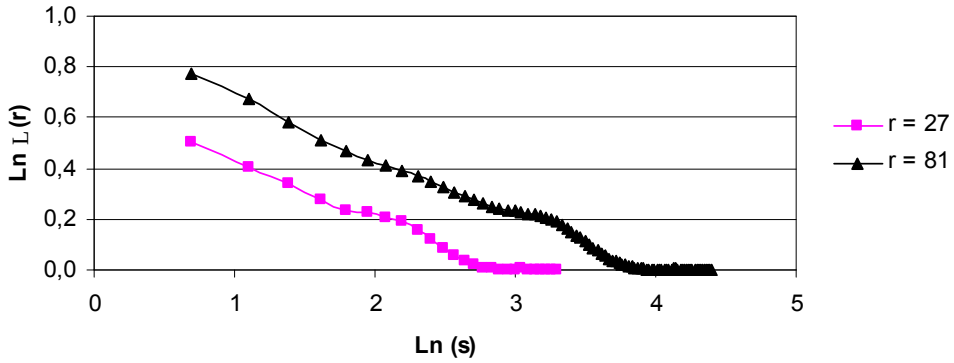

Figure 2.22. Ln x ln plot of Lacunarity versus box size for object of figure 2.7 from the first to the third step. Objects are described at resolution of 9, 27 and 81 voxels.

Figure 2.15 - step 1

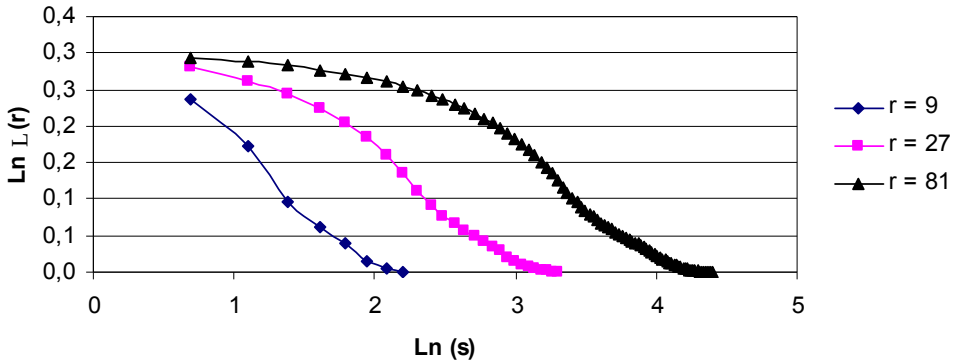

Figure 2.15 - step 2

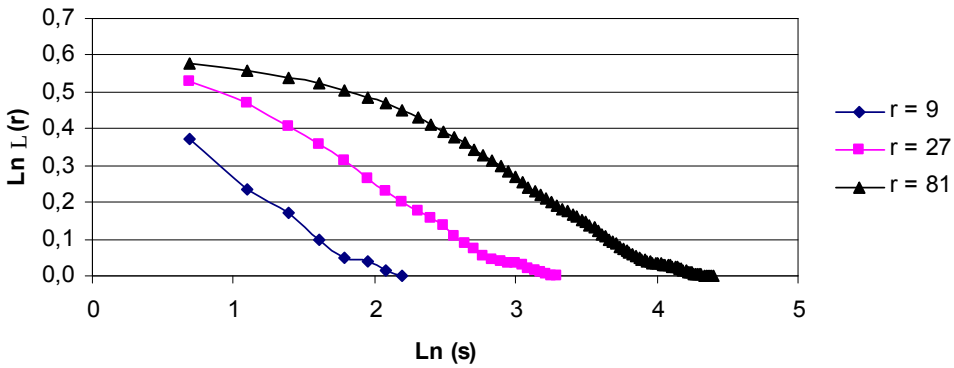

Figure 2.15 - step 3

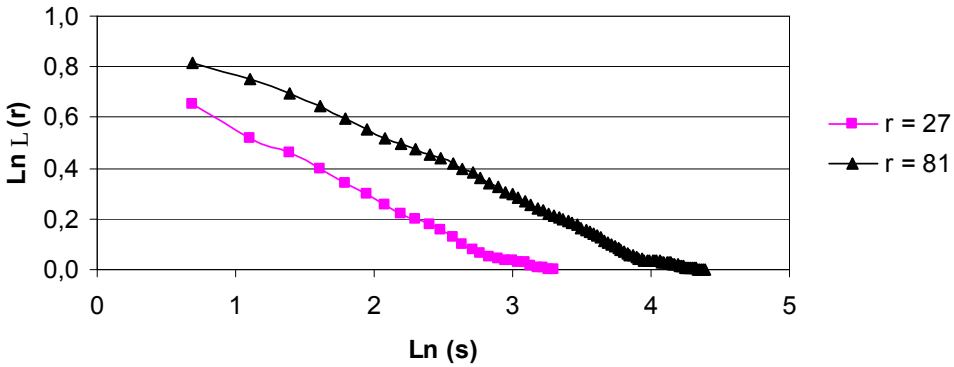

Figure 2.23. Ln x ln plot of Lacunarity versus box size for object of figure 2.17 from the first to the third step when described at resolution of 9, 27 and 81 voxels.

2.2.2 GAN DU PROPOSAL FOR GRAYSCALE IMAGES

The Gan Du proposal to grayscale images (GAN DU and TAT SOON YEO, 2002) is presented here. This method was introduced as an extension to the method previously proposed by Dong (DONG, 2000).

For each *sxs* gliding box, *n(i,j)* is counted differently from the method in (DONG, 2000): let the maximum and minimum pixel values be *g(i,j)* and *b(i,j)*, respectively; then:

$$n(i,j) = g(i,j) - b(i,j) \qquad (2.21)$$

is the contribution of M in the *(i,j)th* gliding box. Taking contribution from all gliding boxes, we have:

$$M = \sum_{i,j} ceil\left[\frac{kn(i,j)}{s}\right] \qquad (2.22)$$

where *k* is the coefficient of z coordinate modification, which is expressed as $k = W/g$, and *g* is the maximum pixel values within the *WxW* window. The *W* here stands for the dimension of the image, the same as the object size, *S*, for the previous section. *Ceil[x]* stands for the ceiling of x (the smallest integral value that is not less than x). Define *n(M,s)* to be the number of gliding boxes with size *s* and mass *M*. It is converted into the probability function *Q(M,s)* by dividing by the total number of boxes:

$$Q(M,r) = \frac{n(M,s)}{(W-s+1)^2} \qquad (2.23)$$

The Lacunarity at scale *s* is defined by the equation 2.20.

2.2.3 FERNANDES PROPOSAL FOR GRAYSCALE IMAGES

The Fernades proposal (FERNANDES and CONCI, 2004a) to grayscale images could be seen as the simplest extension to the binary approach proposed by Alain and Cloitre (ALLAIN and CLOITRE, 1991). This work has not been published yet, but, as it presents another approach to calculate the Lacunarity of grayscale images, we include here

the definition and shown, on the results, the comparison over the other methods described in this section.

In this approach, the mass, *M*, of each *sxs* gliding box, is calculated as the sum of all the gray values of the pixels values on the *(i,j)th* box:

$$M = \sum_{m,n} gray\_value(image(m,n)) \qquad (2.24)$$

This is done for each size *s* in the set of all possible sizes of boxes on an image with size *S*. The probability function *Q(M,s)* is defined as for the previous method (equation 2.23), with *W* equal to the image size *S*. The Lacunarity at scale *s* is also defined by equation 2.20.

2.3 SUCCOLARITY THEORY

Mandelbrot, 1977 defines the Succolarity of a fractal considering that a *succolating* fractal is one that "nearly" includes the filaments that would have allowed percolation; since *percolare* means "to flow through", *succolare* (sub-colare) seems the proper term for "to almost flow through". However, Mandelbrot does not present measures of Succolarity in his book. An approach to compute it is the main discussions of this work.

In mathematics, percolation theory describes the behavior of connected clusters in a random graph. Assume that we have some porous material and we put some liquid on top. The question is: Will the liquid be able to make its way from gap to gap and reach the bottom? (WIKIPEDIA, 2007).

In chemistry and materials science, percolation concerns the movement or filtering of fluids through porous materials. In engineering, it refers to the slow flow of fluids through porous media, but in the mathematics and physics domains it generally refers to simplified regular or random lattice models of random systems, and the nature of the connectivity on them. An important different model of percolation, in a diverse class altogether, is directed percolation, where connectivity along a limit depends upon the direction of the flow (WIKIPEDIA, 2007).

3 CALCULATING SUCCOLARITY

In this section, we present an approach to measure Succolarity. To explain the computation proposal for Succolarity, a very simple binary image is used as an input example of these calculations. First of all, if the image is not binary, a good threshold must be chosen by any automatic method. On this work (as will be explained in the section of results with real images) this step was chosen by heuristic trials.

The Succolarity measures the percolation degree of an image (how much a given fluid can flow through this image). To obtain this, we simulate the draining or percolation capacity of a fluid through the image. From the image to be analyzed (figure 3.1) we obtain, depending on the directions to be considered (figure 3.2), two or more images (figure 3.3). On the example in figures 3.1 to 3.3, four images were obtained, the original image was analyzed horizontally (left to right and right to left) and vertically (top to bottom and bottom to top). Other directions can be applied to the method to generate different images.

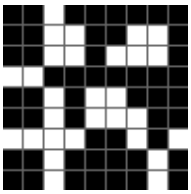

Figure 3.1. Original image (9x9 pixels) to demonstrate the Succolarity.

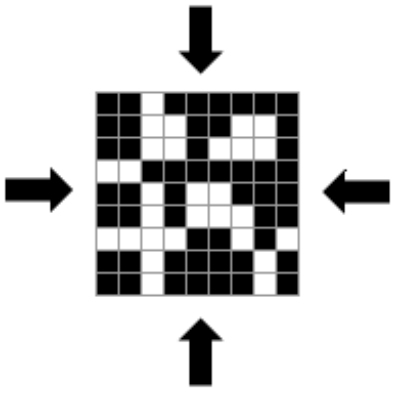

Figure 3.2. Example of four directions that a fluid can try to flood the image.

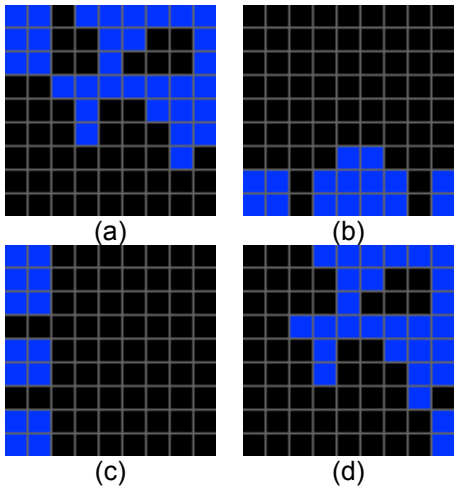

Figure 3.3. Images obtained after the first step of the Succolarity. In blue, the pixels of the flood area; directions: (a) Top to bottom (t2b); (b) Bottom to top (b2t); (c) Left to right (l2r); (d) Right to left (r2l).

The idea of pressure applied to a box is demonstrated in figure 3.4. The pressure grows from left to right on the horizontal case (directions: Letf to right (l2r); and right to left (r2l)) and from top to bottom on the vertical case (directions: Top to bottom (t2b); and bottom to top (b2t)) as can be seen on the figure.

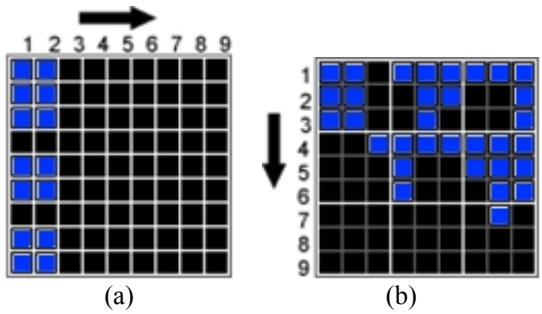

Figure 3.4. Indication of the order of pressure over the boxes: (a) Example of pressure over 1x1 boxes for figure 3.3 (c); (b) Example of pressure over 3x3 boxes for figure 3.3 (a)

3.1 DESCRIBING THE METHOD THROUGH STEP BY STEP ANALYSIS OF AN IMAGE

The method to calculate Succolarity can be described by the four next steps explained:

1 - Coming from the top of the original binary, image all the boundary pixels are considered. If the pixel is empty on the image (in our case we consider black as the absence in the pixel position), it means that a fluild can pass and flood this area. The

existing material pixels (white on the example) are considered as obstacles to the fluid. All the flood areas from a boundary have their neighbors (4 neighbors for each pixels: Top; Bottom; Left and Right) considered on the next step and this process is recursively executed.

2 - The next step is then to divide these flood area of each image (figure 3.3) in equal box sizes (*BS(n)*, where *n* is the number of possible divisions of an image in boxes) like the box counting method. After that the occupation percentage (*OP*) is measured in each box size of each image.

3 - For each box size, *k*, then the sum of the multiplications of the *OP(BS(k)),* where *k* is a number from 1 to *n*, by the pressure *PR(BS(k),pc)*, where *pc* is the position on x or y of the centroid of the box on the scale of pressure) applied to the box are calculated. The pressure varies with the box size because it is applied on the centroid of the box. It also depends on the position of the box to correctly indicate the amount of pressure over it.

The pressure (figure 3.4) is over the centroid of the box, on the horizontal case the *x* position of the centroid while on the vertical case the *y* position is considered.

4 - To make the Succolarity value dimensionless like FD and Lacunarity we divide the value, obtained in equation 3.1, by *PR*, but now considering that the image was totally flooded by the fluid (as if the input image were totally black). The calculation is indicated by the equation 3.1.

$$s\,(BS(k), direction) = \frac{\sum_{k=1}^{n} OP(BS(k)) \times PR(BS(k), pc)}{\sum_{k=1}^{n} PR(BS(k), pc)} \qquad (3.1)$$

There are two ways to divide the image of figure 1 in equal sized boxes. With a dividing factor, *d*, of 9 obtaining boxes of 1x1 pixels and by *d* = 3 obtaining boxes of 3x3 pixels (only considering integer divisions and without considering the dividing factor of 1 of course). These two examples are in figure 3.5.

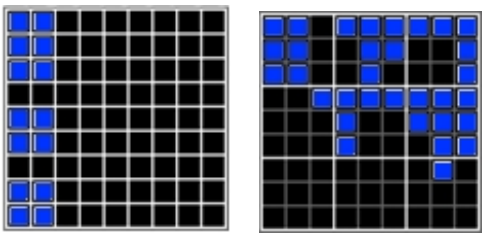

(a) (b)

Figure 3.5. Dividing the intermediate images of figure 3.3 in boxes of two different sizes: (a) Figure 3.3 (c) with d =9, producing boxes of size 1x1 pixels; (b) Figure 3.3 (d) with d = 3, producing boxes of 3x3.

The same method could be applied on 3D images or objects considering 3D boxes to measure the Succolarity values. A synthetic 3D image is used in section 3.3.1 to illustrate numerically this computation.

3.2 EXAMPLE OF THE CALCULUS OF SUCCOLARITY

This section computes, step by step, the results of two directions of the Succolarity for the image considered as input on previous section.

3.2.1 BOX SIZE EQUAL TO 1 PIXEL – DIRECTION LEFT TO RIGHT

On figure 3.5 (a), each box corresponds to a pixel, the occupation percentage then could be only 0 (pixel without fluid) or 100% (pixel with fluid). On this figure we can easily note that 14 boxes have 100% of occupation and the others 67 boxes have 0%. The x positions of the centroid are the same for all of the boxes on the same column in the case of the horizontal percolation (the same occurs with the lines on the vertical percolation). The x value of the centroid is then 0.5 for the boxes on the first column and 1.5 for the second (considering the pressure distribution like the figure 3.4 (a)). Figure 3.5 (a) presents 7 boxes on the first column and 7 more on the second. We have then using the numerator of equation (3.1) obtained the results 7x0.5+7x1.5=14. To compute the Succolarity we then divide this value by the denominator of equation (3.1). This calculus results in 364.5 (= 9x(0.5+1.5+2.5+3.5+4.5+5.5+6.5+7.5+8.5), as the 9 columns suffer pressures between 0.5 to 8.5 and there are 9 boxes on each column. The Succolarity value for the box size 1x1 is then σ (1x1;l2r)=14/364.5≈0.0384.

3.2.2 BOX SIZE EQUAL TO 9 PIXELS (3X3) – DIRECTION TOP TO BOTTOM

On figure 3.5 (b) each box correspond to 3x3 pixels; to calculate the percentage of presence of each box is necessary to divide the number of filled pixels on the box by the area of that box (9 in this case). Figure 3.5 (b) shows 7 boxes with some percentage of occupation and 2 with 0%. The upper left box has 6 pixels, the percentage of that boxes is then 6/9≈0.67. The percentages of occupied boxes of the top of the image respectively from left to right are 0.67, 0.67 and 0.56 (≈5/9), that is, a total of 1.90; on the middle boxes this percentages are 0.11 (≈1/9), 0.56 and 0.89 (≈8/9), a total of 1.56; and on the bottom boxes there are 0, 0 and 0.11. Considering the pressure like in figure 3.4 (b), the y position of the centroid is 1.5 on the three boxes of the top, 4.5 on the three middle boxes and 7.5 on the 3 boxes on bottom of the image. The maximum value possible by a 9x9 image with 3x3 boxes completely flooded is (1.5+1.5+1.5+4.5+4.5+4.5+7.5+7.5+7.5) = 40.5. This value can be seen as the sum of the maximum "pressure" applied to each box.

The Succolarity value is then easily determined by the simple application of equation (3.1). σ (3x3,t2b) ≈ (1.5x1.90)+(4.5x1.56)+(7.5x0.11)/40.5 ≈ 0.2634.

All the results of the Succolarity of figure 3.1 are shown in table 3.1.

		Succolarity (s)			
d	***BS***	**b2t**	**t2b**	**l2r**	**r2l**
9	(1x1)	0.3429	0.2387	0.0384	0.4829
3	(3x3)	0.3292	0.2634	0.0576	0.4691

Table 3.1. Results of the Succolarity of figure 3.1.

These results are shown in the ln x ln plot in figure 3.6. As it can be seen on the y axis (Succolarity logarithm), the value of the Succolarity is multiplied by a factor of 100 before the application of the logarithm. This was made so that the values of the logarithm became positive numbers instead of negative, as the range values of Succolarity varies from 0 to 1.

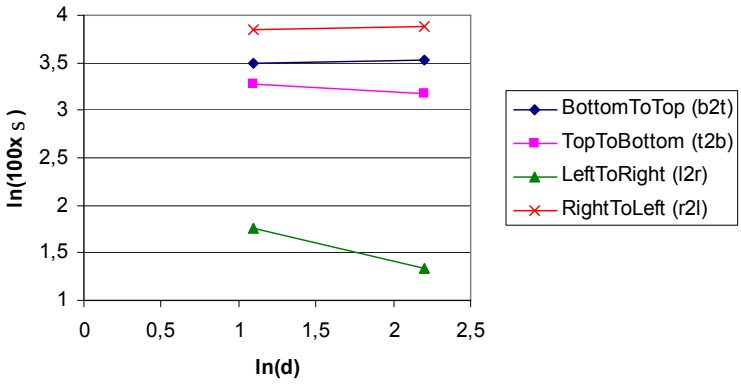

Figure 3.6. Ln x ln plot of Succolarity values for figure 3.1 (described in table 3.1).

3.3 CONSIDERING THE PROPERTIES OF SUCCOLARITY THROUGHOUT IMAGES

This section computes the results of the Succolarity for some synthetic images in order to illustrate characteristics and properties of this measure.

The Succolarity property commented on the beginning of this chapter are demonstrated through the use of the synthetic images in figure 3.7 and its result shown in figures 3.8 and 3.9 (figure 3.7 (b) is equal to figure 3.7 (a) scaled by a multiplied factor of 2). The image in figure 3.7 (a) was tested considering boxes with 1x1, 2x2, 4x4, 5x5, 8x8, 10x10 and 20x20 pixels. Image of figure 3.7 (b) uses boxes with 1x1, 2x2, 4x4, 5x5, 8x8, 10x10, 16x16, 20x20 and 40x40 pixels.

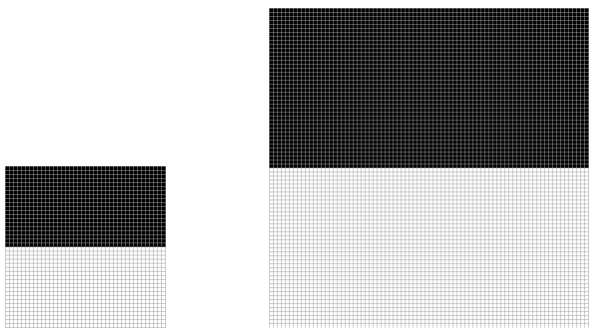

(a) (b)

Figure 3.7. Synthetic images to illustrate the dimensionless property of the Sucolarity, named "image_50%B_50%W": (a) image half-black an half-white with 40x40 pixels; (b) image with the same characteristic and 80x80 pixels.

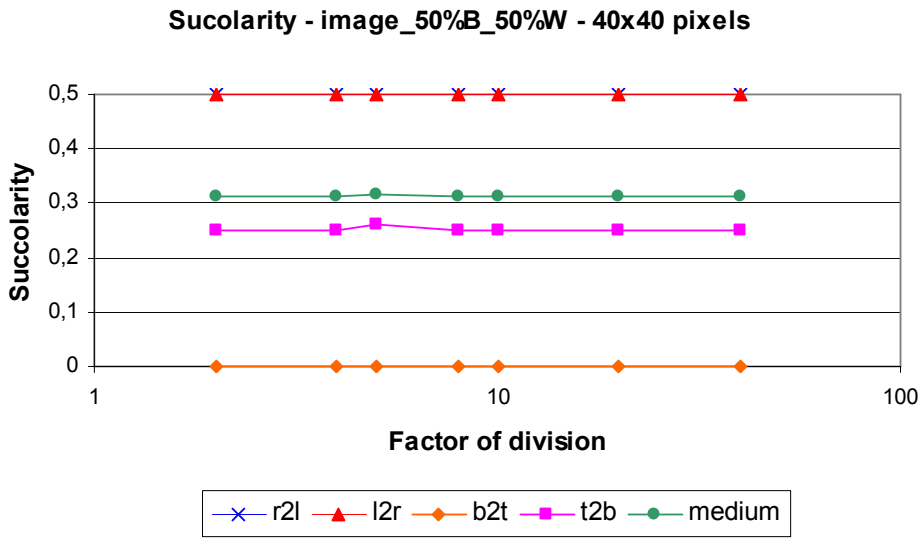

Figure 3.8. Linear X log plot of the result of the Succolarity for the input image in figure 3.7 (a).

By the results in figure 3.8 it is easy to note that the values of Succolarity for the right-to-left (r2l) direction matches the left-to-right (l2r) direction. This is expected as the fluid can flow for half of the image completely on the image of figure 3.7 (a).

The plot for the image in figure 3.7 (b) is shown next, in figure 3.9.

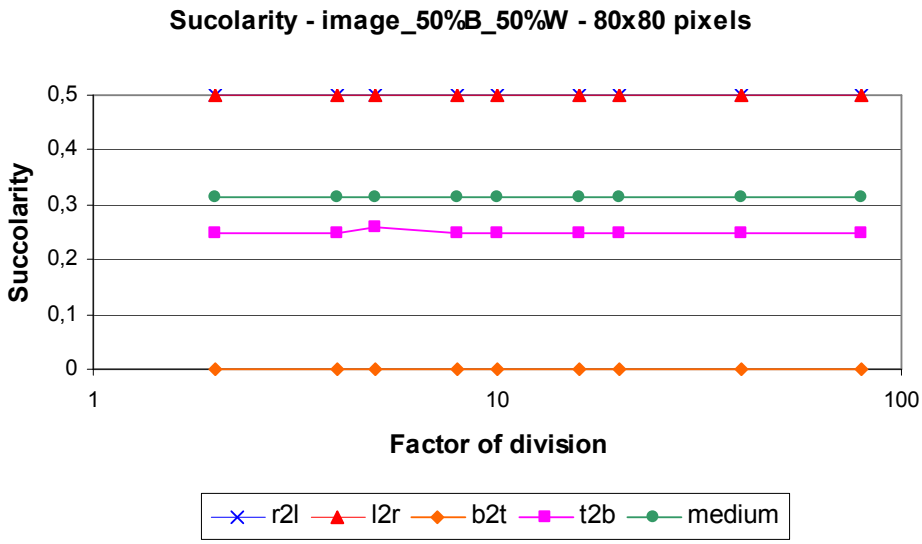

Figure 3.9. Linear X log plot of the result of the Succolarity for the input image in figure 3.7 (b).

The Succolarity resulting plot in figure 3.9 is the same as in figure 3.8, adding two more points which correspond to the new possibilities of division for the new input image. The only point, on both plots, that make the curve different from a line occurs on the top-to-bottom analysis of the Succolarity. This is easily explained by the analysis of the difference of those points. As it can be seen in tables 3.2 and 3.3, the factor of division that corresponds to these points is the same on both results, equal to 5 (marked on tables). Looking at the matching box size and visualizing the box in the images one can easily note that this sizes of boxes are the only that implie on boxes not completely full or empty on the middle of the image. To all the other boxes-sizes the grid formed has only full or empty boxes.

		Succolarity (S)				
d	***BS***	**b2t**	**t2b**	**l2r**	**r2l**	**medium**
40	(1x1)	0	0.25	0.5	0.5	0.3125
20	(2x2)	0	0.25	0.5	0.5	0.3125
10	(4x4)	0	0.25	0.5	0.5	0.3125
8	(5x5)	0	0.25	0.5	0.5	0.3125
5	(8x8)	0	0.26	0.5	0.5	0.315
4	(10x10)	0	0.25	0.5	0.5	0.3125
2	(20x20)	0	0.25	0.5	0.5	0.3125

Table 3.2. Numerical results of Succolarity for the input image in figure 3.7 (a).

		Succolarity (S)				
d	***BS***	**b2t**	**t2b**	**l2r**	**r2l**	**medium**
80	(1x1)	0	0.25	0.5	0.5	0.3125
40	(2x2)	0	0.25	0.5	0.5	0.3125
20	(4x4)	0	0.25	0.5	0.5	0.3125
16	(5x5)	0	0.25	0.5	0.5	0.3125
10	(8x8)	0	0.25	0.5	0.5	0.3125
8	(10x10)	0	0.25	0.5	0.5	0.3125
5	(16x16)	0	0.26	0.5	0.5	0.315
4	(20x20)	0	0.25	0.5	0.5	0.3125
2	(40x40)	0	0.25	0.5	0.5	0.3125

Table 3.3. Numerical results of Succolarity for the input image in figure 3.7 (b).

Other important characteristics to extract from the results shown on the tables is that the image was half flooded by the fluid on the horizontal directions, which implies in a Succolarity result of 0.5 on left-to-right and right-to-left evaluation. The null value (0) of the bottom-to-top analysis occurs because the fluid could not flood from the bottom of the image, as it is totally occluded. The almost linear values of 0.25 for the top-to-bottom analysis indicates the pressure component of the Succolarity once the fluid for this case

also floods half the image, but now the fluid only floods through the areas where the acting pressures is low. As the Sucolarity varies from 0 to 1, one can notice that the contribution of the Succolarity for the non flooded area in this case, if evaluated, will be of 0.75.

Another synthetic image tested is in figure 3.10.

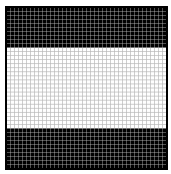

Figure 3.10. Synthetic image to illustrate characteristics of the Sucolarity, named "image_25%B_25%W_25%B" with 40x40 pixels;

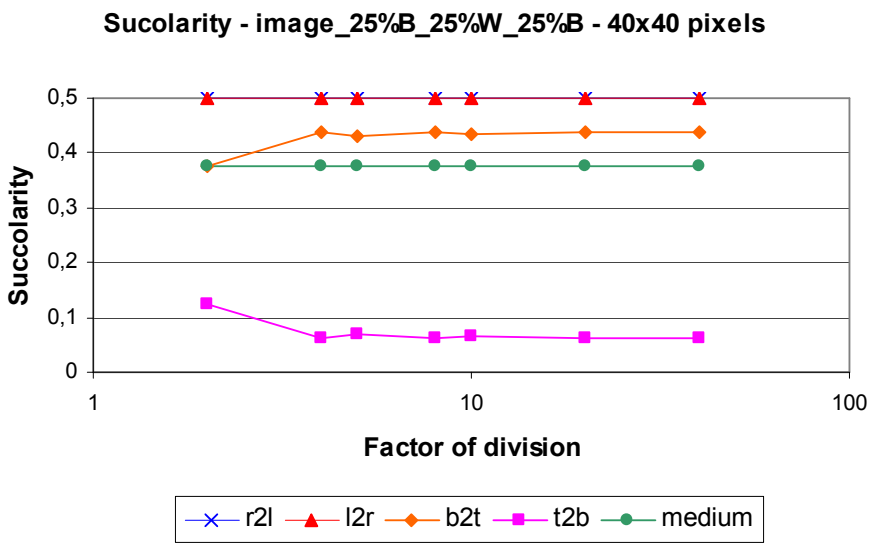

Figure 3.11. Linear X log plot of the result of the Succolarity for the input image in figure 3.10.

Characteristics that could be understood by this plot are that the values for the horizontal analysis are still the same and that the values from the vertical analysis have similar behavior. The horizontal aspect does not change because, on the new image, the fluid can still flood 50% of the image. The differences on the vertical analysis occur because of the associated pressure, which causes, as could be seen by the figure 3.11, greater values for the bottom-to-top analysis over the top-to-bottom, as the pressure grows from top to bottom (for the vertical case).

3.4 EXAMPLE OF THE 3D APPROACH

Figure 3.12 shows the 3D synthetic image used to illustrate the approach of measuring the Succolarity of 3D images or objects. In this image, the voxels are represented as cubes: yellow cubes (including the transparent ones) represent the obstacles to the fluid while the blue cubes already represent the areas where the fluid percolates the image. Figure 3.13 shows the 2D slices that forms the 3D synthetic image in figure 3.12. In these images (figure 3.13), the black squares represent the empty voxels corresponding to the paths that the fluid can flow from the top to the bottom slice of the image. The white squares represent the voxels in the image that corresponds to the obstacles to the fluid flow through the image.

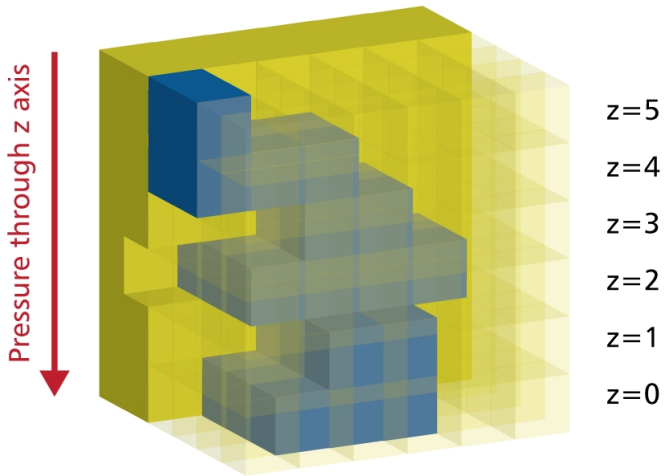

Figure 3.12. 3D Synthetic image used already with the representation of the percolation of fluid (in blue).

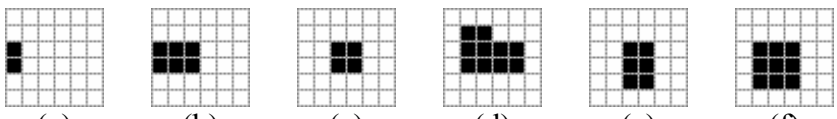

Figure 3.13. Representation through slices of the 3D synthetic image used as input for the 3D approach of the Succolarity: From the upper slice on (a) z = 5 to the bottom slice on (f) z = 0.

The pressure field through the new axis (z) grows from top to bottom, as represented on figure 3.12, then the pressure over the first slice (figure 3.13 (a), z = 5) is smaller than the pressure on the second slice (figure 3.13 (b), z = 4) and so on to the greater pressure that is applied on the last slice (figure 3.13 (f), z = 0).

The dimension of the image represented by the slices in figure 3.12 is 6x6x6: 6 pixels of width; 6 pixels of height and 6 pixels depth. This image has then three possibilities of division: factor of division 2, 3 or 6, having respectively boxes sizes of: 3x3x3; 2x2x2 and 1x1x1 pixels.

For the box of size 1x1x1 we have pressure values through the slices from 0.5 to 5.5. Considering "slice n" as the slice where the value of z = n; the pressure is 5.5 on slice 0. Then we have 2 boxes with pressure 0.5 (slice 5); 6 boxes with pressure 1.5 (slice 4); 4 boxes with pressure 2.5 (slice 3); 10 slices with pressure 3.5 (slice 2); 6 boxes with pressure 4.5 (slice 1); and 9 boxes with pressure 5.5 (slice 0). Considering equation 3.1 and that with boxes of 1x1x1 the boxes are 0 or 100% occupied, the result of Succolarity for box size 1x1x1 is σ (1x1x1,t2b) ≈131.5/648≈0.2029.

For the box size 2x2x2 we have pressure through slices from 1 (slice 4 and 5) to 5 (slice 0 and 1). On slices 4 and 5 we have 2 boxes partially occupied: one with occupation of 75% and the other with 25%. Slices 2 and 3 (with pressure 3 over them) have 5 boxes with some occupation: 2 with 12.5%; 2 with 25% and 1 with 100% of occupation. Slices 0 and 1 have 4 boxes partially occupied: 1 with 12.5%; 1 with 25%; 1 with 50% and 1 with 100% of occupation. Considering the equation 3.1 and the pressure and occupations measured we have the result of Succolarity for this box size of σ (2x2x2,t2b) ≈15.625/81≈0.1929.

With the box size 3x3x3 we have pressure through slices from 1.5 (slices 3, 4 and 5) and 4.5 (slice 0, 1 and 2). On slices 3, 4 and 5 we have 4 boxes partially occupied: 2 with occupation of 3.7% and the two other with 18.5%. Slices 0, 1 and 2 have also 4 boxes with some occupation: 1 with 14.8%; 1 with 22.2%; 1 with 25.9% and 1 with 29.6% occupation. Considering equation 3.1 and the pressure and occupations measured, we have the Succolarity for this box size as σ (3x3x3,t2b) ≈4.8285/24≈0.2012.

The numerical results of Succolarity are shown next on table 3.4.

		Succolarity (s)
d	***BS***	**t2b**
6	(1x1x1)	0.2029
3	(2x2x2)	0.1929
2	(3x3x3)	0.2012

Table 3.4. Numerical results of the Succolarity for the 3D synthetic image represented by in figure 3.12.

4 WHY USE THREE DIFFERENT MEASURES?

The main idea of this section, is to illustrate, through examples, the necessity of using, not just one, but a combination of fractal measures, to help the identification of texture patterns on images. The three characteristics presented in this work explore different aspects of the images in a way that an image could present the same Fractal Dimension for a different Lacunarity; the same Lacunarity for a different Succolarity; and any other combination of results.

The Fractal Dimension (FD) is a measure that characterizes how much an object occupies the space that contains it. FD is a measure that does not change with scale neither with translation nor rotation. Through examples in figures 4.1 and 4.2 some of these aspects can be observed. Lacunarity measures the size and frequency of gaps on the image. Succolarity measures the degree of percolation of an image.

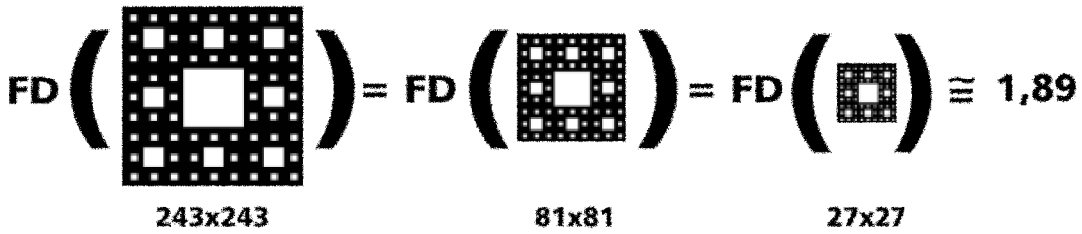

Figure 4.1. Comparison of Fractal Dimension of Sierpinski's carpet with different resolutions: 243x243, 81x81 and 27x27 pixels. FD = log(8)/log(3) ≈1,89. Fractal Dimension does not change with scale.

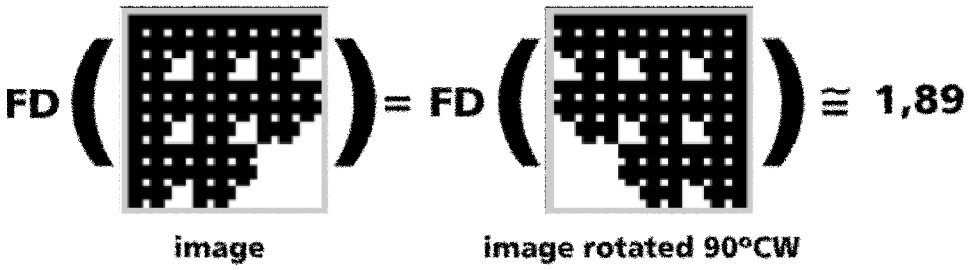

Figure 4.2. Comparison of FD of a fractal with the same Fractal Dimension of Sierpinski's carpet rotated ninety degrees clockwise. Fractal Dimension does not change with rotation.

4.1 FRACTALS WITH THE SAME FRACTAL DIMENSION AND DIFFERENT LACUNARITY AND SUCCOLARITY

This section demonstrates that Fractal Dimension in some cases is not enough to differentiate texture of images. The Fractal Dimensions of the two fractals in figure 4.3 are equal. Nevertheless, it is easily shown by its definitions, that the Lacunarity and Succolarity of those images are different. This is shown in figures 4.4 through 4.7.

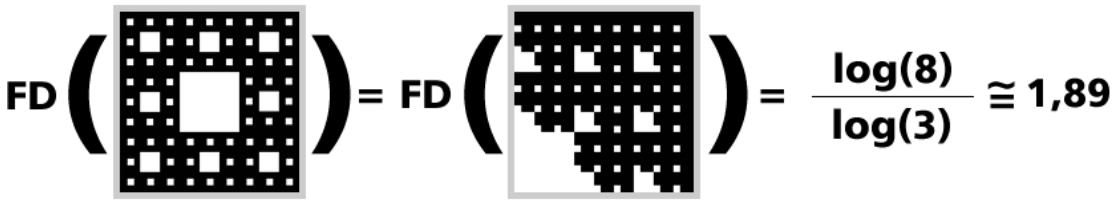

Figure 4.3. Two fractals with the same FD. Sierpinski carpet and another fractal with the same rule of construction: 8 parts with a scale factor of 1/3.

Figures 4.4 and 4.5 illustrates that the fractals in figure 4.3 have different values of Lacunarity.

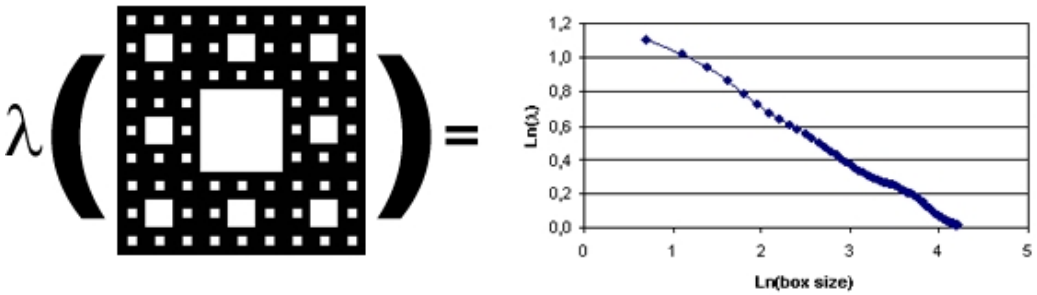

Figure 4.4. Ln x ln plot result of Lacunarity of Sierpinski carpet.

The differences can be better seen after the ln of box size (X axis) is higher than 2 where, in figure 4.4, the ln of Lacunarity is between 0.6 and 0.8, while in figure 4.5, this value is between 0.8 and 1.0.

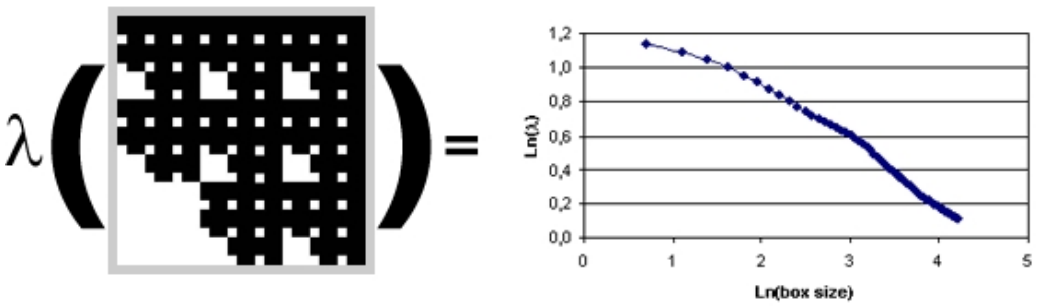

Figure 4.5. Ln x ln plot result of Lacunarity of a fractal with the same FD of the Sierpinski carpet.

In figures 4.6 and 4.7, the difference on the results of Succolarity is easily shown by the ln x ln plots, since the Sierpinski carpet (in figure 4.6) is a totally symmetric fractal, producing equal results in the four directions of analysis of the Succolarity.

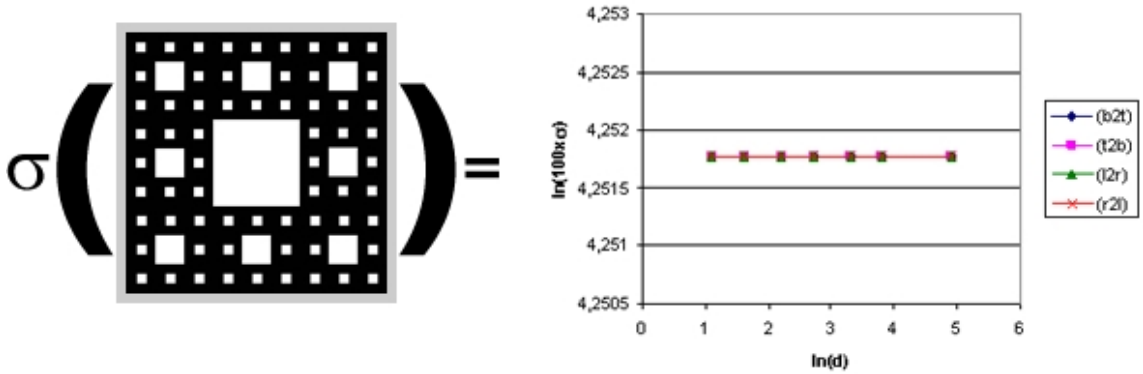

Figure 4.6. Succolarity of Sierpinski carpet.

The fractal in figure 4.7 is only half symmetric, as it can be seen in the ln x ln plot in this figure and by the results in table 4.1.

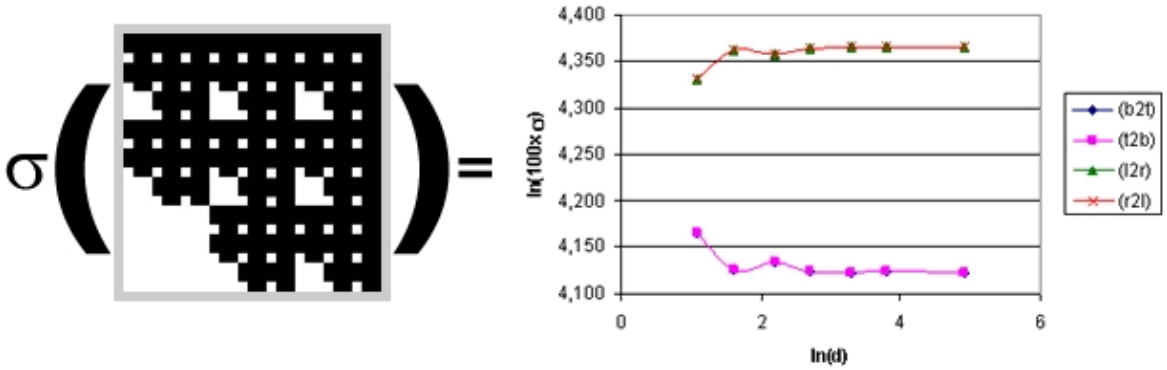

Figure 4.7. Sucolarity of a fractal with the same FD of the Sierpinski carpet.

ln(d)	ln(100x s)			
	b2t	t2b	l2r	r2l
4,9053	4,1236	4,1236	4,3655	4,3655
3,8067	4,1241	4,1241	4,3651	4,3651
3,2958	4,1236	4,1236	4,3655	4,3655
2,7081	4,1249	4,1249	4,3644	4,3644
2,1972	4,1340	4,1340	4,3572	4,3572
1,6094	4,1270	4,1270	4,3627	4,3627
1,0986	4,1648	4,1648	4,3319	4,3319

Table 4.1. Numerical results of the ln x ln Succolarity plot for figure 4.7.

Table 4.1 shows in the first column the logarithm of the dividing factor of the boxes and on the second column the logarithm of the Succolarity times 100. The sub-columns illustrate respectively the results for the directions: bottom to top (b2t); top to bottom (t2b); left to right (l2r) and right to left (r2l). The results in this table made clear that the Succolarity for this image does not change by reversing the direction through the same axis.

4.2 FRACTALS WITH THE SAME FRACTAL DIMENSION AND LACUNARITY AND DIFFERENT SUCCOLARITY

This section illustrates that there are cases where Fractal Dimension and Lacunarity do not differentiate images. Some of these cases could be treated with the Succolarity definition presented here as we can see by the examples of the figures 4.8 through 4.11.

Figure 4.8 illustrates through a synthetic image that Fractal Dimension does not vary with a 90º rotation. This was already observed in figure 4.2.

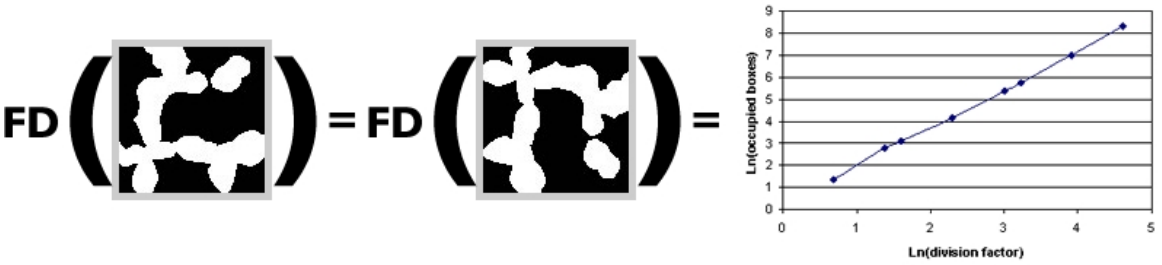

Figure 4.8. Ln x ln plot result of FD by box couting method to a given synthetic image. X axis presents the logarithm of the division factor and Y axis presents the logarithm of the number of occupied boxes. These results show that the FD does not change with rotation.

Figure 4.9 illustrates through the same synthetic image of figure 4.8 that Lacunarity does not vary with rotation as it could be easily expected by its characteristics.

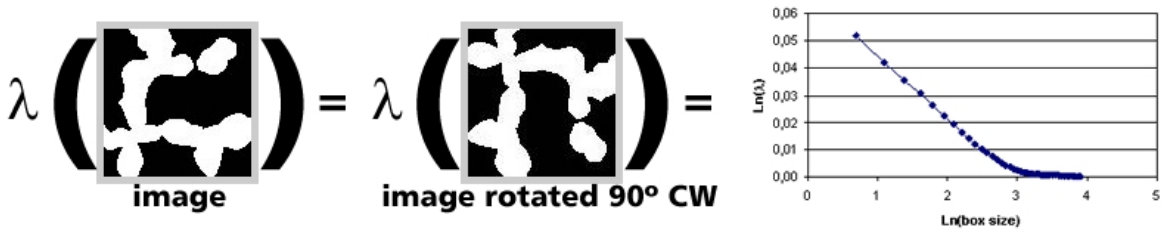

Figure 4.9. Ln x ln plot result of Lacunarity by the gliding box method illustrating that it does not change with rotation.

The results in figures 4.10 and 4.11, also using the same image of figure 4.8, show that Succolarity varies with rotation (on images that were not totally symmetric, of course), and that there are images that have the same FD and Lacunarity and different Succolarity values.

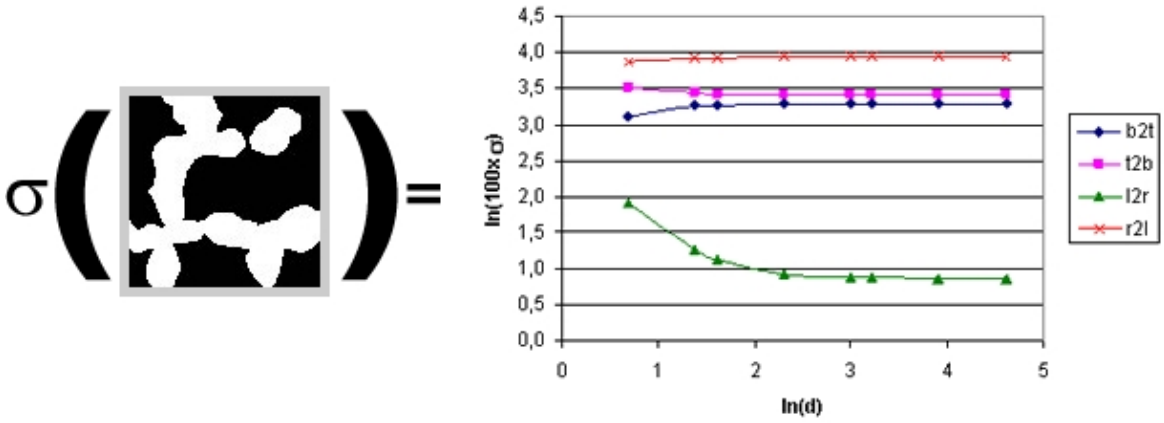

Figure 4.10. Ln x ln plot result of Succolarity of the first image of figure 4.8 by the proposed method.

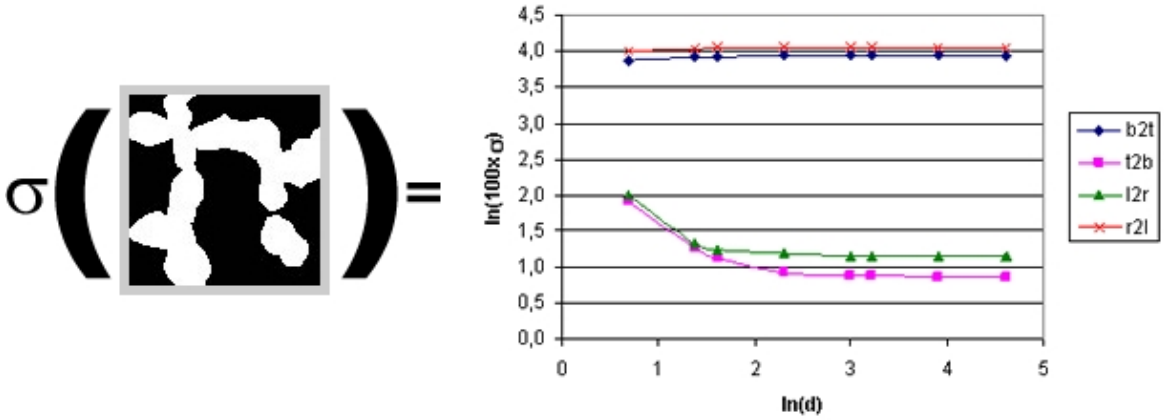

Figure 4.11. Ln x ln plot result of Succolarity of the second image of figure 4.8 by the proposed method.

5 RESULTS ON REAL IMAGES

In this section, the approaches described in the previous sections are used to characterize patterns on real images.

5.1 PREPARING THE IMAGES

This section explains how real images, used in this work, were pre-processed to satisfy the necessities of the implemented methods: Fractal Dimension, Lacunarity and Succolarity. The step for preparing an image consists on using techniques to process it in a way that the result will be better than the original image for use in a specific method.

The pre-processing is useful to increase the quality of the images emphasizing some characteristics that are interesting to a particular method. Three methods implemented here require binary images as input. The medical images of mammograms and carotid artery used here employ a supervised approach to generate the binary version of the images. This was done to guarantee that the binary images resemble the particular features on the original image.

For the Fractal Dimension evaluation, after the threshold, the image edges are also detected before being used in the method. Mathematical morphology was used to find the contour of these images. The binary image, named BI, was eroded by a structuring element in the form of a cross and then, the contour image was the result of the difference of the BI image by the output image of the erosion process (SERRA, 1982 and SOILLE, 1998).

The aerial images of cities used were sent by the author of the paper from which the results are compared on the section 5.3.1. The binary versions of these images were obtained using an unsupervised approach. As it can be seen on section 5.4.1 we adopted a supervised approach in order to classify appropriately the input images as built and non-built areas. The wrong representation of this aspect in the input binary images may lead the method to yield results not corresponding to the results expected.

5.2 RESULTS OF FRACTAL DIMENSION

The method used to calculate the Fractal Dimension for the real images illustrated here was the box counting defined on section 2.1.3.

The real images used here (figures 5.1 (a) and (b)), to illustrate the calculus of the Fractal Dimension implemented, are images from the mammogram database established on a previous work of this research group (CONCI et al., 1999).

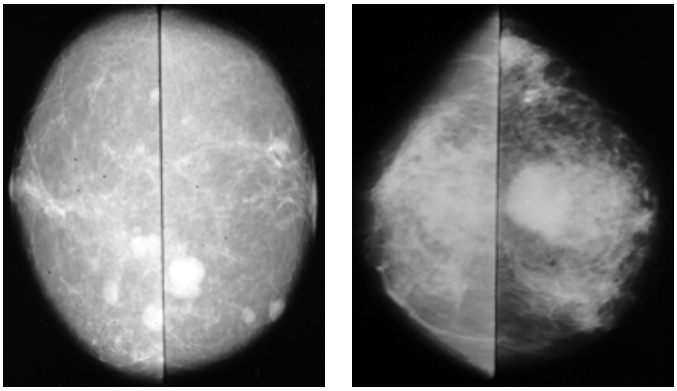

(a) (b)

Figure 5.1. Gray-scale images of tumors (200x230 pixels): (a) ben3 – benign, (b) mal13 - malign.

The images in figure 5.1 were chosen because they represent two types of tumors: one benign and other malign. The benign (figure 5.1 (a)) presents small masses and with more circular shape than the malign case (figure 5.1 (b)). This is more easily seen after the threshold process.

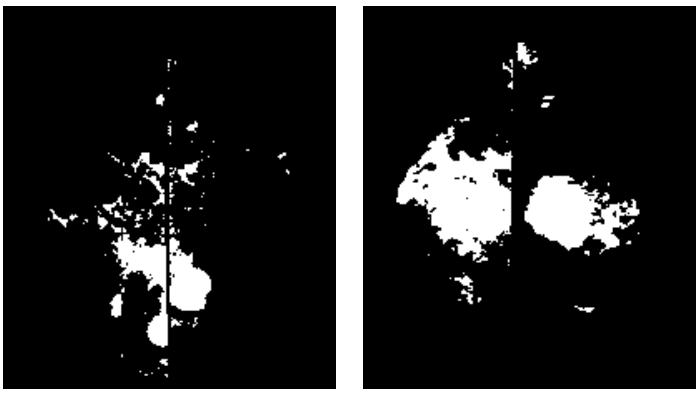

(a) (b)

Figure 5.2. Binary version of images in figure 5.1: (a) threshold = 220, (b) threshold =170.

In the approach used to calculate the Fractal Dimension for the mammograms images on MELO and CONCI, 2007, after the threshold step, the boundaries of the binary images must be obtained. The method to obtain the contour used is the internal contour of mathematical morphology, also named morphological gradient (SOILLE, 1998).

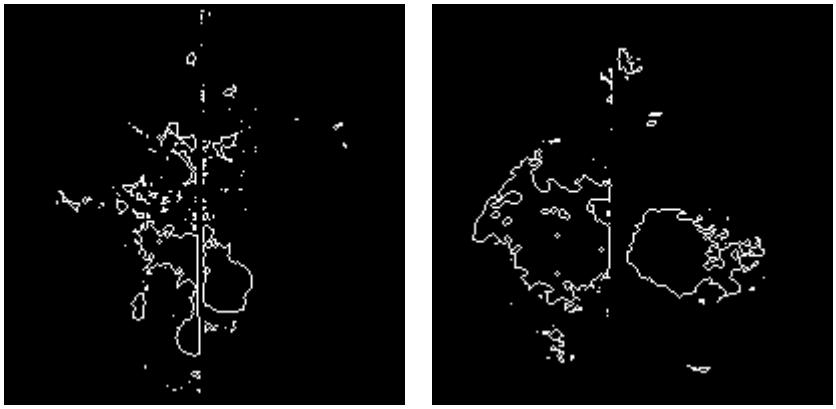

(a) (b)

Figure 5.3. Edges of images in figure 5.2 obtained through mathematical morphology.

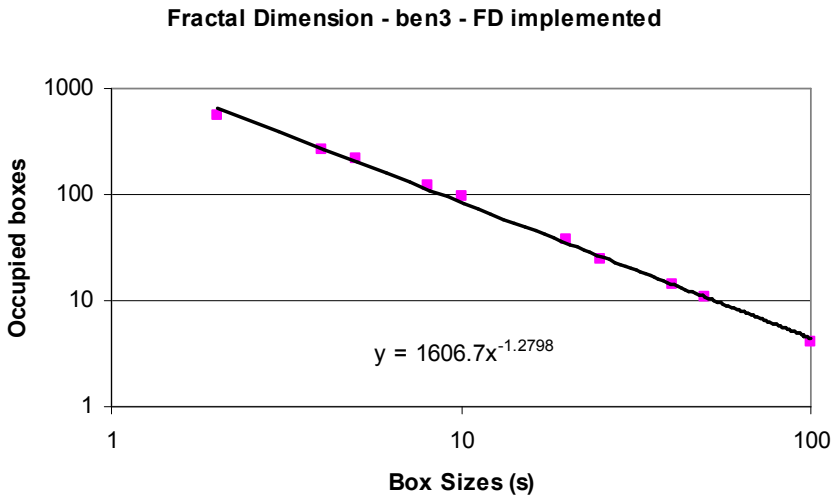

Figure 5.4. Result of the Fractal Dimension of the image of figure 5.3 (a).

For the image in the figure 5.3 (a) the observed result in figure 5.4 was 1.2798 and corresponds to the analysis of benign tumors.

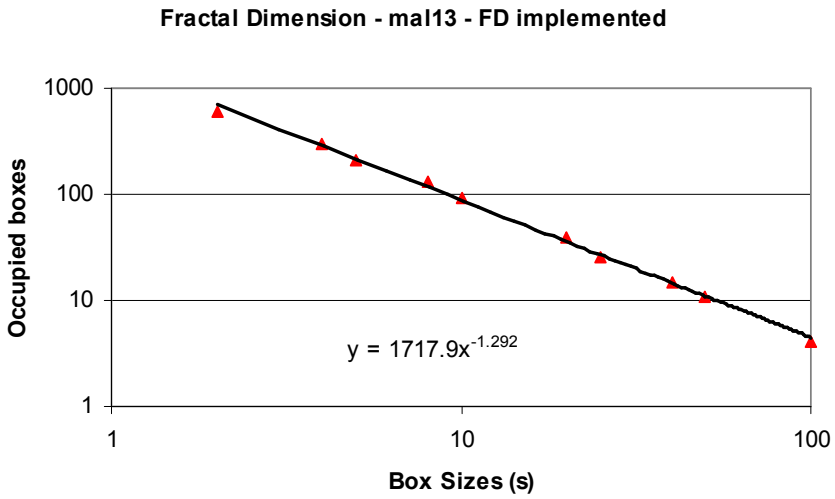

Figure 5.5. Result of the Fractal Dimension of the image of the figure 5.3 (b).

The result observed for the image of the figure 5.3 (b) presents DF = 1.2920, as can be seen in figure 5.5 and corresponds to malign tumors. The value of the Fractal Dimension to the benign tumors is smaller than the result for the malign tumors. This is because figure 5.3 (b) presents more complex edges distributed through the image, causing a bigger occurrence of occupied boxes for this image. Although figure 5.3 (a) presents more mass, they are smaller, simpler and closer to each other than those on the other image.

In order to validate the implementation of the Fractal Dimension here used, the next figures (figures 5.6 and 5.7) illustrate through graphs the results calculated by the method implemented against the results of the FRACLAC (KARPERIEN, 2004), which is a plug-in of IMAGEJ (RASBAND, 1997), a public domain Java image processing program.

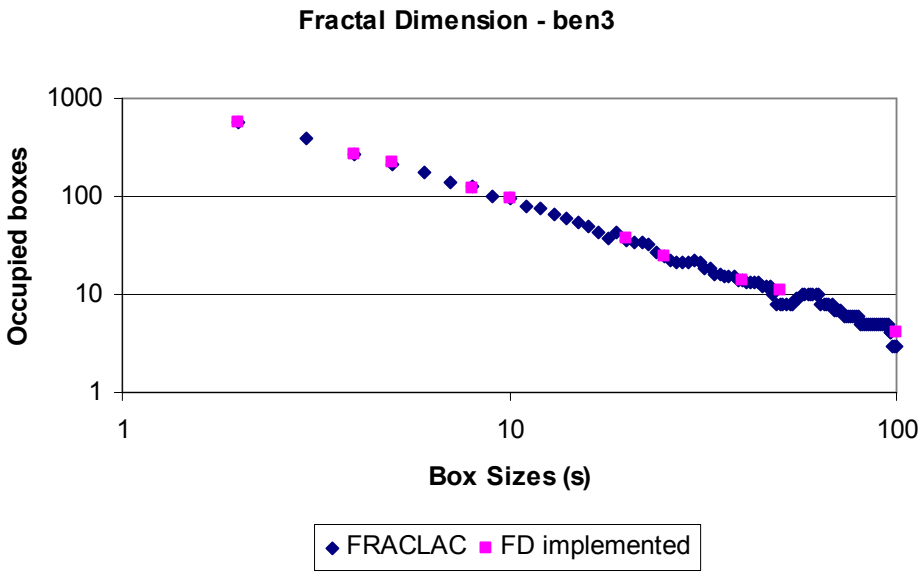

Figure 5.6. Results of Fractal Dimension of the implemented method against the result of FRACLAC corresponding to the benign tumor.

In the results of figure 5.6 one could note that the FRACLAC method computes more box sizes than the method implemented in this work. This is because the approach implemented only considers integer divisions to the windows on the box counting method. As the results for the box sizes that are calculated by the two methods match, the results for the Fractal Dimension obtained for each method are almost the same. As the implemented method considers only integer divisions for the sizes of the boxes, it executes faster than the method implemented in FRACLAC.

The implementation difference to FRACLAC is that the used input images (figure 5.3 (a) and (b)) have to be inverted (each black pixel on the original image becomes white while the white ones become black after the inversion of the image) before entering the other method so that the two methods analyze the same data.

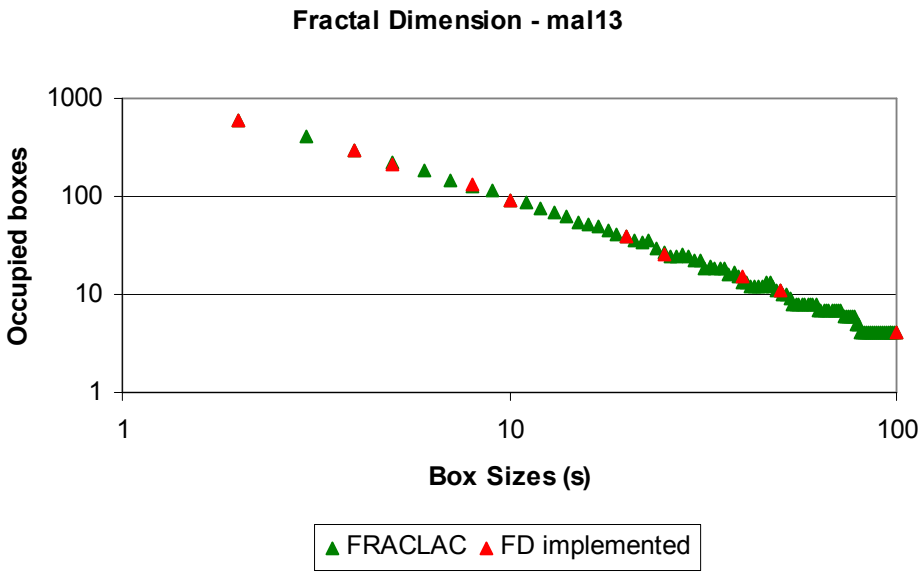

Figure 5.7. Results of Fractal Dimension of the implemented method versus FRACLAC result for malign tumor.

As expected, all the observations made to the results for the benign tumor (figure 5.6) could be observed in figure 5.7.

5.3 RESULTS OF LACUNARITY

The method used to compute the Lacunarity for real images illustrated here was based on the gliding box method, described on section 2.2.

5.3.1 COMPARISONS BETWEEN THE PROPOSED METHOD AND OTHER EXISTING METHODS THROUGH BINARY IMAGES

This section illustrates the results obtained by the Lacunarity calculation implemented on the FRACLAC plug-in (KARPERIEN, 2004) and the method by FERNANDES and CONCI, 2004a compared to the proposed method to calculate Lacunarity. As here, we only compare the Lacunarity, giving as input, black and white images, we expect to obtain the same results, in order to validate the method.

To better illustrate the results, the images used here were already used and discussed on previous works (BARROS FILHO and SOBREIRA, 2005 and BARROS FILHO and SOBREIRA, 2005a). These papers use Lacunarity to distinguish the spatial configuration

of slums from formal constructed areas as well as from other informal areas to contribute for the development of alternative and complementary classifications of these settlements. The goal is to generate complementary mapping and classifications for urban poverty through satellite images.

The images used here (including their binary versions) have been gently provided by Mauro Barros Filho (figures 5.8 and 5.9), one of the authors of the paper BARROS FILHO and SOBREIRA, 2005, to make sure that the results match for the same images. These satellite images were originally captured by the IKONOS (SPACE IMAGING BRAZIL, 2004) and could be freely downloaded through the internet for non-profit research and evaluation purposes.

Four images were used for this analysis(figure 5.8), three from the city of Campinas, SP, Brazil: two regular (orthogonal geometry) samples and one irregular (slum) sample and one image, with an irregular sample, from the city of Rio de Janeiro, Brazil. All images have 270x270 pixels.

(a) (b)

(c) (d)

Figure 5.8. Satellite images from IKONOS: (a) and (b) two regular samples of occupation from Campinas: formal 1 (left) and fomal 2 (right); (c) informal 1: slum of Campinas; (d) informal 2: slum from Rio de Janeiro.

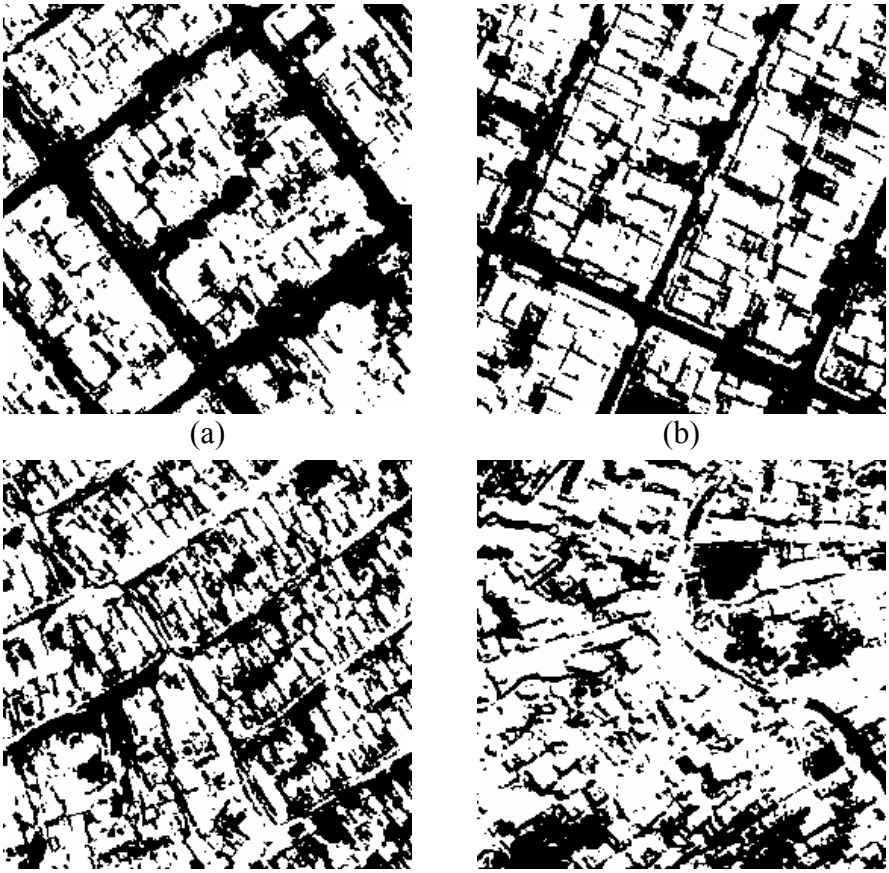

(a) (b)

(c) (d)

Figure 5.9. Binary version of images in figure 5.8.

The FRACLAC plug-in enables some configurations before the calculus of the Lacunarity. Some parameters were set to force the two methods work similarly. These parameters are shown in table 5.1.

Parameter	**Value**
Background color	white
Sizes per series: (0 calculates automatically)	0
Minimum size for scaled, relative and linear series	2 pixels
Maximum box size	25% of the image
Number of pixels to slide boxes (X axis)	1
Number of pixels to slide boxes (Y axis)	1

Table 5.1. Parameters of FRACLAC to calculate the Lacunarity based on the same procedure as the proposed method.

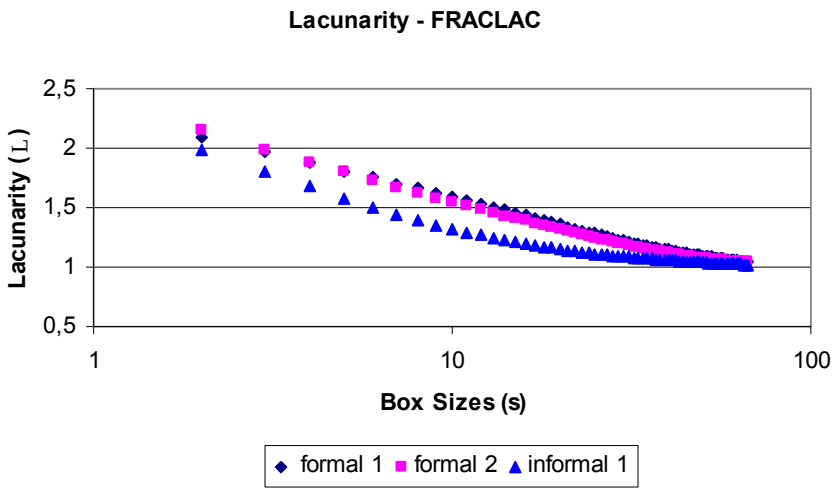

Figure 5.10. Results of Lacunarity obtained from FRACLAC using as input the images of Campinas in figure 5.9.

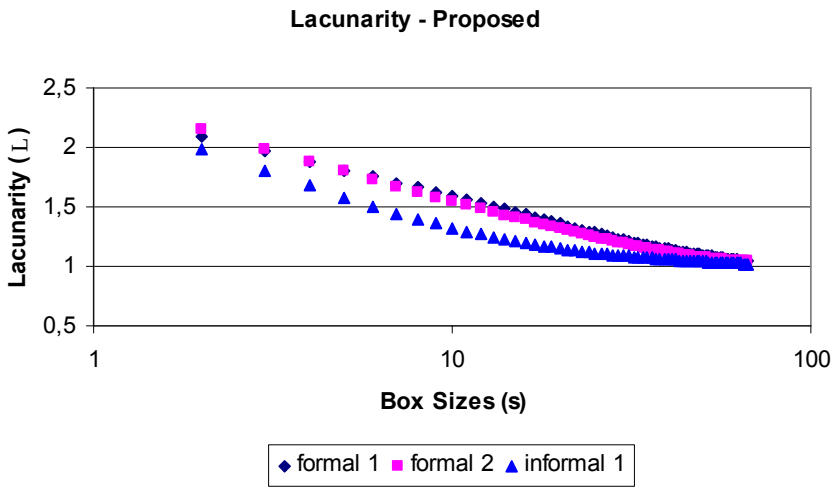

Figure 5.11. Results of Lacunarity obtained from the proposed method using as input the images of Campinas in figure 5.9.

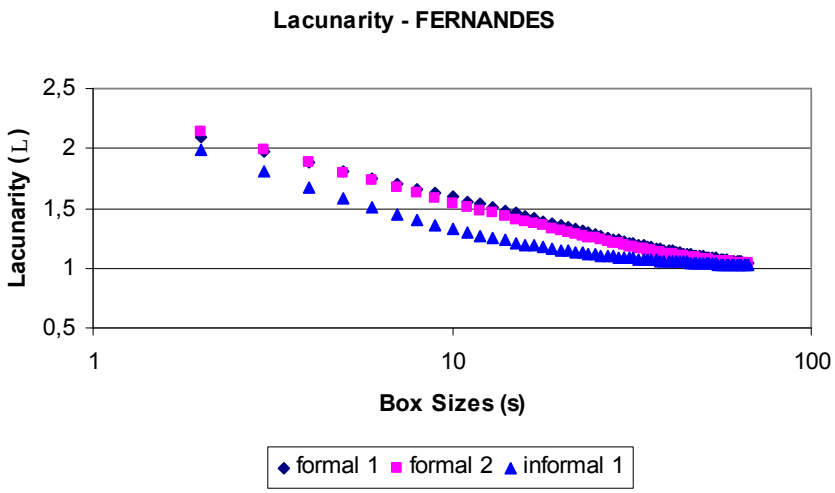

Figure 5.12. Results of Lacunarity obtained from the method on FERNANDES and CONCI, 2004a using as input the images of Campinas in figure 5.9.

As we can see in figures 5.10 to 5.12, the results are the same (regarding some values that diverges on the order of 10^{-4}), as expected. It is important to note that, for particularities of implementations, the images in figure 5.9 were inverted considering its colors (black pixels became white and white pixels became black) before the processing at the FRACLAC application.

The results in figure 5.10 to 5.12 show that the Lacunarity values of the images formal 1 and formal 2, are practically the same, while the values from informal 1 diverges. Lacunarity permits to distinguish two groups of configuration and texture. The regular (orthogonal) areas present, in average, higher values of Lacunarity, probably a consequence of the outstanding emptiness of spaces, associated to large and regular avenues, and overall low density. On the other hand, when analyzing the slums, the result is low Lacunarity, indicating low permeability, resulting from typical feature of such urban structures: highly dense occupation and tortuous alleys (BARROS FILHO and SOBREIRA, 2005a).

Other comparison made using the results of the slum images (figures 5.8 (c) and (d)) are shown next in figures 5.13 to 5.15.

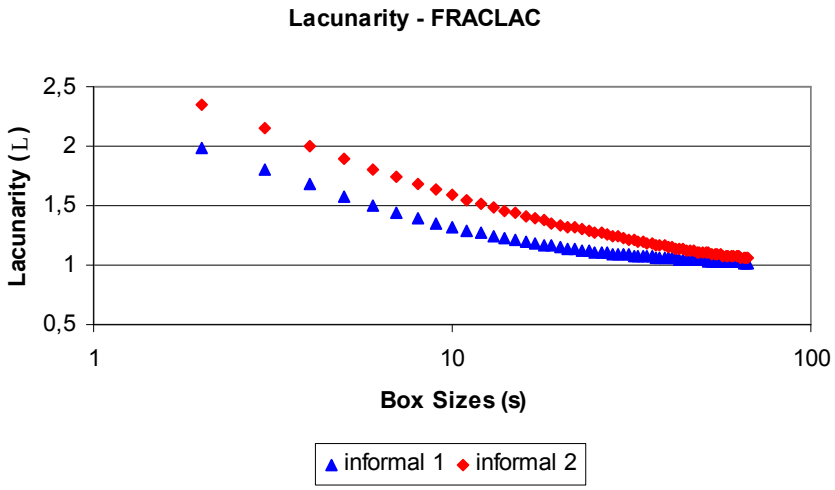

Figure 5.13. Results of Lacunarity obtained from FRACLAC using as input the images of slums in figure 5.7: (c) informal 1 and (d) informal 2.

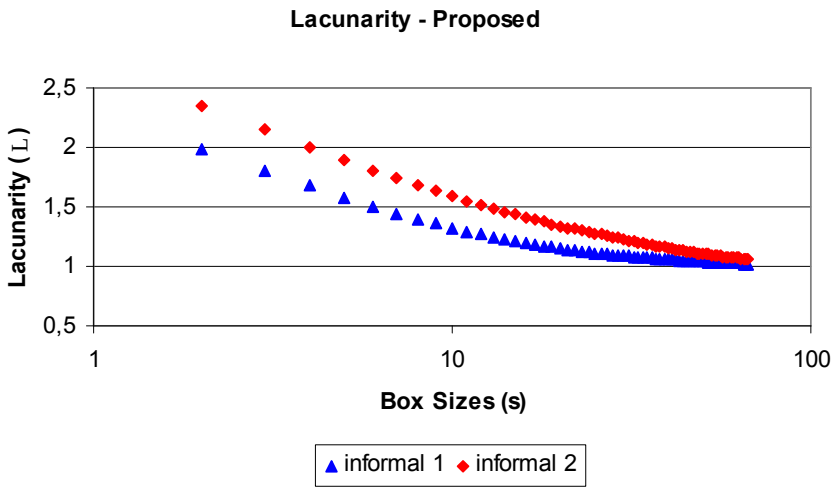

Figure 5.14. Results of Lacunarity obtained from the proposed approach using as input the images of slums in figure 5.9: (c) informal 1 and (d) informal 2.

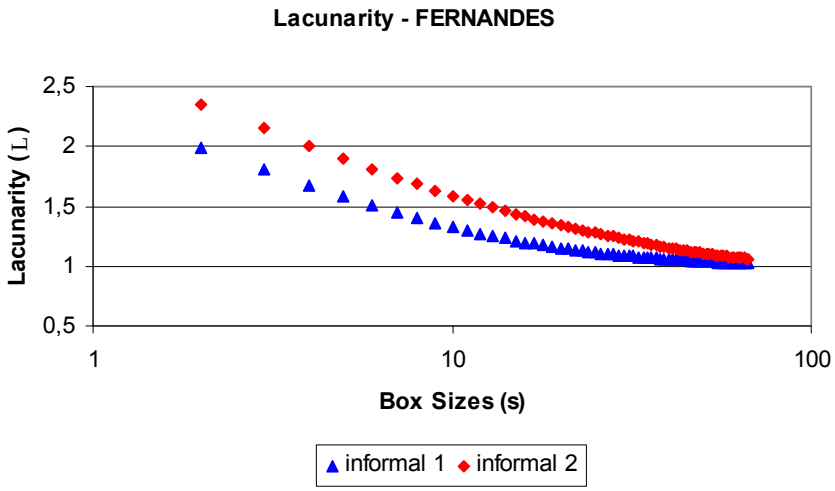

Figure 5.15. Results of Lacunarity obtained from the method on FERNANDES and CONCI, 2004a using as input the images of slums in figure 5.9: (c) informal 1 and (d) informal 2.

The results on the plots of figures 5.13 to 5.15 are the same, as expected, as observed before in figures 5.10 to 5.12 (neglecting some values that diverge on the order of 10^{-4}).

Contrary to expectations, the two irregular areas diverge considerably in their Lacunarity patterns. If one observes the results and at the same time analyze the spatial configuration, one will understand that differences result from morphological and social particularities of each community. Informal 2 (figure 5.9 (d)) presents higher Lacunarity values than informal 1 (figure 5.9 (c)) due to the presence of some green areas that elevates its Lacunarity values as it could affect the process of threshold (BARROS FILHO and SOBREIRA, 2005a).

5.3.2 COMPARISON BETWEEN BINARY AND GRAYSCALE APPROACHES TO CALCULATE THE LACUNARITY OF MAMMOGRAMS

This section illustrates the results obtained by the Lacunarity evaluation. The three approaches to analyze gray-scaled images described on the section 2.2 and 2.2.1 were compared with the approaches in sections 2.2.2 and 2.2.3. The input images used are the images of figure 5.1 modified to have the width equal to height (figure 5.16). To modify the images, parts that do not represent important information (like tummors) were

excluded from new images in figure 5.16. The thresholds used were represented in figure 5.17, other thresholds used are observed next, in figure 5.18.

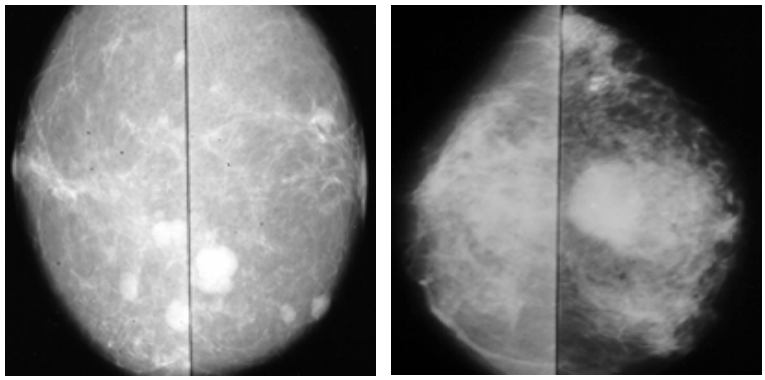

(a) (b)

Figure 5.16. Gray-scale images of tumors (figure 5.1) rescaled to (200x200 pixels): (a) ben3 – benign, (b) mal13 - malign

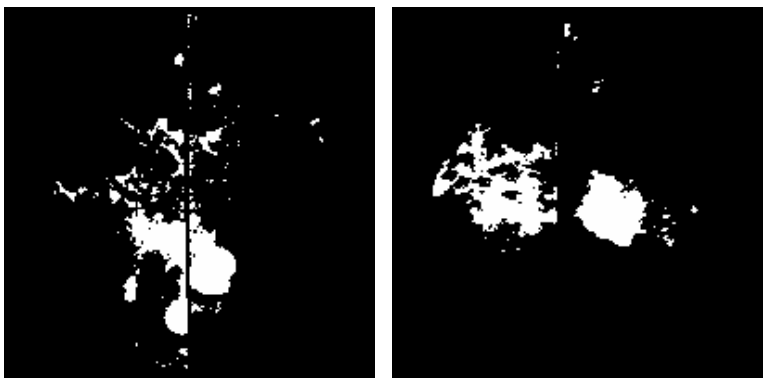

(a) (b)

Figure 5.17. Binary version of images in figure 5.16: (a) threshold = 220, (b) threshold =180.

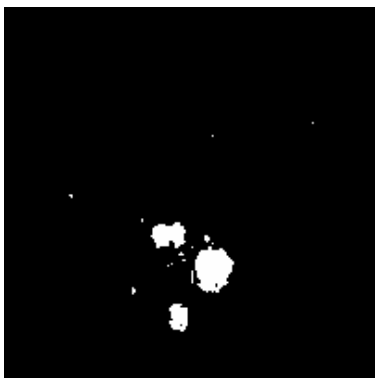

(a)

Figure 5.18. Another binary version of image in figure 5.16: (a) threshold = 240.

Results of all approaches are shown next in ln x ln plots (figures 5.19 to 5.26).

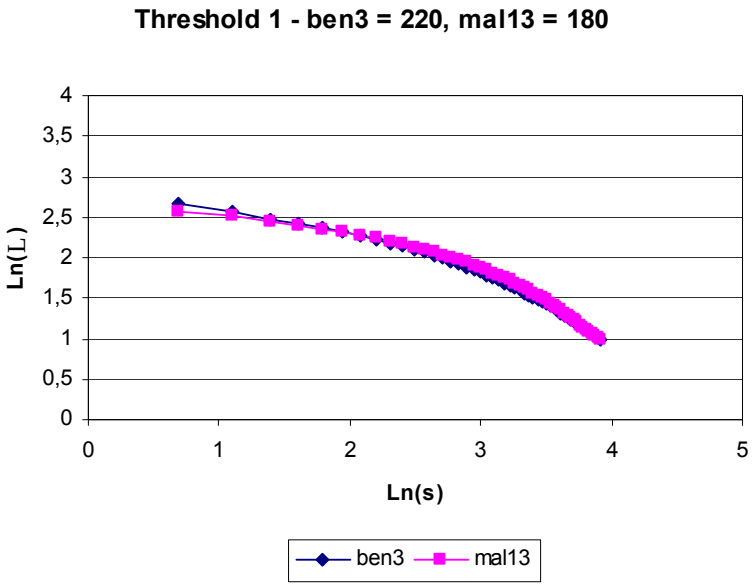

Figure 5.19. Result of the binary version of the Lacunarity for the input images in figure 5.17.

The Lacunarity plots (figures 5.19; 5.20 and 5.21) show important features to notice: (1) the Lacunarity values reflect the degree gaps; (2) the Lacunarity curves is closer to a straight line as more self-similar is the image; and (3) the Lacunarity values reveals the aspects of gaps distribution over the entire image, enabling the detection of the presence of hierarchical structures, homogeneity in gaps distribution, random or self-similar behavior.

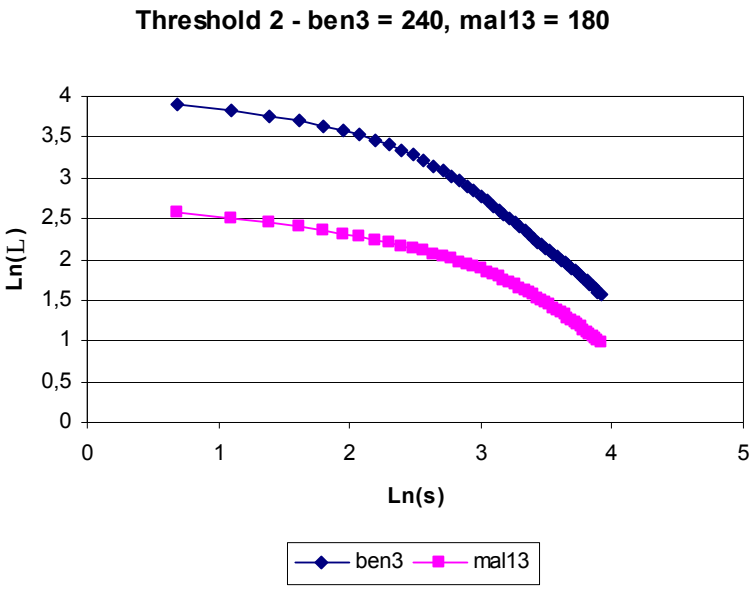

Figure 5.20. Result of the binary version of the Lacunarity for the input images in figure 5.18.

Next, in figures 5.21 and 5.22, the plots for the 3D proposed methods are shown over the same scale of the plots for the binary Lacunarity (figures 5.19 and 5.20) to better compare the results.

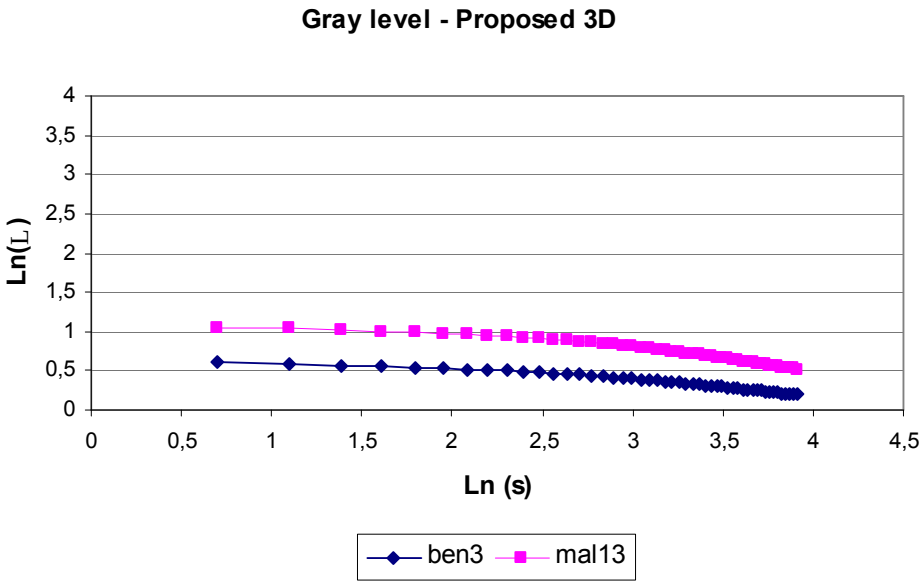

Figure 5.21. Result of the gray-scale version of the 3D approach Lacunarity for the input images in figure 5.16 through the scale on y from 0 to 4.

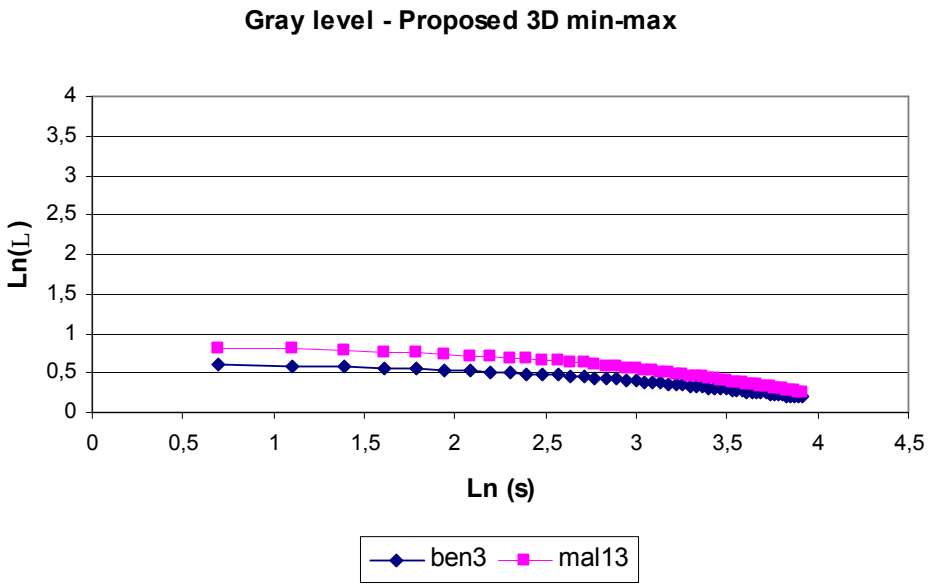

Figure 5.22. Result of the gray-scale version of the 3D min-max approach Lacunarity for the input images in figure 5.16 through the scale on y from 0 to 4.

Figures 5.21 and 5.22 present similar results; as the intensity levels on the images change almost from 0 to 255 on both images. These figures (5.21 and 5.22) also show that the Lacunarity plots generated by the gray-scale versions of the Lacunarity (3D and 3D min-max) could be better or worst separated in comparison with the results of the binary version of the Lacunarity (figures 5.19 and 5.20), depending on the threshold values used.

This single comparison shows that the gray-scale method is better to characterize the type of tumor in these images than the binary method. The main reason is that on the gray-scale method more data is considered on the processing of the Lacunarity, and there is no risk of information loss. The extra amount of data processed on this method implies in a higher processing cost, turning this method more time consuming.

Other approaches developed to gray-scale images and defined in section 2.2 have their results demonstrated through the plots in figures 5.25 and 5.26. The results of the proposed methods (3D and 3D min-max) are again represented in figures 5.23 and 5.24 using a more appropriated scale to compare the results with the plots in figure 5.25 and 5.26 (all plots with the same scale).

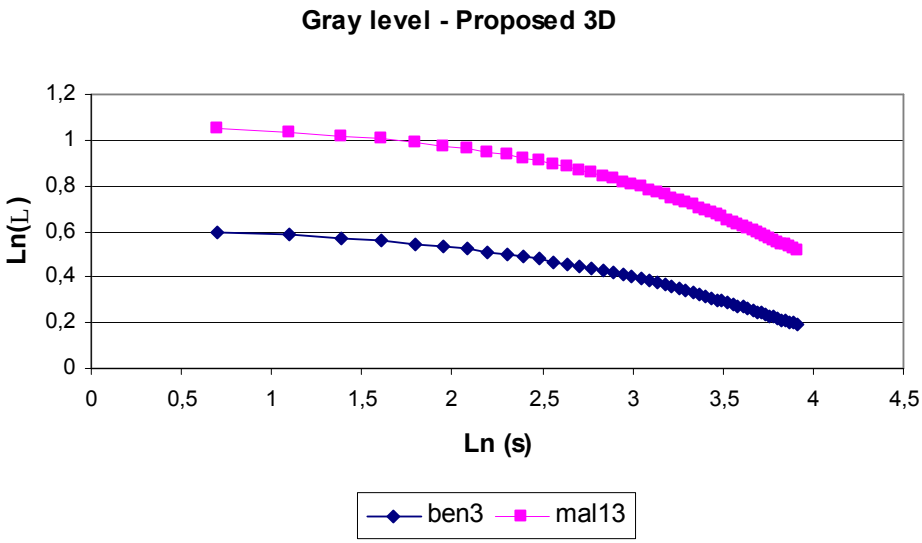

Figure 5.23. Result of the gray-scale version of the 3D approach Lacunarity for the input images in figure 5.16 through the scale on y from 0 to 1.2.

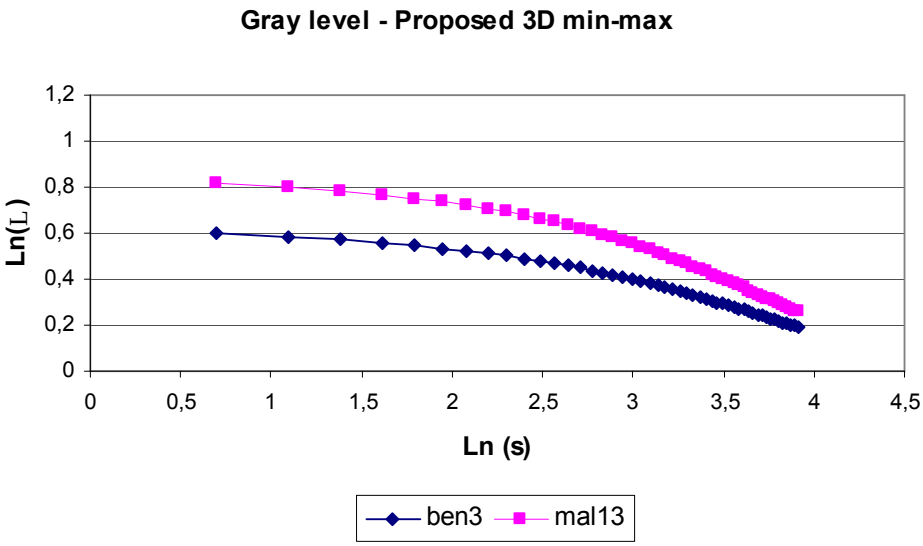

Figure 5.24. Result of the gray-scale version of the 3D min-max approach Lacunarity for the input images in figure 5.16 through the scale on y from 0 to 1.2

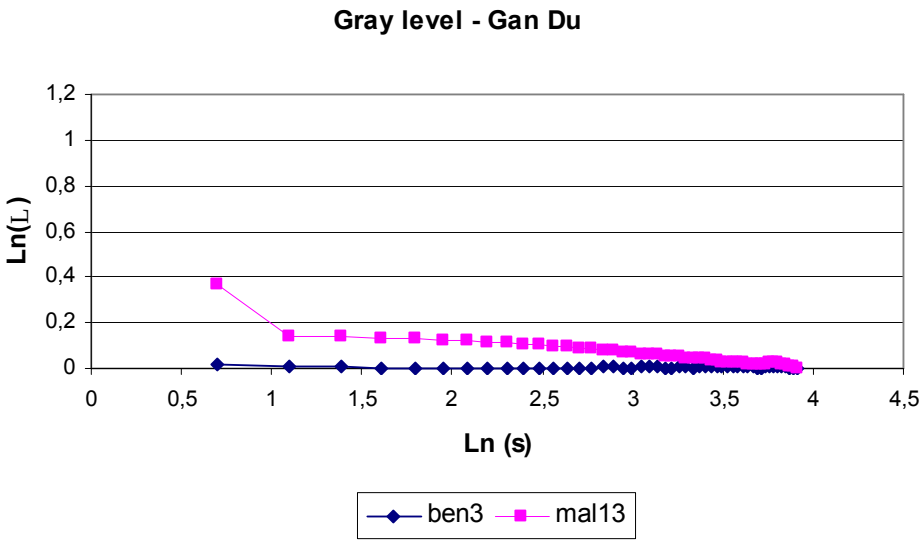

Figure 5.25. Result of the gray-scale version of the Gan Du approach Lacunarity for the input images in figure 5.16 through the scale on y from 0 to 1.2.

Considering the plots, one could easily see that the Gan Du approach (plot in figure 5.25) has similar results to the Fernandes approach (plot in figure 5.26). The Fernandes approach is a little better separated than the Gan Du approach to greater boxes as it can be seen if one looks carefully at the values of the Lacunarity when the logarithm of the box size (ln(s)) goes from 3 to 4.

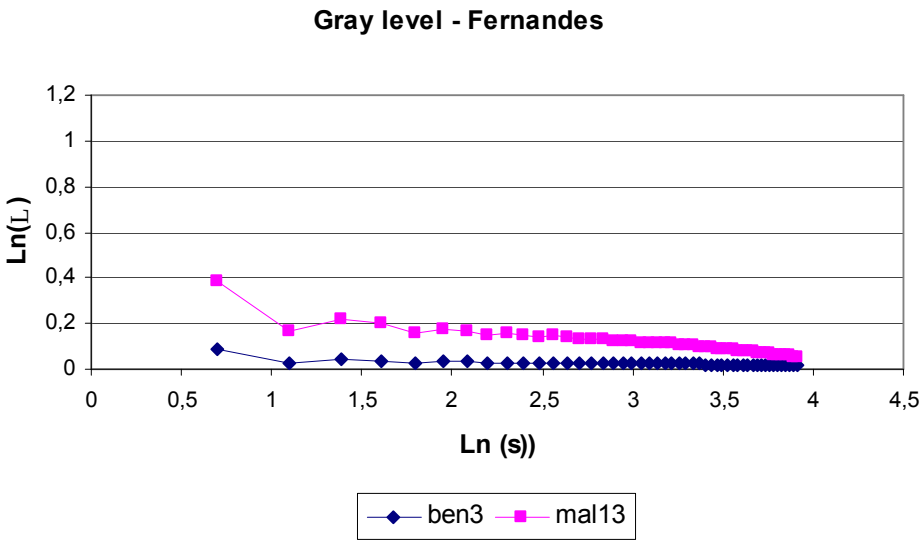

Figure 5.26. Result of the gray-scale version of the Fernandes approach Lacunarity for the input images in figure 5.16 through the scale on y from 0 to 1.2.

Comparing figures 5.23 through 5.26 one thing that could be noticed is that the obtained values by the proposed methods (figure 5.23 and 5.24) are bigger than for the other approaches. Another important fact is that the plots for the proposed approaches are better separated than for the other approaches. These differences are probably due to the occurrence of empty 3D gliding boxes in the method proposed when the gliding process reaches a height greater than the most pixel values of the image.

5.4 SUCCOLARITY RESULTS

5.4.1 SUCOLARITY AS A COMPLEMENTARY MEASURE TO LACUNARITY CHARACTERIZATION OF SOCIAL ASPECTS OF CITIES

Considering that cities are systems with fractal features because they are the result of a non-linear logic, whose patterns cannot be measured by usual concepts and tools from classical geometry (BATTY and LONGLEY, 1994; FRANKHAUSER, 1997; SOBREIRA and GOMES, 2000). We use here these types of images as input to the new proposed fractal measure, called Sucolarity. The idea of this section is to demonstrate the results of Succolarity as a complementary measure to Lacunarity, as Lacunarity is complementary to Fractal Dimension.

The particular problem of characterizing social aspects of cities and differentiate informal and formal areas fit very well to the concepts of Succolarity. Normally a great difference between formal and informal areas lies on the width of the streets, bigger on the formal area. Also, quite often the alleys that exist on informal areas do not communicate with neighboring streets. This could be better explained if one could imagine that is not as easy for a car to drive through all the parts of an informal area like it is in a formal area.

With this in mind, together with the concepts on sections 2.3 and chapter 3, the images used in this section are the same of the section 5.3.1. The image in figure 5.9 (c) were inverted to be used in the method because in Succolarity the black pixels represent the possibility of percolation (the streets) and the white ones represent the obstacles (the constructions). The inverted version represents better this idea (figure 5.27).

(a) (b)

Figure 5.27. Better binary representation of the satellite image from Campinas SP (informal) (a) original image; (b) Binary version of (a).

Figure 5.28 shows a plot with the average result of the Succolarity (this average is a simple sum of the four directions of Succolarity analysis: left to right, right to left, top to bottom and bottom to top divided by four) for the same sample used to compare the Lacunarity on previous section. The three images from Campinas are here evaluated.

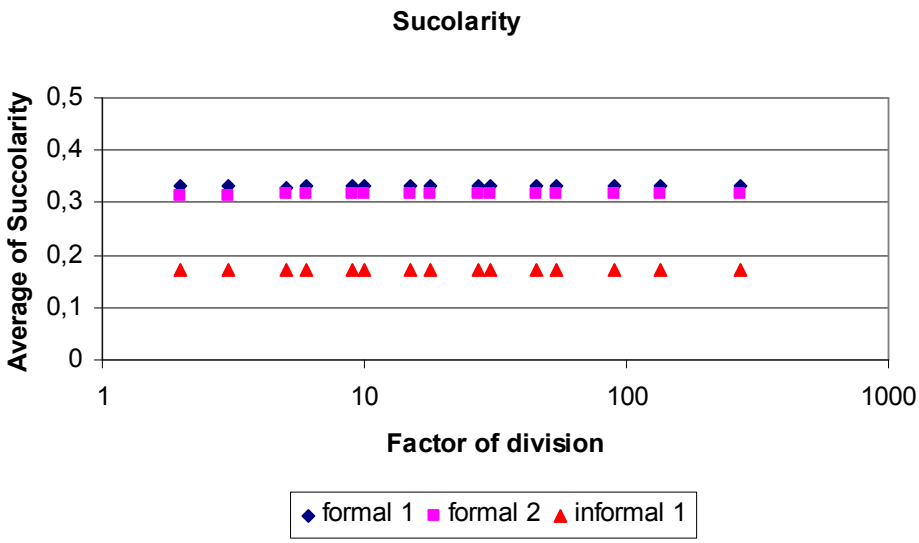

Figure 5.28. Results of Succolarity average obtained from the proposed method using as input the images of Campinas in figure 5.9 (a) – formal 1 and (b) – formal 2 and the image in figure 5.27 (b) – informal 1.

Figure 5.29 illustrates the advantages of using the Succolarity over the Lacunarity for this example. The informal areas, seen through the results, produce graphs better separated, showing that Succolarity is a good measure to characterize this kind of pattern.

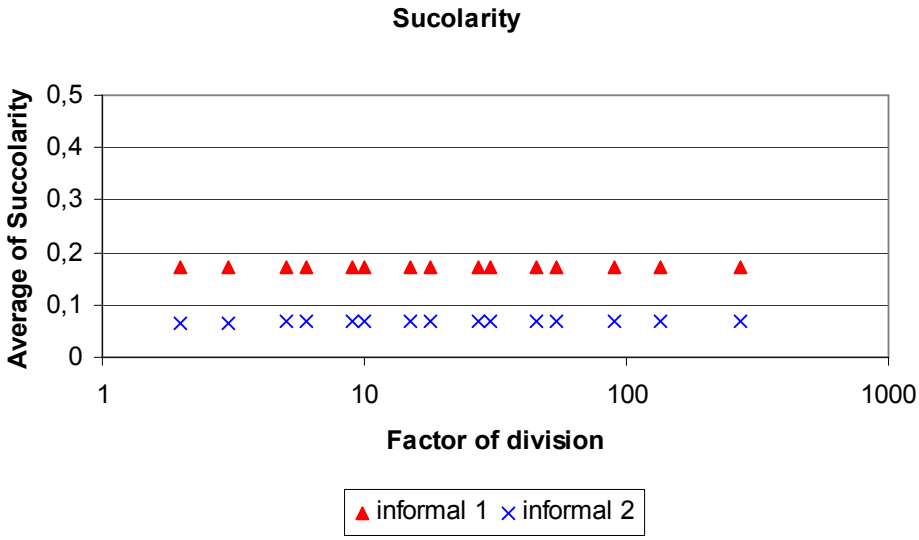

Figure 5.29. Results of Succolarity average obtained from the proposed method using as input the images of Campinas in figure 5.27 (b) – informal 1 and the image in figure 5.9 (d) – informal 2.

Another important point is that these results are the average results of Succolarity in a way that, for a specific application, as we will see on the next section, only one or a particular number of directions could be measured, as considered useful for the problem to be solved.

On graphs of figures 5.30 to 5.33 one can see that, through other type of analysis, the results of Succolarity could be used to distinguish formal from informal areas.

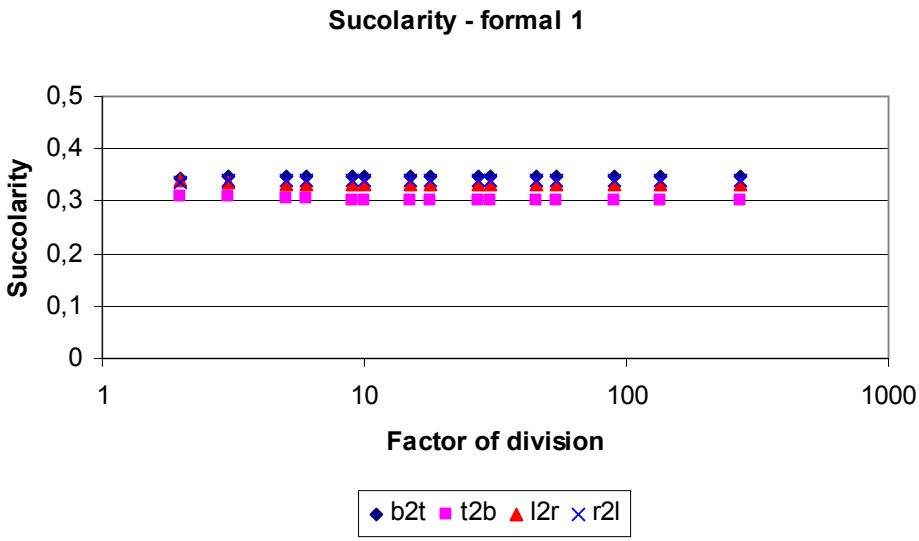

Figure 5.30. Results of Succolarity of the image in figure 5.9 (a).

Next results, figure 5.30 to 5.33, illustrate the results of Succolarity considering four directions that a fluid can flood the original image: bottom to top (b2t); top to bottom (t2b); left to right (l2r); right to left (r2l). Figures 5.30 and 5.31 demonstrate that, on formal areas, the results do not vary considerably with the direction. This is easily explained when we think that formal areas usually have a great number of large streets that go from lots of points to others including points where some streets cross others.

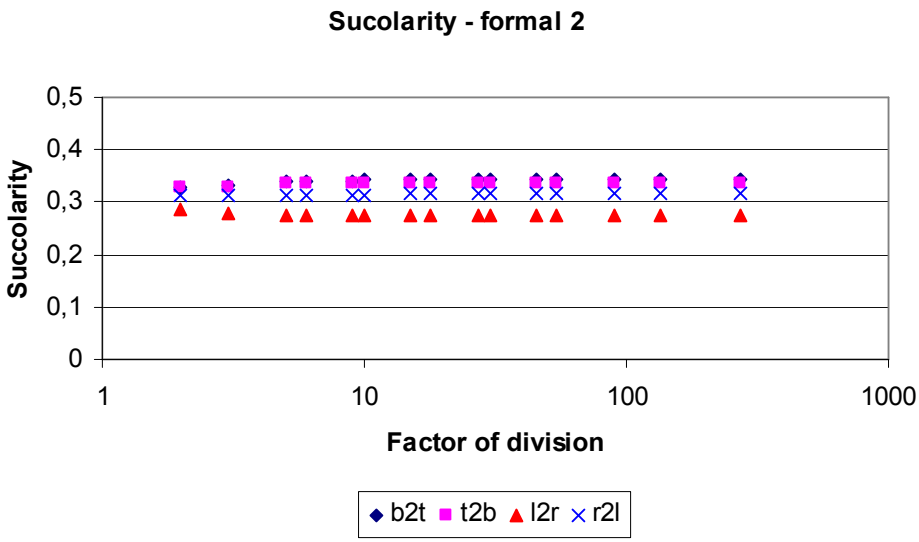

Figure 5.31. Results of Succolarity of the image in figure 5.9 (b).

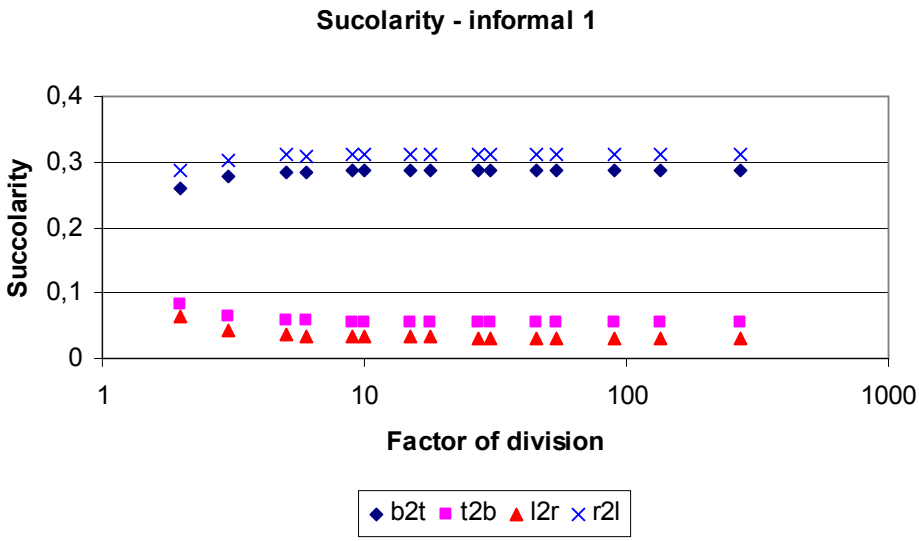

Figure 5.32. Results of Succolarity of the image in figure 5.27 (b).

Figures 5.32 and 5.33, which are results of Succolarity of informal areas, demonstrate that, in this kind of occupation, the direction used on the evaluation presents great impact on the results. While, for the analyzed formal areas, the difference in the values is on hundredths for Succolarity; for the informal areas, this difference is in decimals.

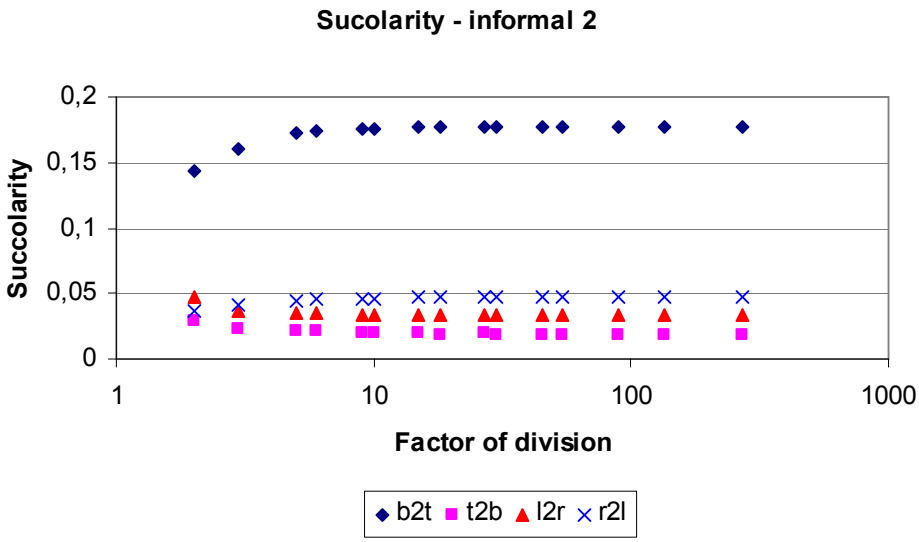

Figure 5.33. Results of Succolarity of the image in figure 5.9 (d).

The numerical values of Succolarity in the plots of this section are represented in tables 5.2 through 5.5 to better illustrate the differences on the results.

Factor of division	Succolarity				
	b2t	t2b	l2r	r2l	Average
270	0,3489	0,3023	0,3330	0,3415	0,3314
135	0,3489	0,3023	0,3330	0,3415	0,3314
90	0,3489	0,3023	0,3330	0,3415	0,3314
54	0,3489	0,3023	0,3330	0,3415	0,3314
45	0,3489	0,3023	0,3330	0,3415	0,3314
30	0,3489	0,3024	0,3330	0,3415	0,3315
27	0,3488	0,3023	0,3330	0,3415	0,3314
18	0,3489	0,3026	0,3330	0,3413	0,3314
15	0,3487	0,3024	0,3330	0,3413	0,3314
10	0,3486	0,3028	0,3331	0,3407	0,3313
9	0,3489	0,3033	0,3339	0,3414	0,3319
6	0,3482	0,3035	0,3339	0,3412	0,3317
5	0,3473	0,3035	0,3313	0,3380	0,3300
3	0,3487	0,3075	0,3357	0,3384	0,3326
2	0,3430	0,3085	0,3400	0,3354	0,3317

Table 5.2. Numerical results of Sucolarity of formal 1: figures 5.30 and 5.28.

Factor of division	Succolarity				
	b2t	t2b	l2r	r2l	Average
270	0,3432	0,3364	0,2752	0,3152	0,3175
135	0,3432	0,3364	0,2752	0,3152	0,3175
90	0,3432	0,3364	0,2752	0,3152	0,3175
54	0,3432	0,3364	0,2752	0,3152	0,3175
45	0,3432	0,3364	0,2751	0,3152	0,3175
30	0,3431	0,3364	0,2753	0,3152	0,3175
27	0,3432	0,3364	0,2752	0,3151	0,3175
18	0,3431	0,3364	0,2753	0,3151	0,3175
15	0,3428	0,3362	0,2754	0,3152	0,3174
10	0,3424	0,3361	0,2754	0,3147	0,3172
9	0,3415	0,3354	0,2756	0,3148	0,3168
6	0,3410	0,3355	0,2758	0,3145	0,3167
5	0,3408	0,3358	0,2755	0,3139	0,3165
3	0,3326	0,3294	0,2783	0,3121	0,3131
2	0,3295	0,3286	0,2847	0,3113	0,3135

Table 5.3. Numerical results of Sucolarity of formal 2: figures 5.31 and 5.28.

Factor of division	Succolarity				
	b2t	t2b	l2r	r2l	Average
270	0,2870	0,0543	0,0317	0,3113	0,1711
135	0,2870	0,0543	0,0317	0,3113	0,1711
90	0,2870	0,0543	0,0317	0,3113	0,1711
54	0,2870	0,0543	0,0318	0,3113	0,1711
45	0,2870	0,0543	0,0317	0,3113	0,1711
30	0,2869	0,0543	0,0318	0,3113	0,1711
27	0,2869	0,0544	0,0319	0,3112	0,1711
18	0,2868	0,0546	0,0321	0,3111	0,1711
15	0,2866	0,0547	0,0322	0,3112	0,1712
10	0,2861	0,0553	0,0327	0,3103	0,1711
9	0,2862	0,0556	0,0333	0,3104	0,1714
6	0,2845	0,0568	0,0350	0,3086	0,1712
5	0,2828	0,0574	0,0358	0,3107	0,1717
3	0,2765	0,0645	0,0424	0,3030	0,1716
2	0,2595	0,0823	0,0637	0,2867	0,1730

Table 5.4. Numerical results of Succolarity of informal 1: figures 5.32; 5.28 and 5.29.

Factor of division	Succolarity				
	b2t	t2b	l2r	r2l	Average
270	0,1768	0,0189	0,0332	0,0469	0,0690
135	0,1768	0,0189	0,0332	0,0469	0,0690
90	0,1768	0,0189	0,0332	0,0469	0,0690
54	0,1768	0,0190	0,0332	0,0469	0,0690
45	0,1768	0,0190	0,0333	0,0468	0,0690
30	0,1767	0,0190	0,0333	0,0468	0,0690
27	0,1767	0,0191	0,0333	0,0468	0,0690
18	0,1765	0,0190	0,0334	0,0467	0,0689
15	0,1764	0,0193	0,0336	0,0466	0,0690
10	0,1757	0,0195	0,0336	0,0463	0,0688
9	0,1757	0,0199	0,0334	0,0461	0,0688
6	0,1742	0,0207	0,0349	0,0453	0,0688
5	0,1723	0,0217	0,0358	0,0448	0,0686
3	0,1600	0,0234	0,0373	0,0414	0,0655
2	0,1440	0,0287	0,0470	0,0373	0,0642

Table 5.5. Numerical results of Sucolarity of informal 2: figures 5.33 and 5.29.

5.4.2 APLICATION OF SUCCOLARITY TO MEDICAL IMAGES

To demonstrate that Succolarity, like the other fractal measures, is a powerful method to characterize real images, an application of the Succolarity to vascular diagnosis is shown in this section. The two examples of images (SIZE and DUNCAN, 2006) demonstrate a carotid with and without occlusion. On first image named H53022B, figure 5.34, there is an internal carotid artery plaque, on the second H53031B, figure 5.35, there

is an internal carotid artery occlusion. Parts of the original image that contains only textual information were removed from the two images. The result images are both 480x240 pixels.

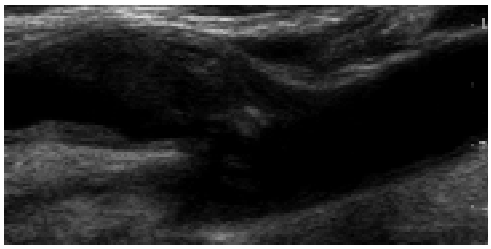

Figure 5.34. H53022B of the vascular-web database (SIZE and DUNCAN, 2006). Internal carotid artery plaque.

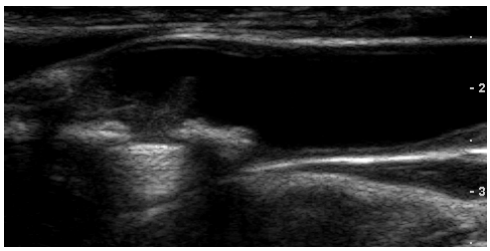

Figure 5.35. H53031B of the vascular-web database (SIZE and DUNCAN, 2006). Internal carotid artery occlusion.

In figures 5.34 and 5.35 it is not easy to visualize the occlusion that occurs in figure 5.35 and does not occur in figure 5.34. These images were submitted to heuristic tests to determine good values of threshold. The results of the threshold of these images are shown in figures 5.36 and 5.37.

Figure 5.36. Threshold of the image in figure 5.34. Value of threshold heuristically chosen was 18.

Figure 5.37. Threshold of the image in figure 5.35. Value of threshold heuristically chosen was 15.

After the threshold, it is easier to note that figure 5.37 has a complete occlusion and figure 5.36 has a partial obstruction. The next two images (5.38 and 5.39) show the intermediate images generated during the executing of the method proposed to calculate the Succolarity of the input image in figure 5.36.

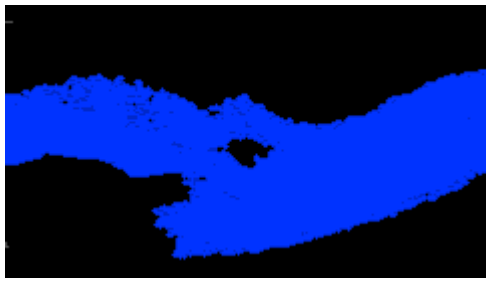

Figure 5.38. Intermediate image for the direction left to right (l2r) for the input image 5.36.

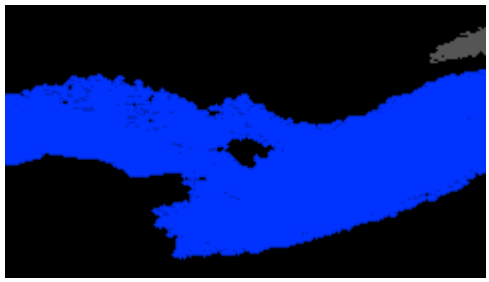

Figure 5.39. Intermediate image for the direction right to left (r2l) for the input image 5.36.

The two following images (figures 5.40 and 5.41) show the intermediate images generated during the executing of the method proposed to calculate the Succolarity for the input image in figure 5.37.

Figure 5.40. Intermediate image for the direction left to right (l2r) for the input image 5.37.

Figure 5.41. Intermediate image for the direction right to left (r2l) for the input image 5.37.

The ln x ln plots of the Succolarity are shown in figure 5.42 and 5.43.

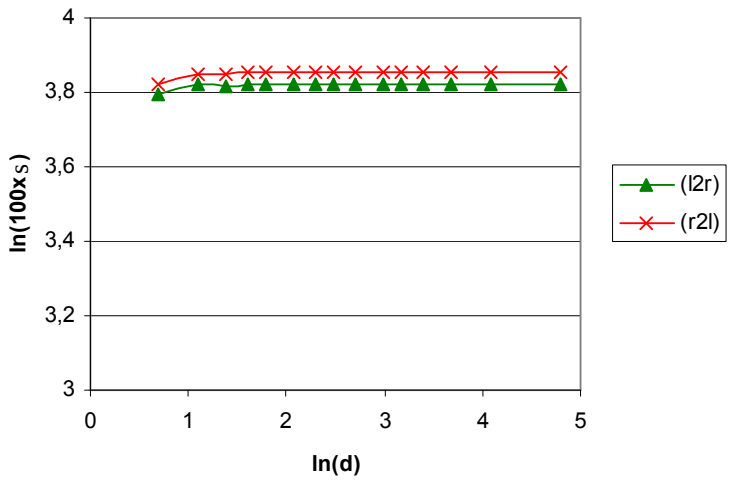

Figure 5.42. Ln x ln plot of the Succolarity for figure 5.36.

Table 5.6 shows the Succolarity numerical values for the image H53022B (figure 5.36). Table 5.7 shows the Succolarity numerical values for the image H53031B (figure 5.37).

		Succolarity (S)	
d	BS	l2r	r2l
120	(4x2)	0.4575	0.4727
60	(8x4)	0.4575	0.4727
40	(12x6)	0.4575	0.4727
30	(16x8)	0.4574	0.4726
24	(20x10)	0.4574	0.4726
20	(24x12)	0.4575	0.4726
15	(32x16)	0.4574	0.4725
12	(40x20)	0.4572	0.4723
10	(48x24)	0.4572	0.4723
8	(60x30)	0.4570	0.4720
6	(80x40)	0.4573	0.4720
5	(96x48)	0.4565	0.4709
4	(120x60)	0.4547	0.4687
3	(160x80)	0.4569	0.4702
2	(240x120)	0.4446	0.4566

Table 5.6. Numerical values of Succolarity of the threshold H53022B. d is the factor of division. BS the box size (width x height).

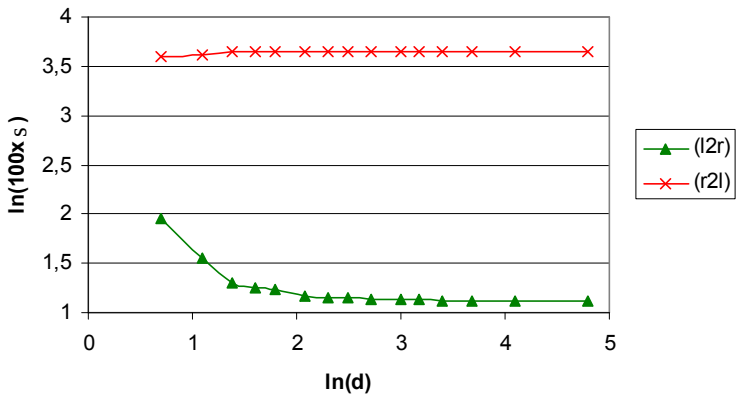

Figure 5.43. Ln x ln plot of the Succolarity for figure 5.37.

		Succolarity (S)	
d	**BS**	**l2r**	**r2l**
120	(4x2)	0.0307	0.3869
60	(8x4)	0.0307	0.3869
40	(12x6)	0.0308	0.3869
30	(16x8)	0.0308	0.3868
24	(20x10)	0.0310	0.3868
20	(24x12)	0.0310	0.3867
15	(32x16)	0.0313	0.3865
12	(40x20)	0.0317	0.3864
10	(48x24)	0.0315	0.3862
8	(60x30)	0.0323	0.3858
6	(80x40)	0.0343	0.3845
5	(96x48)	0.0347	0.3848
4	(120x60)	0.0369	0.3828
3	(160x80)	0.0470	0.3743
2	(240x120)	0.0705	0.3654

Table 5.7. Numerical values of Succolarity of the threshold H53031B. d is the factor of division. BS the box size (width x height).

The direction considered on the results was only horizontal because the vessels on the images are on this direction.

In the non occluded image the results on the curve to l2r and r2l almost match as we can see by the figure 5.42. But when an obstacle is present on the analyzed image, the l2r and r2l curves differs significantly as could be seen in figure 5.43.

6 CONCLUSIONS AND FUTURE WORKS

This chapter describes the conclusions about the fractal measures implemented and proposed as well as the directions to future works.

6.1 CONCLUSION

Throughout the results of the three types of fractal measures: Fractal Dimension; Lacunarity and Succolarity for all the real images used here we see, that fractal measures are very good to characterize a variety of kinds of images. Like many other works we continue here demonstrating the usability of fractal measures on medical diagnosis. The proposed measure, Succolarity, is also evaluated using medical images as input.

6.1.1 FRACTAL DIMENSION

The Fractal Dimension is already largely used to characterize patterns on a great number and kinds of application. The use on this work of the box counting method is only to confirm the idea that FD is a very good approach for texture analysis. The same type of images, mammograms, where used in this work to illustrate FD and Lacunarity uses. In both cases, we could say that fractal measures are very useful in the characterization of mammograms. Both methods could be used to compose a feature vector that, on a decision step, could help in the identification of the occurrence or not of malign tumors by mammograms.

The results from the implemented method against the results from FRACLAC validate the results obtained with the implementations.

6.1.2 LACUNARITY

The use of Lacunarity for texture identification in objects or image analysis is also considered in this work. Lacunarity has several practical advantages over other indices of texture analysis: its computation is simple to implement; it exhaustively samples the image to quantify changes and self-similarity with scale and it can be used for analysis of natural or synthetic images.

This work presents a method for estimation of LL of any kind of 3D object or image. It is not a simple extension of the usual Lacunarity characterization of 1D sets because it considers many local aspects as: resolution, generation and box size in images representation. Moreover, image now is an element of the 3D space, which means that its gaps distribution may consider the grey level representing the z coordinate.

The proposed approach is used for Lacunarity computation of an approximation of fractal objects and real images. The experimental results show the characteristics of texture recognition obtained using the Lacunarity as a feature extracted from an image. Although single value can be used for characterizations aspects of an area like a filter, the use of Lacunarity values combined as log x log (ln x ln) or even linear x log graphs are much more representative for the characterization of the texture of all images. It is the change of the Lacunarity values over different gliding box sizes that yields greater amount of information. The combination of these values captures pattern over the entire range of scales from the minimum grid to a given percentage of the entire image, or a representative percentage of the image.

The use of a single value of Lacunarity extracted from a single box size is of limited value and meaningless as a basis for comparing different images. The more useful feature of Lacunarity is the amount of information gained by computing it over a range of box sizes. It is especially interesting if resolution, r, also change. For each object, the Lacunarity representation can be calculated for box (cubes) sizes ranging from s=2 to r incrementing one voxel at the box size each time.

The plots that compare the results obtained from our approach versus the FRACLAC to calculate the Lacunarity show that the values match on the simple case, that is, the binary version of Lacunarity.

The plots compare the results of the Lacunarity for the gray-scale images illustrating that the proposed methods characterizes better the differences on the mammograms tested against the method proposed by Fernandes (not published yet) and the one proposed by Gan Du (GAN DU and TAT SOON YEO, 2002). The disadvantage of the proposed methods is that they are more computationally expensive than the others.

6.1.3 SUCCOLARITY

The results of the experiments on real images show that the method is very useful as a new feature to integrate other characteristics on pattern recognition processes. The notions of Succolarity described on MANDELBROT, 1977 were respected and the measure could be seen as a natural evolution of the FD and Lacunarity. The other advantage of the method is to be simple, easy and fast to be calculated.

Analyzing the Succolarity results for the city pictures, it is easy to notice that, depending on the intention of the classification, the method is better suited than the Lacunarity. The main gain of the Succolarity is that the method enables not one, but lots of ways to analyze the results, once the user knows something about what kind of information he wants to extract from the image, more he can take advantage of the representation of the result. The user could use different directions, combining it or not, depending on the problem in question. These were illustrated by the cities results of Succolarity, which uses four directions, and the vascular medical images results, that use only two directions.

Like the Lacunarity, our proposal to Succolarity computation considers the use of log x log (ln x ln) or linear x log plots instead of a single value. The Succolarity values over different box sizes gives essential information useful to the pattern recognition process.

Succolarity is a great measure, that is very useful, not only for the type of images used here, but to generic images, that present some information associated with direction or flow. Among the applications are the study of percolation of petroleum and natural gas through semi-porous rock; where the theory can help to predict and improve the productivity of natural gas and oil (WIKIPEDIA, 2007).

6.2 FUTURE WORKS

This section talks about the possible continuation works and new ways to calculate the Lacunarity and Succolarity to enhance the results obtained so far.

6.2.1 LACUNARITY

The method proposed here to calculate the Lacunarity of gray-scale images was the same method used to calculate the Lacunarity of 3D objects. This method presents good results but is computationally expensive, and because of that it is not useful to real time texture segmentation applications. A future work then is to develop an algorithm that makes use of all the information in the gray-scale image, like was used here, that could be used on automatic identification needs.

6.2.2 SUCCOLARITY

As future work, it is suggested modeling of a gray scale version of the .Succolarity, which will avoid the threshold step on 8 bit images. The initial intention is to keep the method easy to understand and implement as well as keep it faster to execute like the binary version described here.

An idea is also to consider the use of the Succolarity results obtained as texture filters as coefficients (as the Hurst coefficient).

Another application for the Succolarity method, beyond the ones described in this work, is on the study or prevention of the reservoir induced earthquakes (induced seismicity). Some evidence exists to link the development of larger dams with the occurrence of seismic events. In seismically active areas, a reservoir may advance the occurrence of earth tremors (possibly resulting in more frequent but smaller magnitude events). The relationship between water percolation, seismic events and the mechanisms by which a reservoir could causes earthquakes are not wholly understood and there is considerable debate on the subject (WORLD BANK, 2007).

REFERENCES

(ADDISON, 1997) ADDISON, P. S., **Fractals and Chaos: An Illustrated Course**, Napier University, Edinburgh; Institute of Physics Publishing, Publishing Ltd; London, 1997.

(ALLAIN and CLOITRE, 1991) ALLAIN, C., CLOITRE, M., **Characterizing the lacunarity of random and deterministic fractal sets**, Physical Review A, 44, pp. 3552-3558, 1991.

(AMORIN et al, 2001) AMORIN, H. P., VELLASCO, M. M., CONCI, A., LEVY, A. F. S., **Reconhecimento de Defeitos em Equipamentos Elétricos de Alta Tensão Utilizando a Teoria Fractal e as Redes Neurais Artificiais**, XVI SNPTEE, Seminário Nacional de Produção e Transmissão de Energia Elétrica, CTEEP, EPTE., 2001.

(AQUINO and CONCI, 1998) AQUINO, F. R. and CONCI, A., **Fractal Image Coding by Multi-Scale Selection Based on Block Complexity**, Proceedings of 8th International Conference on Engineering Design Graphics and Descriptive Geometry - ICECGDG - Austin, Texas, USA, July 31-August 3, vol. 2 , pp. 495-499, Edited by ISCG-International Society for Geometry and Graphics, 1998.

(AZEVEDO and CONCI, 2003) AZEVEDO, E. and CONCI, A., **Computação Gráfica – Teoria e Prática**, 1ª. ed. Elsevier Ltda., Rio de Janeiro, 2003.

(BADII and POLITI, 1987) BADII, R. and POLITI, A., **Renyi dimensions from local expansion rates**, Physical Review, 35-3, pp. 1288-1293, Fecbruary 1987.

(BARABÁSI and STANLEY, 1995) BARABÁSI, A. L., STANLEY, H. E., **Fractal Concepts in Surface Growth**, Cambridge University Press, New York, USA, 1995.

(BARNSLEY et al., 1988) BARNSLEY, M. F., DEVANEY, R. L., MANDELBROT, B. B., PEITGEN, H. O., SAUPE, D., **The Science of Fractals Images**, Springer-Verlag, New York, 1988.

(BARROS FILHO and SOBREIRA, 2005) BARROS FILHO, M. N. M. and SOBREIRA, F. A., **Assessing texture pattern in slums across scales: an unsupervised approach.**

In: CASA Working Paper, Centre for Advanced Spatial Analysis, University College London, London, n. 87, 2005. Link: http://www.casa.ucl.ac.uk/working_papers/paper87.pdf.

(BARROS FILHO and SOBREIRA, 2005a) BARROS FILHO; M. N. M.; SOBREIRA, F. A. J. **Analysing spatial patterns in slums: a multiscale approach**. In: CONGRESSO INTERNACIONAL DE PLANEJAMENTO URBANO REGIONAL INTEGRADO E SUSTENTÁVEL, São Carlos (SP). São Carlos: PLURIS, 2005.

(BATTY and LONGLEY, 1994) BATTY, M., LONGLEY, P. **Fractal Cities: Geometry of Form and Function**. 1 ed. London: Academic Press, 1994.

(BLOCK et al., 1990) BLOCK, VON BLOH, W. and SCHELLNHUBER, H. J., **Efficient box-counting determination of generalized fractal dimensions**, Physical Review A, 42, 4, pp. 1869-1874, 1990.

(BROWN, 2005) BROWN, A., **Fractal landscapes**, Link: http://www.fractal-landscapes.co.uk, 2005

(CHA, 1992) CHA, K. L., **Fractal-based texture analysis**, ICCS/ISITA Conference Proceedings - Communications on the Move, Singapore, pp. 102–106, Nov. 1992.

(CHEN et al., 1989) CHEN, C. C., DAPONTE, J. S. and FOX, M. D., **Fractal feature analysis and classification in medical imaging**, IEEE Transactions on Medical Imaging, vol. 8, pp. 133–142, June 1989.

(COELHO and CONCI, 2000) COELHO, F. F. S., CONCI, A., **Investigation of Meteorological Satellite Images Using Multifractal Analysis**, Abstracts do CILAMCE 2000, 21st Iberian Latin American Congress on Computational Methods in Engineering , IMPA, Rio de Janeiro, Edited by Luiz Eloy Vaz, ISBN 85-901717-1-x , p. 148. Trabalho completo em CD of XXI CILAMCE - CILAMCE'2000, December 2000.

(COELHO and CONCI, 2001) COELHO, F. S. and CONCI, A., **An Efficient Approach to Compute the Hausdorff dimension of images**, IEEE - EURASIP Workshop on Nonlinear Signal and Image Processing, Hyatt Regency Baltimore, Baltimore, Maryland USA, June 2001.

(CONCI, 1999) CONCI, A., **Texture Classification of Lansat Images Using Fractal Dimension and Bands**, Anais do GisBrasil99 - V Congresso e Feira para Usuários de Geoprocessamento da América Latina Salvador, Bahia, Brasil, CD Módulo de Tecnologia-Coleta de Dados- Sensoriamento Remoto, July 1999.

(CONCI et al., 1996) CONCI, A. , CAMPOS, C. F. J. , PROENÇA, C. B., **Using Fractal Dimension to Identify Texture Variation**, proceedings of Second International Conference on Non-linear Dynamics, Chaos, Control and Their Applications in Engineering Science ICONNE'96, in Chap. 2 Chaotic Phemomena of Nonlinear Dynamics, Chaos Control and Their Applications to Engineering Science- ISBN – 65-900351-1-5, edited by J. M. Balthazar, D./T. Mook & J. M. Rosario, São Pedro , SP, pp. 174-178, August 1996.

(CONCI et al., 1997) CONCI, A., CAMPOS, C.F.J. and PROENÇA, C. B., **Using Fractal Dimension to Identify Texture Variation** in Chap. 2 Chaotic Phenomena of Nonlinear Dynamics, Chaos Control and Their Applications to Engineering Science - ISBN – 65-

900351-1-5, edited by J. M. Balthazar, D./T. Mook & J. M. Rosario , AAM/RBCM pp. 174-178, 1997.

(CONCI et al., 1999) CONCI, A., SOARES, L. M., VIANNA, A. D., **Identification of Benign and Malignant Lesion by Feature Extraction on Mammographic Images**, Applied Mechanics in Americas, v. 6, pp. 53-56, 1999.

(CONCI and AQUINO, 1999) CONCI A. and AQUINO, F., **Fractal Image Coding Based on Block Complexity**, Journal for Geometry and Graphics , Heldermann Verlag, Germany, ISSN 1433-8158, v. 3, pp. 57-64, 1999.

(CONCI and AQUINO, 1999a) CONCI A., and AQUINO, F., **Using Adaptive Contraction for Fractal Image Coding Based in Local Fractal Dimension**, proceedings of SIBGRAPI'99, Edited by IEEE Computer Society, ISBN: 0-7695-0481-7/99 Technical Session, pp. 231-239, 1999.

(CONCI and AQUINO, 2002) CONCI, A., AQUINO, F. R., **Codificação Fractal de Imagens**, Chapter 16 in Anais do I Congresso de Dinâmica, Controle e Aplicações. Editado por J. M. Balthazar, M. Boaventura, G. N. Silva e M. Tsuchida . Sociedade Brasileira de Matemática Aplicada e Computacional - SBMAC - palestra convidada do I DINCON - ISBN- 85-86883-05-0. 1ª. Escola Temática de Dinâmica e Controle, São José do Rio Preto, SP, v. 1, pp. 365-402, July 2002

(CONCI and AQUINO, 2005) CONCI, A., AQUINO, F. R., **Fractal Coding Based on Image Local Fractal Dimension**. Computational & Applied Mathematics (CAM), ISSN: 0101-8205, SBMAC, Special Issue on Dynamics, Control and Their Applications - Guest Editors: J M Balthazar and G N Silva, pp. 26-40, January 2005.

(CONCI and CAMPOS, 1996) CONCI, A. CAMPOS,C. F. J., **An Efficient Box-Counting Fractal Dimension Approach for Experimental Image Variation**

Characterization, Processing IWISP'96 - 3rd International Workshop on Image and Signal Processing - Ed. by B.G. Mertzios & P. Liatsis ISBN 0444825878 - Elsevier Science B.V., Manchester, UK, pp. 665-668 , November 1996.

(CONCI and CASTRO, 2002) CONCI, A, and CASTRO, E. M. M. M., **Image mining by content**, Journal of Expert Systems with Application, Devon, UK, Ref.: ESWA 1003, Elsevier Science, UK, v. 23, Issue 4, pp. 377-383, 2002

(CONCI and MONTEIRO, 2000) CONCI, A. and MONTEIRO, L. H., **Multifractal Characterization of Texture-Based Segmentation**, IEEE - ICIP 2000, Proceedings of the International Conference on Image Processing on paper and CD-ROM - ISBN 0 7803 6300 0, Vancover, Canada, pp. 792-795, September 2000.

(CONCI and MONTEIRO, 2000a) CONCI, A. and MONTEIRO, L. H., **An Approach to Estimate the Hausdorff Dimension of Textures**, ICONNE 2000, Proceedings of the Third International Conference on Nonlinear Dynamics, Chaos Control and Their Applications to Engineering Science- ISBN – 65-900351-1-5, edited by J. M. Balthazar, D./T. Mook & J. M. Rosario , ABCM & AAM, Campos do Jordão, SP, vol. 1, pp. 100-112, July 2000.

(CONCI and MONTEIRO, 2002) CONCI, A. and MONTEIRO, L. H., **An Approach to Estimate the Hausdorff Dimension of Textures**, Chapter 4: Aplicon - Applications, in: Nonlinear Dynamics, Chaos Control and Their Applications to Engineering Science: Applications of Nonlinear Phenomena - ISBN: 85-900351-6-6, edited by J. M. Balthazar, P. B. Goncalves, R. M. F. R. F. Brasil, I. L. Caldas, F. B. Rizatto, Publised by ABCM, AAM, SBMAC, SIMAI, v. 6, pp. 307-316, 2002.

(CONCI and NUNES, 2001) CONCI, A. and NUNES, E.O., **Multi-bands image analysis using local fractal dimension**, proceedings of SIBGRAPI 2001, Florianopolis, SC, pp. 91-98, 2001.

(CONCI and PROENÇA, 1997) CONCI, A. and PROENÇA, C. B., **A Box-Counting Approach to Color Image Segmentation**, ICIP'97- IEEE 4th International Conference on Image Processing, Santa Barbara, California, USA, v. I, pp. 228-230, October 1997.

(CONCI and PROENÇA, 1997a) CONCI, A. and PROENÇA, C. B., **Fractal Image Analysis for the Textile Industry**, Proceedings of EDUGRAPHICS'97 - Third International Conference on Graphics Education - COMPUGRAPHICS'97 - Sixth International Conference on Computational Graphics and Visualization Techniques, Vilamoura, Algarve, Portugal, pp. 137-144, December 1997.

(CONCI and PROENÇA, 1998) CONCI, A. and PROENÇA, C. B., **A Fractal Image Analysis System for Fabric Inspection Based on Box-Counting Method**, Computer Netwoks and ISDN Systems, v. 30, Issue 20-21, pp. 1887-1895 Edited by Elsevier Science, November 1998.

(DONG, 2000) DONG, P., **Test of a new lacunarity estimation method for image texture analysis**, International Journal of Remote Sensing, v. 21, Issue 17, pp. 3369–3373, Nov. 2000.

(EINSTEIN et al., 1998) EINSTEIN, J., Hai-Shan Wu, Gil, J., **Self-affinity and lacunarity of chromatin textures in benign and malign breast epithelial cell nuclei**, Physical Review Letters, 80, pp. 397-400, 1998.

(FALCONER, 1990) FALCONER, K. J., **Fractal Geometry: Mathematical Foundations and Applications**, University of Bristol; John Wiley & Sons Ltd; England, 1990.

(FERNANDES and CONCI, 2004) FERNANDES, J. L., CONCI, A., **A Lacunaridade na Caracterização Espacial de Padrões**, proceedings of III Congresso Temático de

Dinâmica e Controle da SBMAC, Dincon-2004, UNESP/Campus de Ilha Solteira, ABCM, Tec Art Editora, Ilha Solteira, SP, Brazil, pp. 1432-1492, May 2004.

(FERNANDES and CONCI, 2004a) FERNANDES, J. L., CONCI, A., **Uso da lacunaridade no controle de qualidade visual de padrões industriais**, proceedings of III NATIONAL CONGRESS OF MECHANICAL ENGINEERING, Belém, PA, Brazil, August 2004.

(FOLEY et al., 1990) FOLEY, J.D., DAM, A.V., FEINER, S.K. and HUGHES, J.F., **Computer Graphics – Principles and Practice**, 2ª. ed. Addison Wesley, Reading, 1990.

(FRANKHAUSER, 1997) FRANKHAUSER, P. **Fractal analysis of urban structures**, In: HOLM, E. (Edit). Modelling space and networks: Progress in theoretical and quantitative geography. Umea: Gerum Kulturgeografi, pp. 145-181, 1997.

(FRAZER et al., 2005) FRAZER, G. W., WULDER, M. A., NIEMANN, K. O., **Simulation and quantification of the fine-scale spatial pattern and heterogeneity of forest canopy structure: A lacunarity-based method designed for analysis of continuous canopy heights**, Forest Ecology and Management, v. 214, pp. 65-90, 2005.

(GAN DU and TAT SOON YEO, 2002) GAN DU and TAT SOON YEO, **A novel lacunarity estimation method applied to SAR image segmentation**, IEEE Transactions on Geoscience and Remote Sensing, v. 40 – 12, pp. 2687-2691, 2002

(GONZALEZ and WOODS, 2000) GONZALEZ, R. C. and WOODS, R. E., **Processamento de Imagens Digitais**, 1ª. ed. Edgard Blücher Ltda, São Paulo, Brazil, 2000.

(GRASSBERGER, 1981) GRASSBERGER, P., **On the Hausdorff dimension of fractal attractors**, Journal of Statistical Physics, v. 26 – 1, pp. 173-179, 1981.

(KARPERIEN, 2004) KARPERIEN, A., **FRACLAC**, Link: http://www.geocities.com/akarpe@sbcglobal.net/box.html.Charles Sturt University, Australia, 2004.

(KELLER et al., 1989) KELLER, J. CROWNOVER, R. CHEN, S., **Texture description and segmentation through fractal geometry**, Computer Vision, Graphics, and Image Processing, v. 45, pp. 150-166, 1989.

(KOCH, 1904) KOCH, H. von, **Sur une courbe continue sans tangente, obtenue par une construction geometrique elementaire**, Arkiv for Matematik 1, 6810704, 1904.

(LISBERGER, 1982) LISBERGER, S., **Tron**, Disney, USA/Taiwan, California, USA, 1982.

(MANDELBROT and VAN NESS, 1968) MANDELBROT, B.B., VAN NESS, J., **Fractional Brownian motion, fractional noise and applications**, SIAM Review, 10, 1968.

(MANDELBROT, 1977) MANDELBROT, B., **The fractal geometry of nature, W. H. Freeman and Company**., San Francisco, 1977.

(MCINTYRE and WIENS, 2000) MCINTYRE, N. E. and WIENS, J. A., **A novel use of the lacunarity index to discern landscape function**, Landscape Ecology, 15, pp. 313-321, Springer Netherlands, 2000.

(MELO et al., 2006) MELO, R. H. C.; VIEIRA, E. A.; CONCI, A., **Characterizing the lacunarity of objects and image sets and its use as a technique for the analysis of textural patterns** on Advanced Concepts for Intelligent Vision Systems - ACIVS 2006 –

Lecture Notes in Computer Science, Publisher Springer Berlin / Heidelberg, IEEE Benelux Signal Processing Chapter, v. 4179, pp. 208-219, Antwerp, Belgium, September 2006.

(MELO et al., 2006a) MELO, R. H. C.; VIEIRA, E. A.; CONCI, A., **Comparing two approaches to compute lacunarity of mammograms** on proceedings of 13th International Conference on Systems, Signals and Image Processing - IWSSIP'06, Co-organised by the Budapest University of Technology and Economics, Hungary and Technical University of Kosice, Slovak Republic, in cooperation with IEEE, IEEE Region 8, IEE, IEEE Hungarian Section, EURASIP, ISBN: 80-89082-09-2, pp. 299-302, Budapest, Hungary, 2006.

(MELO and CONCI, 2007) MELO, R. H. C., CONCI, A., **Identificação de tumores dos seios pela análise de suas imagens** on I Encontro Nacional de Engenharia Biomecânica - ENEBI 2007. organized by: ABCM, UFMG and IME.

(MÜSSIGMANN, 1992) MÜSSIGMANN, U., **Texture Analysis by Fractal Dimension**. In: J.L.Encarnação, PEITGEN, H. O., SAKAS, G., ENGLERT, G. (eds.): Fractal geometry and Computer Graphics. Springer-Verlag, Berlin, pp. 217-230, 1992.

(NUNES and CONCI, 2001) NUNES, E.O. and CONCI, A., **Determinação da Dimensão Fractal de Conjuntos de Pontos à Imagens de Satélites**, Applicon 2001, Proceedings of Applicon, Sao Carlos, SP, Brazil, July 2001

(PAPOULIS, 1965) PAPOULIS, A., **Probability, Random Variables, and Stochastic Processes**, In: McGraw-Hill Series in Systems Science, McGraw-Hill, New York, 1965.

(PEITGEN et al., 1992) PEITGEN, H. O., JÜRGENS, H., SAUPE, D., **Chaos and Fractals: New Frontiers of Science.** Springer-Verlag, New York, 1992.

(PENTLAN, 1984) PENTLAN, A., **Fractal-based description of nature scenes**, IEEE Transactions on Pattern Analysis and Machine Intelligence, v. 10, pp. 661–674, May 1984.

(PIZZOLATO, 2003) PIZZOLATO, D. **CxImage**, Link: http://www.codeproject.com/bitmap/cximage.asp?target=CxImage, 2003.

(PLOTNICK et al., 1993) PLOTNICK, R.E., GARDNER, R.H., O'NEILL, R.V., **Lacunarity indices as measures of landscape texture**, Landscape Ecology, Springer Netherlands, v. 8, pp. 201-211, 1993.

(PROENÇA et al, 1999) PROENÇA, C. B. CONCI, A., SEGENREICH, S., **Comparação de Técnicas de Segmentação e de Dimensão Fractal visando a Detecção Automática de Falhas Têxteis**, Applied Mechanics in Americas, Proceedings of VI Pan American Congress of Applied Mechanics - PACAM and 8th International Conference on Dynamic Problems in Mechanics, v. 6, pp. 381-384, Rio de Janeiro, Brazil, January 1999.

(RASBAND, 1997) RASBAND, W., **ImageJ**. Link: http://rsb.info.nih.gov/ij/, National Institute of Mental Health, Bethesda, Maryland, USA, 1997.

(RAUCH, 2007) RAUCH, E., **Introduction to Lacunarity**. Link: http://www-swiss.ai.mit.edu/~rauch/lacunarity/lacunarity.html.

(SARKAR and CHAUDHURI, 1992) SARKAR, N. and CHAUDHURI, B. B., **An efficient approach to estimate fractal dimension of textural images**, Pattern Recognition, 25, pp. 1035-1041, 1992.

(SARKAR and CHAUDHURI, 1994) SARKAR, N. and CHAUDHURI, B. B. **An efficient differential box-counting approach to compute fractal Dimension of Image**, IEEE Trans. Syst. Man and Cybernetic, v. 24, 1, pp. 115-120, 1994.

(SERRA, 1982) SERRA, J., **Image Analysis and Mathematical Morphology,** Academic Press Inc., Orlando, ISBN 0-12-637240-3, 1982.

(SIZE and DUNCAN, 2006) SIZE, G. P., DUNCAN, R. K., **Vascular-Web**, Link: http://www.vascular-web.com, 2006.

(SOBREIRA and GOMES, 2000) SOBREIRA, F., GOMES, M., **The Geometry of Slums**, Working Paper Series, CASA – Centre for Advanced Spatial Analysis – University College London, London, n. 30, 2000.

(SOILLE, 1998) SOILLE, P., **Morphological Image Analysis,** Springer – Verlag Inc., Berlin, ISBN 3-540-65671-5, 1998.

(SPACE IMAGING BRAZIL, 2004) Space Imaging do Brasil, Link: http://www.spaceimaging.com.br/, 2004.

(VIEIRA AND MELO, 2004) VIEIRA, E. A., MELO, R. H. C., **Granulometria: Uma Aplicação para Contagem e Medição de Grãos em Imagens Digitais**, Monografia Dep. de Ciência da Computação - Universidade Federal Fluminense para Obtenção do Grau de Bacharel, 2004.

(WALKER, 2007) WALKER, J., **Fractal Food: Self-Similarity on the Supermarket Shelf**, Link: http://www.fourmilab.ch/images/Romanesco/, 2007.

(WATT and POLICARPO, 1998) WATT, A.H. and POLICARPO, F., **The Computer Image**, Addison-Wesley, ISBN 0-201-42298-0, 1998.

(WEISSTEIN, 2006) WEISSTEIN, E. W., **Mathworld: The Web's Most Extensive Mathematics Resource**, Link: http://mathworld.wolfram.com/, 2006.

(WIKIPEDIA, 2007) WIKIPEDIA, **Percolation, Percolation theory and Percolation thresholds** , 2007

(WORLD BANK, 2007) WORLD BANK, **Hydro Power: Reservoir Induced Earthquakes (Induced Seismicity)**, Link: http://www.worldbank.org/html/fpd/em/hydro/rie.stm, 2007.

(ZEMECKIS, 2004) ZEMECKIS, R., **The Polar Express: An IMAX 3D Experience (USA) (IMAX version)**, Warner Bros, California, USA, 2004.